Vaccinia Virus' E3 Protein Inhibits Cellular Recognition of Canonical dsRNA and ZRNA

by

Samantha Cotsmire

A Thesis Presented in Partial Fulfillment
of the Requirements for the Degree
Doctor of Philosophy

Approved August 2021 by the
Graduate Supervisory Committee:

Bertrand Jacobs, Chair
Arvind Varsani
Brenda Hogue
Shelley Haydel

ARIZONA STATE UNIVERSITY

December 2021

ABSTRACT

Poxviruses such as monkeypox virus (MPXV) are emerging zoonotic diseases. Compared to MPXV, Vaccinia virus (VACV) has reduced pathogenicity in humans and can be used as a partially protective vaccine against MPXV. While most orthopoxviruses have E3 protein homologues with highly similar N-termini, the MPXV homologue, F3, has a start codon mutation leading to an N-terminal truncation of 37 amino acids. The VACV protein E3 consists of a dsRNA binding domain in its C-terminus which must be intact for pathogenicity in murine models and replication in cultured cells. The N-terminus of E3 contains a Z-form nucleic acid (ZNA) binding domain and is also required for pathogenicity in murine models. Poxviruses produce RNA transcripts that extend beyond the transcribed gene which can form double-stranded RNA (dsRNA). The innate immune system easily recognizes dsRNA through proteins such as protein kinase R (PKR). After comparing a vaccinia virus with a wild-type E3 protein (VACV WT) to one with an E3 N-terminal truncation of 37 amino acids (VACV E3Δ37N), phenotypic differences appeared in several cell lines. In HeLa cells and certain murine embryonic fibroblasts (MEFs), dsRNA recognition pathways such as PKR become activated during VACV E3Δ37N infections, unlike VACV WT. However, MPXV does not activate PKR in HeLa or MEF cells. Additional investigation determined that MPXV produces less dsRNA than VACV. VACV E3Δ37N was made more similar to MPXV by selecting mutants that produce less dsRNA. By producing less dsRNA, VACV E3Δ37N no longer activated PKR in HeLa or MEF cells, thus restoring the wild-type phenotype. Furthermore, in other cell lines such as L929 (also a murine fibroblast) VACV E3Δ37N, but not VACV WT infection leads to activation of DNA-dependent activator of IFN-regulatory factors (DAI) and induction of necroptotic cell death. The same low dsRNA mutants demonstrate that DAI activation and necroptotic induction is independent of classical dsRNA. Finally, investigations of spread in an animal model and replication in cell lines where both the PKR and DAI pathways are intact determined that inhibition of both pathways is required for VACV E3Δ37N to replicate.

ACKNOWLEDGEMENTS

I would like to thank my committee members for their support and guidance over the years. I would especially like to thank Dr. Jacobs for being my mentor and teaching me to approach problems with creative solutions. I would like to thank Dr. Arvind Varsani for his positivity, compassion, and contagious excitement for teaching. I would like to thank Dr. Brenda Hogue for teaching me virology and for suggesting valuable experiments through the years. I would like to thank Dr. Shelley Haydel for her insights and pushing me to have endpoints for experiments and projects.

I would first like to thank the members of the Jacobs lab who trained me specifically Dr. Karen Kibler and Dr. Trung “Joe” Huyhn without your patience and support this would not have been possible. I would also like to thank Dr. Heather Koehler, Nobuko Fukushima, and James Bonner both for being great coworkers and for their ongoing support and friendship. I have appreciated our conversations about biology and life in general. I would like to thank Shizuka Barclay, Hamed Alattar, and Clayton Foster for not just being great undergrads but also for their exceptional enthusiasm for research. I would also like to thank the other members of Dr. Jacobs’ lab for productive discussion and collaboration specifically Dr. Jeffrey Langland, Dr. Karen Denzler, Dr. Latha Kannan, Dr. Negin Blattman, Dr. Sambhavi Subramanian, Dr. Mateusz Szczerba, Dr. Brian Johnson, Dr. Lydia Meador, Dr. Susan Holechek, Megan McCaughan, Jackie Sicalo, Johanne Ma Angelee Alonso Gerstel, Kimberly Velarde, Aradhana Kasimsetty, Corwin Bernard, William Martelly, and Sean Dunn. I would finally like to thank the former grad students of Dr. Jacobs’ lab specifically Dr. William Arndt and Dr. Stacy White whose work I built off of for my thesis.

I would like to thank ASU School of Life Sciences and the School for Engineering of Matter, Transport and Energy for their support with coursework and funding. I would also like to thank the Graduate and Professional Student Association for funding to attend conferences.
I would like to thank my loved ones for their enduring patience and emotional support even if from far away. In particular, Dr. Sri Krishna for his friendship, love, and support; I don’t know how I

would have made it through this without you. My Mom for always demonstrating incredible work ethic and perseverance growing up; I'm excited to get to see you more. My brother for always being someone I can talk to even if it's been too long since our last call; I am so proud of the man you have become and couldn't hope for a better sibling.

TABLE OF CONTENTS

Page

LIST OF TABLES

Table Page

LIST OF FIGURES

Figure Page

CHAPTER 1
INTRODUCTION

Poxviruses in the Modern Era

The SARS-CoV-2 pandemic virus increased public awareness of the dangers of seemingly innocuous viruses emerging as human threats. Furthermore, it has demonstrated the ability of a viral pathogen to adversely affect not only our health but also our economy (1, 2). In addition to this society-altering pandemic, Zika virus and Ebola have both caused recent epidemics. Each of these outbreaks were discovered after the viruses began spreading throughout communities causing increased disease in humans. These incidents have demonstrated the importance of studying emerging infectious diseases before they become major outbreaks.

Monkeypox virus (MPXV) recently arrived in the United States of America after an infected individual flew from Lagos, Nigeria to Dallas, Texas (with a brief layover in the Atlanta, Georgia airport) on July 7, 2021 (3). The infected person was likely exposed to the virus as part of the ongoing outbreak in Nigeria that began with a single introduction into humans after severe flooding in 2017 (4, 5). Since the outbreak began, four other infected patients have travelled to the UK, Israel, and Singapore leading this to become the first outbreak where infected persons have left Africa (6). Monkeypox virus's only previous visit to the USA was in 2003 when an exotic pet importer accidentally brought infected animals from Ghana leading to the 37 confirmed human cases and 10 suspected cases across the Midwest (7). Subsequent testing of the imported animals yielded positive results for culturable MPXV or detectable MPXV DNA in 2 pouch rats, 9 dormice, and 3 rope squirrels (8). Once the animals reached the US, they were housed in a facility with prairie dogs which were later sold as pets; all infected people had a bite or evidence of prolonged close contact with an infected prairie dog (7). Fortunately, both of the MPXV imports to America have been from the West African clade and not the Central African clade (9). The West African clade does not transmit well from person to person and is rarely lethal compared to the Central African clade (9). However, in the 2017 Nigerian outbreak, MPXV in the

West African clade has been observed spreading through close human contact or in the UK, through contaminated hospital bedsheets (4, 10).

When the animal care team at a Scandinavian research institution first discovered MPXV following an outbreak in monkey colonies recently imported from Singapore, they did not expect that it would be pathogenic in humans (11). That changed 12 years later in 1970 when the virus was isolated from a human patient in the Democratic Republic of Congo who was being tested for smallpox (12). While we know that MPXV has a host reservoir, we do not know what it is except that it is likely a rodent (13). Possible culprits include rope squirrels, Gambian pouch rats, African dormice, and sun squirrels which have all tested positive for MPXV or MPXV reactive antibodies after trapping in the wild (13). Since 1970, scientists have been identifying increasing MPXV cases due to several factors. After smallpox eradication, MPXV became easier to identify, and over time, fewer people had pre-existing immunity from cross-protection by the smallpox vaccine, Vaccinia virus (VACV) (14). Furthermore, more humans and animals are interacting leading to increased opportunities for infection from the host reservoir (14). It is suspected that the outbreak in Nigeria was able to occur because the flooding forced all mammals to congregate in limited high, dry ground (14). As we continue to encroach on animal territories and global warming radicalizes the weather leading to unusual migration patterns, we will likely see even more MPXV infections in humans. Fortunately, the current MPXV outbreak is a strain less pathogenic in humans, however the virus could mutate to spread more easily or become more lethal. We aim to get ahead of this threat by identifying ways that MPXV evades the host immune response and may evolve to become more human specific.

The Poxvirus Lifecycle

Poxviruses have a broad animal host range and can cause disease in humans after zoonosis (15). Depending on the virus and host, they can spread through skin contact or through aerosols (16). After infecting the host the viruses exhibit broad cellular tropism. Heparin sulfate, chondroitin sulfate, sulfatides, phosphatidylinositol, and the matrix laminin have all been

implicated in mediating poxvirus-cell binding (17–23). While no single cell receptor is responsible for poxvirus binding, a multiprotein complex on the virus facilitates binding and entry (16, 24) (Figure 1-1A). Once poxviruses enter the cell, they undergo an uncoating process (Figure 1-1B). Poxviruses undergo the first stage of uncoating by removal of the lipid envelope which occurs by fusion to either the outer cell membrane or fusion to endosomal membranes, depending on the virus entry mechanism (25).

Figure 1-1: Poxvirus lifecycle

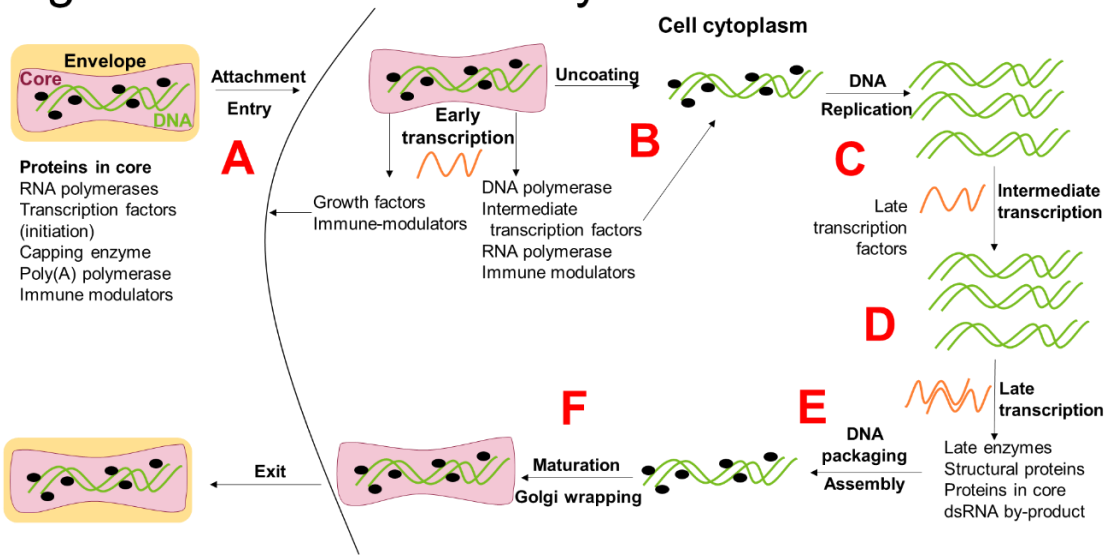

Figure 1-1 Poxvirus Lifecycle. A) Poxviruses attach to the cell without binding a single specific receptor. B) After entering the cell, the virus undergoes early transcription and DNA uncoating of its nucleoprotein complex. C) DNA replication begins, and late transcription factors are transcribed. D) Late transcription begins leading to formation of double-stranded RNA (dsRNA). E) Newly synthesized genomes are packaged and the nucleoprotein core begins assembly. F) Protein core undergoes maturation and Golgi wrapping.

Once fusion is complete, the viral cores begin the second stage of uncoating which requires viral mRNA and protein synthesis (26–29). Because poxviruses have double-stranded DNA genomes that replicate entirely in the cytoplasm, they must incorporate their own

transcriptional machinery into the virion (16). Early gene expression covers approximately one half of all Vaccinia genes and have distinct promoters (30). Poxviruses carry their own topoisomerase, DNA helicase, and a multi-subunit DNA-dependent RNA polymerase into the cell in their core (28, 29, 31).The early RNA polymerase has homology to eukaryotic RNA polymerase II (32–34). Part of their RNA polymerase complex are two enzymes responsible for cap synthesis and attachment to the mRNA (35–39). Genes encoding early transcripts contain a *cis*-acting viral termination factor to stall the RNA polymerase (40, 41). Upon terminating transcription, the poxvirus' polyadenylation polymerase completes their mRNA (42). As the early transcripts are being synthesized the genome is released from the core allowing the genome to be fully released and DNA synthesis to begin (Figure 1-1C).

DNA synthesis of poxviruses does not depend on a specific origin sequence but rather occurs in the ends of the genome in hairpin regions (43, 44). A poxvirus expressed helicase-primase begins DNA replication by synthesizing RNA primers (45). The poxvirus DNA polymerase then begins catalyzing DNA and is capable of generating branched molecules likely to be allowing for recombination events (46–48). Intermediate transcription also begins at this time (Figure 1-1D). Previously, it was thought that intermediate transcription only contained late transcription factors, but extensively controlled deep sequencing has determined that many poxvirus genes are driven by both intermediate and late promotors (30). Late VACV transcripts form the pathogen-associated molecular pattern (PAMP), double-stranded RNA (dsRNA) (49–51). Late genes do not encode the cis-acting transcription terminator signals, leading to formation of long transcripts (16). When the genes are on opposing strands of DNA, complementary mRNA are formed which hybridize and form dsRNA (30). Late transcripts are short lived in HeLa cells with half-lives of 13 minutes, compared to early transcripts with half-lives of 120 minutes (52, 53). Recent studies have demonstrated that the short half-life of late mRNAs is likely due to selective decapping of dsRNAs and degradation by the host exonuclease XrnI (54–56). Furthermore, VACV takes advantage of the decapping process to regulate selective translation of late mRNAs

(57). These data suggest that dsRNA is formed as a means of regulating poxvirus gene expression during late transcription.

Next, the newly replicated genomes and structural proteins generated during late transcription begin DNA packaging and assembly (Figure 1-1E). DNA enters crescent immature virions before they close into spheres (58, 59). The mechanism for wrapping VACV in a Golgi-derived membrane is uncertain and complicated by multiple types of virions and exit strategies (16, 60, 61). One such strategy is to use the retrograde Golgi pathway allowing VACV and MPXV to be wrapped in a double-membrane envelope allowing exocytosis (62).

Host Cell recognition of dsRNA

Double-stranded RNA (dsRNA) is a potent pathogen associated molecular pattern (PAMP) recognized by many cellular pathways (Figure 2). The IFN stimulated gene, PKR, can recognize dsRNA and dimerize, leading to autophosphorylation (Figure 1-2A) (63–65). Once PKR is phosphorylated, the protein can then go on to phosphorylate eIF2a and shut down total protein translation (63, 66, 67). Once PKR has been activated, it can also induce apoptosis or signal induction of antiviral cytokines through IRF-1 and NF-κβ (68–71), although there is conflicting data about whether the dsRNA binding and subsequent PKR catalytic activity are required for NF-κβ activation (72, 73). Additionally, PKR has been implicated in necroptosis, but not after stimulation with dsRNA (74). Finally, PKR can inhibit vaccinia virus replication if VACV has been deleted of a critical dsRNA inhibitory protein (70, 75, 76).

Another dsRNA sensing antiviral pathway is the oligoadenylate synthetase pathway (OAS) which does not have a traditional dsRNA binding domain (Figure 1-2B) (77). It binds to a sequence specific motif and induces formation of modified adenosine chains which activate RNase L to degrade mRNAs (77–81). RNase L can then degrade RNA bound to OAS (82, 83). The adenosine deaminase acting on RNA (ADAR) protein is also a dsRNA editing enzyme and edits adenosine to inosine which destabilizes dsRNA structures (Figure1- 2C) (84, 85). Treatment with IFN induces splice site changes with ADAR transcripts leading ADAR to express a 150 kDa

protein with a Z-form nucleic acid binding domain (86, 87). Furthermore, ADAR is inhibited during VACV infection (88, 89).

Figure 1-2: dsRNA sensing pathways

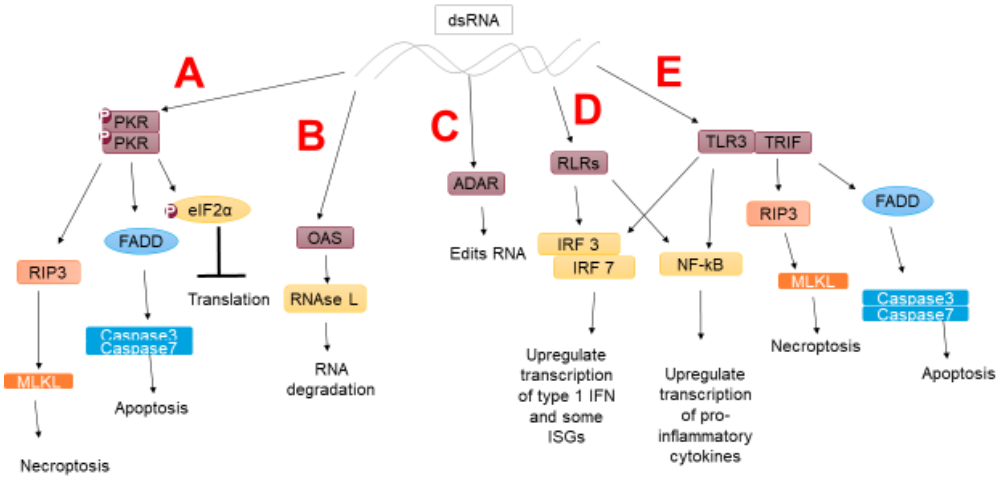

Figure 1-2 dsRNA Sensing Pathways. A) PKR senses dsRNA, dimerizes, and autophosphorylates. It can then interact with RIP3 leading to necroptosis, activate apoptosis through BCL-2, or phosphorylate the transcription initiation factor eIF2α preventing translation. B) The OAS family of proteins sense RNA and interact with RNAse L leading to RNA degradation. C) ADAR binds to dsRNA and edits the Adenosines to Inosines leading to wobble base pairing and destabilization of dsRNA binding. D) RIG-like receptors (RLRs), RIG-I and MDA5 are both capable of binding to dsRNA leading to activation of IRF3/7 and NF-kB which induce transcription of inflammatory cytokines E) TLR3 binds to dsRNA in endosomes and can lead to activation of IRF3/7, NF-kB, and apoptosis. It also has a RHIM domain and can induce necroptosis.

Rig-like receptors (RLRs) such as RIG-I and MDA5 both bind dsRNA. RIG-I binds short dsRNA, and MDA5 binds long dsRNA (Figure 1-2D) (90). In both RIG-I and MDA5, the proteins bind to dsRNA, undergo post-translational modifications, and then undergo oligimerization and a conformational change to form a tube-like structure around the dsRNA (91–94). Once the filament structure is formed, the proteins become active and can relocate to the mitochondrial protein

MAVS (95–97). MAVS then leads to activation of IRF3/7 and NF-κβ which initiate transcription for pro-inflammatory/antiviral cytokines (98–101). TLR3 recognizes dsRNA and initiates a TRIF-mediated immune response (Figure 1-2E) (102). TLR3 activation leads to IRF3 activation and upregulation of antiviral cytokines (103). Additionally TLR3 activation has been implicated in PANoptosis (pyroptosis, apoptosis, and necroptosis) which induces cell death inhibiting viral replication (80, 104, 105).

Necroptosis

Necroptosis is a highly inflammatory cell death first discovered in L929 cells treated with TNFα following VACV infection where they determined that it was not only caspase independent, but relied on active caspase inhibition (Figure 1-3) (106). Necroptosis can be initiated in many different ways, the first to be described were through TNF-R, TRAIL-R and Fas (107). When activated through ligand binding, the receptors can undergo one of three pathways. First, in the absence of RIP1, a signaling cascade is initiated to upregulate antiviral proteins in the cell. Next when RIP1 is present and caspase is uninhibited, the cell will undergo apoptosis (107–109). Finally, when caspase is inhibited or not expressed, RIP1 induces necroptosis (110, 111). RIP1 and RIP3 interact to form a complex known as the ripoptosome which can go on to activate MLKL (109, 112–115). MLKL undergoes the first step of activation when phosphorylated at a serine site (Ser345 in mouse, Ser355 in human) (116–118). Next MLKL is transported to the cell membrane where it undergoes tyrosine phosphorylation by TAM kinases and oligomerization (119–123). MLKL then manipulates phosphotidylserines to puncture a hole in the cell membrane killing the cell (124–126).

TLR 3 and TLR 4 can also initiate RIP1-independent necroptosis through interactions between TRIF and RIP3 (104, 127). PKR has been implicated in induction of necroptosis but never after activation by dsRNA (74). Finally, DAI initiates RIP1-independent necroptosis after activation with PAMPs (128–133).

Figure 1-3: Inducers of necroptosis

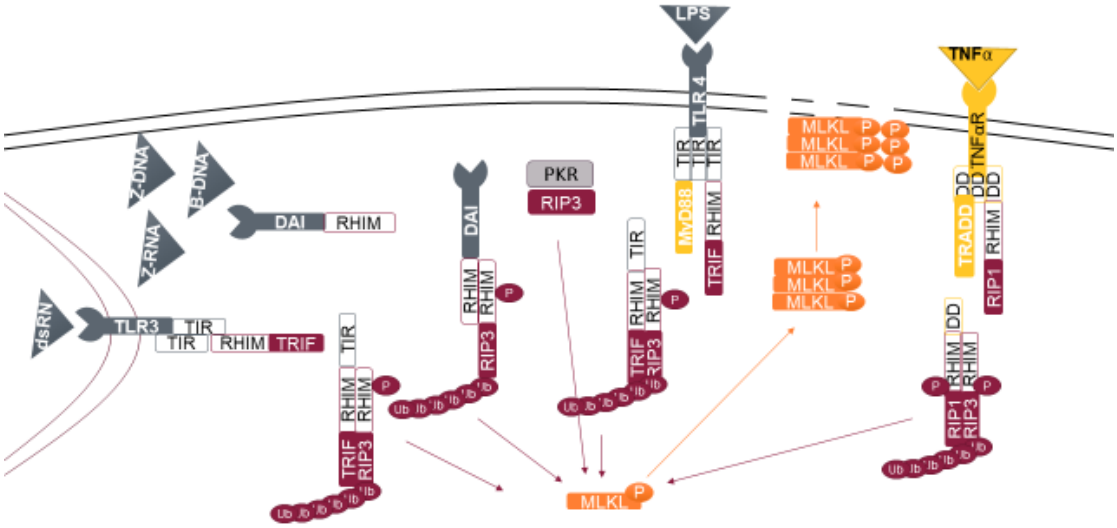

Figure 1-3 Inducers of Necroptosis. DAI can induce necroptosis through direct interactions with RIP3. TLR3 and TLR4 can induce necroptosis through TRIF interactions with RIP3. TNF can induce RIP1-RIP3 dependent necroptosis. In every case, once RIP3 has been activated, it goes on to activate MLKL through serine phosphorylation. MLKL trimerizes, relocates to the membrane and undergoes tyrosine phosphorylation. It then creates pores in the cellular membrane leading to rapid cell death.

Z-form Nucleic Acid

Normally nucleic acid helices are right-handed with dsDNA commonly found in the B-form and dsRNA commonly found in the A-form, but Z-form nucleic acid (ZNA) is a left-handed helix (134). Both dsRNA and dsDNA can convert to the Z-form (134, 135). Conversion from A- or B- to Z-form is not usually energetically favorable and was first found in instances of relieving steric hindrance in supercoiling or regions of high transcription (136–139). Formation of ZNA is somewhat sequence dependent favoring GC rich regions over AT rich regions (137, 140). There are several cellular proteins that have ZNA binding domains (ZBD) that are involved with host-pathogen sensing. ADAR has a ZBD, can bind to ZNA *in vitro*, and can interact with host

nucleic acids (87, 88, 141–143). It has not yet been elucidated why ADAR would need a ZBD when it has functioning dsRNA binding domains. However, ADAR interacts with MDA5 and MDA5 is hypothesized as a possible location for ZNA formation (144, 145).

DAI (sometimes called ZBP1) also has two ZBDs with high sequence homology to ADAR's ZBDs (146). DAI has been implicated to interact with RIP3 following viral infection (128, 131, 147, 148). In influenza virus infected cells DAI leads to viral inhibition through PANoptosis (148–152). In MCMV and HSV DAI sensing leads to necroptosis (153–155). DAI can also lead to necroptosis following systemic inflammation, but it is not clear what nucleic acid is being sensed in these cases (152, 156). VACV can also induce DAI-dependent necroptosis after infection by mutant VACV in tissue culture and in mice (130, 131, 147, 157).

The only viruses with a protein with an identified ZBD are poxviruses. The VACV protein, E3, has two domains, a C-terminal dsRNA binding domain and an N-terminal ZBD (158, 159). Both of these domains are critical for evasion of the innate immune response in cultured cells and pathogenesis in mice (160–162). The C-terminus sequesters dsRNA and interacts with PKR to fully prevent activation (163–166). Despite having a ZBD, the N-terminus of E3 was first implicated in PKR inhibition (76, 159, 163, 167). The mechanism by which E3's N-terminus sequesters dsRNA is unclear. The ZBD of E3 is highly conserved with the ZBD of ADAR and DAI and the ZBD of these proteins can be interchanged to rescue replication and pathogenesis (87, 131, 168). Deletion of the ZBD from VACV E3 leads to necroptosis through DAI recognition (130, 131, 147). Because E3 is so critical for inhibition of nucleic acid sensing in a VACV infection, it is highly conserved in most orthopoxviruses (167, 169). The only orthopox virus it is not conserved in is MPXV. The MPXV E3 homologue contains a deletion in the first methionine leading to formation of a truncated E3 protein. However, MPXV is still somehow able to subvert the restrictions of VACV E3 N-terminal deletion mutants (167).

Figure 1-4: Research overview

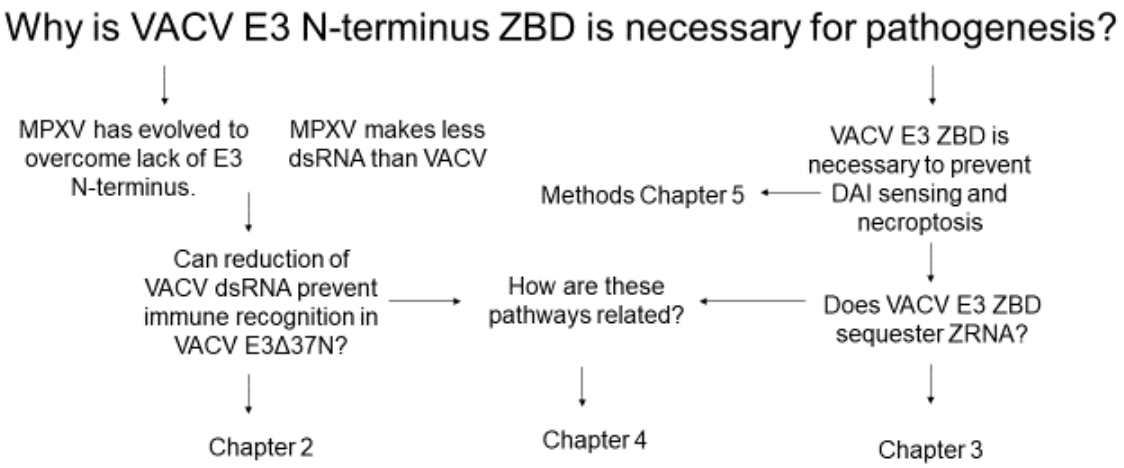

Figure 1-4 Research Overview. This demonstrates the organization of the questions being posed in this dissertation.

Research Overview

The primary goal of this dissertation is to better understand the role that VACV E3 protein's N-terminus plays in inhibiting cellular recognition of virus nucleic acids (Figure 1-4). In order to better understand this, I primarily used the VACV E3 N-terminal deletion mutant VACV E3Δ37N. Determining a mechanism of action has been complicated over time by different results depending on what cell type was used. Three model cell lines have been identified by previous members of the lab. First, MEF 129 cells selectively inhibit VACV E3Δ37N through PKR recognition of late dsRNA (Chapter 2) (76). Next, L929 cells have been demonstrated to inhibit VACV E3Δ37N exclusively through DAI induction of necroptosis (Chapter 3) (130). Finally, multi-step viral growth of JC cells correlates to intracranial pathogenesis (Chapter 4) (Figure 1-5) (170–172). Furthermore, the method of inhibition for VACV E3Δ37N intracranial and intranasal pathogenesis and spread are still not well-defined (Chapter 4).

Figure 1-5 Replication in JC cells and Intracranial LD50s are correlated.

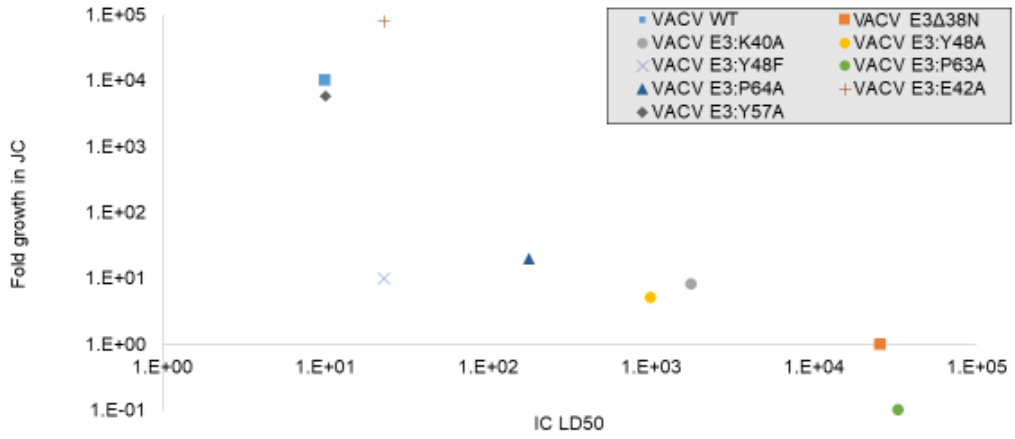

Figure 1-5 Replication in JC Cells and Intracranial LD50s are Correlated. This figure is modified from a previous student's research (172). The X-axis indicates the intracranial LD50, and the Y-axis indicates fold change in titer from 0 days post infection to 3 days post infection in JC cells. Various point mutants of E3 in the N-terminus were used.

I first decided to gain a better understanding of how VACV evades dsRNA recognition by PKR by comparing PKR activation in VACV E3Δ37N to MPXV. Previous research determined that MPXV both evades the PKR response and makes less dsRNA (167, 173). I hypothesized that low dsRNA in MPXV disallowed PKR activation despite its lack of an E3 N-terminus. In Chapter 2 of this study, I generated two low dsRNA producing mutants of VACV E3Δ37N. These mutants did not lead to PKR activation in HeLa or MEF 129 cells, which confirmed my hypothesis.

Next I wanted to elucidate the role of ZNA binding in both VACV E3 and in DAI. TheL929 cell model system which inhibits VACV E3Δ37N solely through the DAI-RIP3-MLKL necroptosis pathway was used (130). In Chapter 3, I determined that the nucleic acid recognized by DAI was structurally identifiable by a Z-NA antibody and that it was RNA. I also determined DAI recognition of VACV E3Δ37N depended solely on early mRNA transcription and not on protein synthesis or late transcription. Finally, I demonstrated that the dsRNA conversion to ZRNA after early

transcription was distinct from canonical late dsRNA formation by using low dsRNA VACV E3Δ37N mutants (131). I also developed methods for studying the necroptosis pathway in Chapter 5 (147).

Finally, I tried to determine how these two pathways interact in complex cell systems and in animal models. In Chapter 4, JC cells were used since multi-step growth correlates to intracranial infections in mice (172). In JC cells, DAI and PKR jointly inhibit VACV E3Δ37N. I determined that it took both reduction of dsRNA and inhibition of RIP3 kinase activity to restore viral replication in JC cells. Additionally, unlike L929, the low dsRNA VACV E3Δ37N viruses had partially restored cell viability demonstrating DAI alone does not drive viral inhibition. Furthermore, reduction of dsRNA in VACV E3Δ37N restored spread to spleen after intranasal infections but did not restore intracranial pathogenesis. By demonstrating that neither DAI nor PKR was solely responsible for inhibiting virus, I determined that the VACV E3 N-terminus critically inhibits host recognition of ZRNA and dsRNA.

CHAPTER 2

MONKEYPOX VIRUS EVADES PKR BY MAKING LESS DOUBLE-STRANDED RNA THAN VACCINIA VIRUS

Abstract

Poxviruses such as vaccinia virus (VACV) and monkeypox virus (MPXV) produce late RNA transcripts that extend beyond the transcribed gene and hybridize to form double-stranded RNA (dsRNA). Because the innate immune system can easily recognize dsRNA, poxviruses produce several proteins to mask dsRNA and to inhibit the downstream dsRNA signaling. One critical VACV protein E3 contains a dsRNA binding domain in its C-terminus and a domain that binds to Z-form nucleic acids in its N-terminus which must also be present for pathogenicity in murine models. Previous studies have compared a vaccinia virus with a wild-type E3 protein (VACV WT) to one with an E3 N-terminal truncation of 37 amino acids (VACV E3Δ37N), phenotypic differences appeared in several cell lines. In HeLa and MEF129 cells, dsRNA recognition pathways such as PKR become activated during VACV E3Δ37N infections but not VACV WT infections. While most orthopoxviruses have E3 homologues with highly homologous N-termini, the MPXV homologue, F3, has an N-terminal truncation of 37 amino acids. However, MPXV does not activate PKR in HeLa or MEF 129 cells. Additionally, our investigation determined that MPXV accumulates less dsRNA than VACV. We made VACV E3Δ37N more similar to MPXV by selecting mutants that produces less dsRNA. By producing less dsRNA, VACV E3Δ37N no longer activated PKR in HeLa or MEF 129 cells restoring the wild-type phenotype. This suggests that MPXV evolved to produce less dsRNA to circumvent loss of the E3 N-terminus.

Introduction

Monkeypox virus (MPXV) is an emerging infectious orthopox virus that can cause lethality in humans with an unknown host reservoir (174). Due to recent outbreaks, studying how it can be pathogenic in humans is becoming increasingly important (10, 175, 176). While MPXV infections can be lethal in humans, Vaccinia virus (VACV), the vaccine used to eradicate smallpox, replicates in humans but is rarely lethal (174, 177). Both poxviruses have large dsDNA genomes and replicate entirely in the cytoplasm. They produce double-stranded RNA (dsRNA) as a by-product at late times post infection. However, MPXV synthesizes less dsRNA than VACV throughout the course of infection (173). dsRNA is a highly immunogenic nucleic acid because it is not commonly found in eukaryotic cells. In order to prevent recognition of dsRNA by host innate immune proteins, VACV makes a protein called E3 (162, 178). VACV E3 has a dsRNA binding domain in its C-terminus and a Z-form nucleic acid binding domain in its N-terminus (159). The MPXV homologue of VACV E3, F3, has a mutation in its start codon leading it to produce a protein without the first 37 amino acids of E3 (167, 179).

Previous research demonstrates that without the E3 protein, dsRNA can be detected by protein kinase R (PKR) in host cells, leading to loss of replication (76, 159, 162, 178). PKR is inducible in cells by type 1 interferon (IFN) and recognizes dsRNA through a dsRNA binding domain (180, 181). Upon binding dsRNA, PKR dimerizes and autophosphorylates causing it to become activated (182). Once PKR is activated, it phosphorylates the eukaryotic initiation factor 2 α (eIF2α) preventing recruitment of the large ribosome to the translation complex and halting cellular translation (183, 184). We hypothesize that MPXV evades detection by PKR by making less dsRNA than VACV and test this using low dsRNA producing VACV E3 N-terminal deletion mutants.

Materials and Methods

Cells. BSC 40 cells were maintained in Dulbecco's Modified-Minimal Essential Medium (DMEM, Cellgro) supplemented with 5% FBS. MEFs (129/SV background) were generated from embryos as previously described (76) and were maintained in DMEM supplemented with 10% heat-inactivated FBS (HI FBS). FBS was heat-inactivated by incubation at 56°C for 30 minutes. PKR-/- MEFs (129/SV background) were generously provided by Lynda Morrison (185) from Saint Louis University and were maintained in DMEM with 10% FBS. HeLa F2 cells were a kind gift from George Pavlakis, NCI and were maintained in DMEM 5% FBS. Infections were carried out in HeLas using DMEM, 5% FBS, 2 mM L-glutamine, and NEAA.

Small molecules. For IFN treatment, cells were pre-treated with 1000 units of recombinant mouse α-interferon at 37°C for 18 hours. Isatin β-thiosemicarbazone (IBT) was used to increase dsRNA made by VACV and select for low dsRNA producing mutants. IBT was resuspended in acetone at 22.7015 mM before neutralizing the pH by diluting the IBT/acetone in 2N NaOH 20% (v/v) to produce a stock solution with a concentration of 4.5 mM IBT. Treatments of HeLa with IBT were done by adding media supplemented with 60 μM IBT at 30 minutes post infection.

Viruses. The vaccinia virus Western Reserve strain (VACV) was used throughout this study with the unmodified virus designated VACV WT. VACV deleted of E3 (VACV ΔE3) or containing a 37 amino acid N-terminal truncation of E3 (VACV E3Δ37N) were generated as previously described (162). VACV with a wild-type E3 and mutation in the A24R gene confirmed to give low dsRNA (VACV mutA24-1) were a generous gift from Richard Condit's lab (186, 187). Monkeypox virus strain WRAIR 76-1 (MPXV) of the West African clade was used in this study. VACV E3Δ37N with reduced dsRNA were generated by treating VACV E3Δ37N virus infected BSC 40s with 60 μM IBT for 48 hours while plaques formed. Individual plaques were picked from the monolayer, and virus from each plaque was titered in the presence and absence of 60 μM IBT. Viruses confirmed to have reduced dsRNA were designated VACV E3Δ37N IBTR3 and VACV E3Δ37N IBTR7. Co-infections between MPXV and VACV E3Δ37N were performed under biosafety level 3 (BSL-3) conditions all other infections were conducted in a dedicated BSL-2 virus lab in accordance with protocols approved by Arizona State University.

Growth kinetics. Cells were seeded in 12 well plates to be 80% confluent at the time of infection. For multi-step kinetics, cells were infected with an MOI of 0.01 of the indicated virus for 1 hour then washed 3 times with warm media before the overlay with growth medium. Infected cells were incubated under normal growth conditions until they were harvested by scraping into media at the indicated times. After subjecting samples to three freeze-thaw cycles, the titers of VACV, the VACV recombinants, and MPXV were determined by plaquing in the permissive cell line, BSC 40. Single-step kinetics were done using the same protocol except that an MOI of 5 was used.

Co-infections. HeLa cells were infected with virus at a total MOI of 10 with VACV WT, MPXV, VACV E3Δ37N, VACV E3Δ37N IBTR3, and VACV E3Δ37N IBTR7. Cells were also co-infected by combining MPXV (MOI 5) with VACV E3Δ37N (MOI 5), VACV E3Δ37N IBTR3 (MOI 5), or VACV E3Δ37N IBTR7 (MOI5) for a total MOI of 10 (5 MPXV + 5 VACV).

RNA isolation. RNA was isolated from mock or infected cells as indicated 9 hours post infection. Cells were harvested by scraping into ice cold PBS and centrifugation prior to lysis. Cells were lysed in RNase-free conditions on ice for 5 minutes in 175 µL of Qiagen buffer RLN (50 mM Tris-Cl pH 8.0, 140 mM NaCl, 1.5 mM $MgCl_2$, 0.5% (v/v) Nonidet P-40, 1 mM DTT) before centrifugation to remove cellular debris. RNA was subsequently purified from lysates using Qiagen's Rneasy Mini Kit according to the manufacturer's protocol.

RT-PCR Methods cDNA was generated from 500 ng total RNA using PrimeScript RT reagent kit (Takara). Samples were amplified using PrimeTime Gene Expression Master Mix (IDT) on a CFX Connect Real-Time PCR detection system (BioRad). Primer sets for MPXV and VACV genes were previously described (167, 173).

Statistics. Error bars displayed indicated standard error. Statistical significance was calculated in Excel using a two tailed, unpaired, student's T test. P values are as reported in figures.

Results

Generation of VACV E3Δ37N producing low dsRNA. In order to determine if MPXV evades PKR activation by making less dsRNA, we made a more MPXV-like VACV E3Δ37N by generating

low dsRNA producing mutants. VACV E3Δ37N plaques were picked from the 60 μM IBT treated BSC40s, and virus from each plaque was titered in the presence and absence of 60 μM IBT. Ten IBT plaques with high yields were chosen for further analysis (Figure 1A). Because selective pressure by IBT is not high enough to eliminate all non-mutant plaques, IBT sensitivity curves were conducted to confirm resistance (Figure S1). VACV WT, VACV mutA24R, VACV E3Δ37N, and MPXV VACV IBT sensitivity curves were also measured for comparative analysis. mutA24R is a previously characterized low dsRNA producing VACV with a WT E3 and nonsense mutation in the VACV RNA polymerase subunit gene A24R (186). Two viruses, plaques 3 and 7 (VACV E3Δ37N IBTR3 and VACV E3Δ37N IBTR7 respectively) were selected for further analysis. Plaque 3 was selected due to its similarity to the control VACV mutA24R. Plaque 7 was selected because it was resistant to IBT at low concentrations (<60 μM) and sensitive to IBT at high concentrations (60 and 120 μM). The IBT curves of these plaques are demonstrated in Figure 1B.

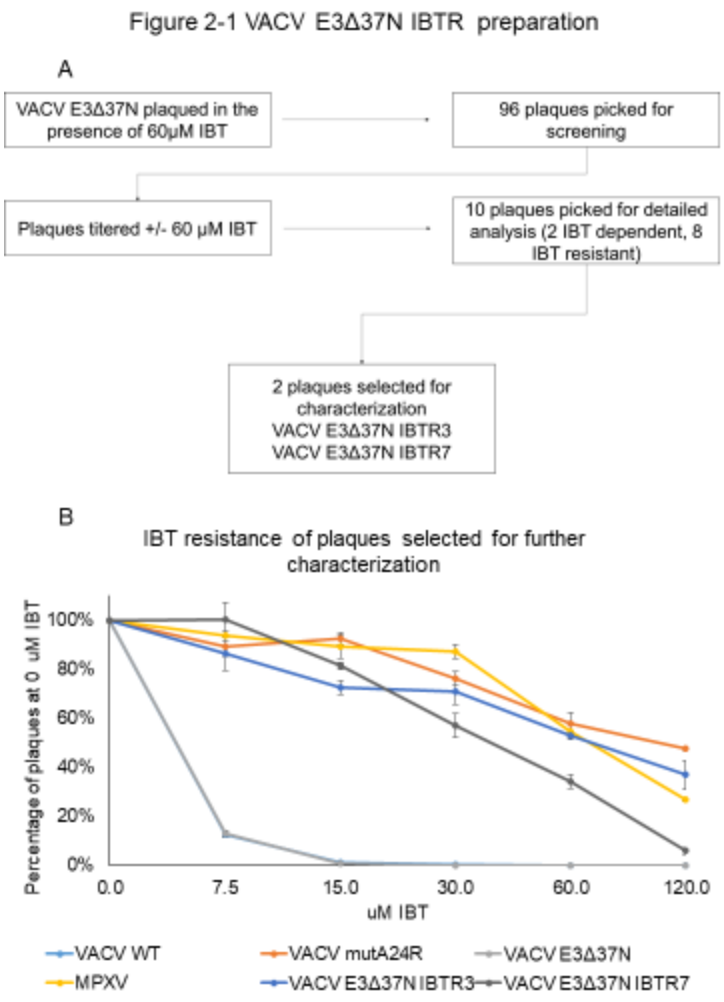

Figure 2-1: Generation and Selection of VACV E3Δ37N Producing Low dsRNA. VACV E3Δ37N virus infected BSC 40s at an MOI of 0.01. They were treated with 60 μM IBT for 48 hours while plaques formed. Plaques were then overlaid with 1.5% agarose gel in a Tris-Cl buffer and incubated at 37°C for 4 more hours. Individual plaques were picked from the monolayer and stored in Tris-Cl pH 10. After 3 freeze thaws, virus from each plaque was titered in the presence and absence of 60 μM IBT. Two plaques that only grew under 60 μM IBT selection were set aside (data not shown) and eight plaques with high yields in the presence and absence of 60 μM IBT were chosen for further analysis (A). 6 wells of BSC40 monolayers of 6 well dishes were infected with 100 pfu of VACV WT, VACV mutA24, VACV E3Δ37N, MPXV, or VACV E3Δ37N plaques 3 and 7 picked in the presence of IBT. At 30 minutes post infection, cell media with either 0, 7.5, 15, 30, 60, or 120 μM IBT was added. Two days later, cells were stained with crystal violet and plaques were counted. The experiment was conducted in triplicate, and results were graphed (B). Error bars represent standard error.

VACV E3Δ37N IBTR mutants produce less dsRNA than VACV E3Δ37N. To confirm that these mutants were IBT resistant due to low dsRNA rather than reduced interaction with IBT, we first

measured dsRNA in infected cells by slot blot (Figure 2-2A). VACV WT and VACV E3 Δ37N had similar levels of dsRNA with and without IBT treatment. VACV E3Δ37N IBTR3 and VACV E3Δ37N IBTR7 had 2 fold less detectable dsRNA than VACV E3Δ37N (Figure 2-2B). While VACV WT and VACV E3Δ37N both had an increase of one fold or more dsRNA after treatment with 60 µM IBT, VACV mutA24R, VACV E3Δ37N IBTR3, and VACV E3Δ37N IBTR7 all had less than half a fold increase in detectable dsRNA with IBT treatment compared to mock treated. This demonstrated that there was less total dsRNA in the infected IBTR mutants.

In addition to looking at reduction of total dsRNA, we wanted to determine how much dsRNA was not bound to E3 or was “free dsRNA”. To measure free dsRNA, we fixed cells with formaldehyde which fixes protein-nucleic acid interactions. Figure S1A demonstrates mock, VACV WT, and VACV ΔE3 infected cells fixed with formaldehyde at 6 hours post infection and stained for dsRNA by flow cytometry. Figure S1B demonstrates a dot blot of cells infected with mock, VACV WT, and VACV ΔE3 and harvested at the same time without fixation. These are quantified and compared in Figure S1C where there is no statistical difference between VACV WT and VACV ΔE3 in the dot blot. However by flow cytometry there are 50% dsRNA positive cells in the VACV ΔE3 infection and less than 2% in the VACV WT infected cells. This demonstrates that we can use flow cytometry to measure free dsRNA.

We measured free dsRNA for our VACV E3Δ37N IBTR mutants in HeLa cells infected with VACV WT, VACV ΔE3, VACV mutA24R, VACV E3Δ37N, VACV E3Δ37N IBTR3, VACV E3Δ37N IBTR7, and MPXV (Figure 2-2C). There was more free dsRNA in cells infected with VACV E3Δ37N (25% positive) than VACV WT (5% positive) and infected cells treated with IBT made more dsRNA as previously reported (173). Treatment of cells with 60 µM IBT led to a 10 fold increase in detectable free dsRNA in VACV WT infected cells but not in VACV mutA24R. MPXV, VACV E3Δ37N IBR3, and VACV E3Δ37N IBTR7 infected cells did not have high rates of dsRNA staining in either the mock or IBT treated cells. In cells without IBT treatment, the levels of free dsRNA in VACV WT, MPXV, VACV mutA24R, VACV E3Δ37N IBTR7 are statically different

than VACV E3Δ37N. This indicates that reducing the total dsRNA during an infection can allow the truncated E3 protein to fully inhibit what little dsRNA remains.

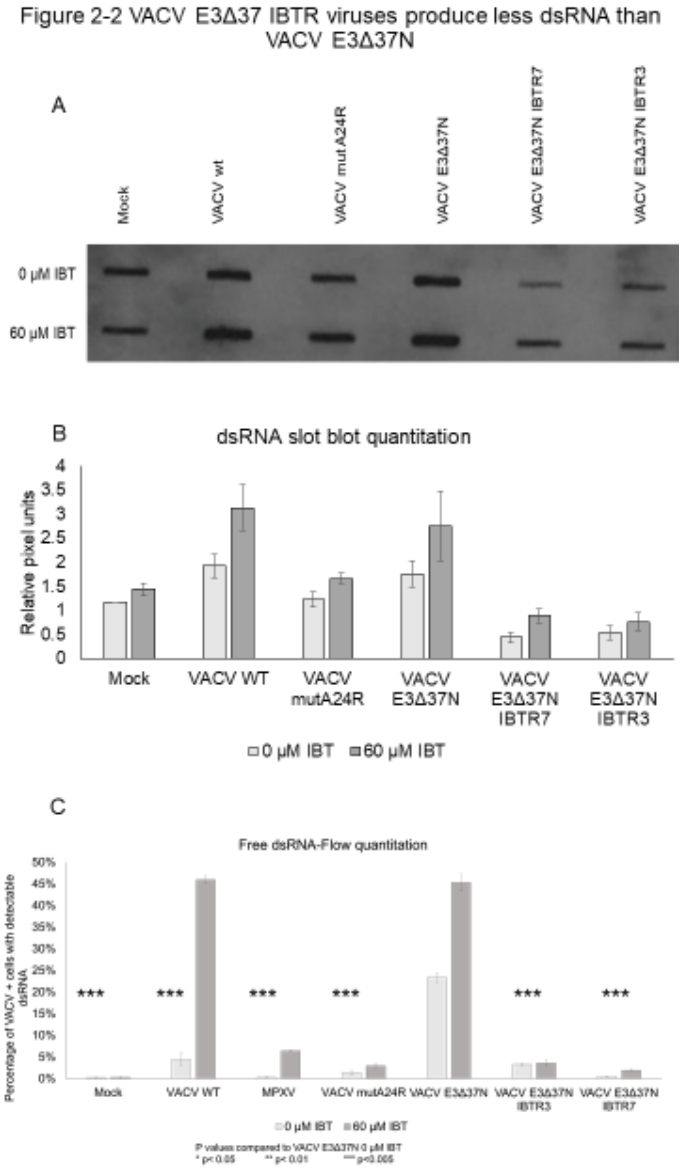

Figure 2-2: VACV E3Δ37 IBTR Viruses Produce Less dsRNA than VACV E3Δ37N

HeLa cells were infected at an MOI of 5 for 9 hours with mock, VACV WT, VACV mut A24, VACV E3Δ37N, VACV E3Δ37N IBTR3, and VACV E3Δ37N IBTR7. RNA was harvested from infected cells. RNA was hybridized to a Nitran membrane using a slot blot apparatus and probed for dsRNA using an antibody in triplicate (A). Bands were quantified using ImageJ and plotted (B). HeLa cells were infected at an MOI of 5 for 9 hours with mock, VACV WT, VACV mut A24, VACV E3Δ37N, VACV E3Δ37N IBTR3, VACV E3Δ37N IBTR7, and MPXV and treated with 0 or 60 μM IBT. Cells were fixed at 9 hours post infection with BD Cytofix/Cytoperm™ and stained overnight with a rabbit polyclonal antibody against VACV and the mouse monoclonal J2 antibody against dsRNA structure. Cells were stained with secondary fluorescent antibody and analyzed by flow cytometry. VACV + cells were gated and the percent of those cells positive for dsRNA was plotted on a bar graph (C). The experiment was conducted in biological triplicates.

Error bars for these experiments represent standard error. Statistical significance was calculated using a student's 2 tailed, unpaired T test. P values are as indicated.

Reduction of dsRNA is necessary and sufficient to evade PKR activation. In order to determine if the reduction of dsRNA was sufficient to elude PKR detection, we evaluated cells infected with VACV E3Δ37N IBTR mutants for activated PKR. MEF 129 cells from WT or PKR -/- mice were pre-treated with IFNα to stimulate PKR production and infected with VACV WT, VACV ΔE3, VACV E3Δ37N, VACV E3Δ37N IBTR3, VACV E3Δ37N IBTR7, and MPXV and harvested at either 6 or 9 hours post infection (HPI) as indicated in Figure 2-3A. Because mouse PKR-P antibodies are not commercially available and activated PKR phosphorylates eIF2α to inhibit translation, we probed for eIF2α-P in cells harvested from WT or PKR -/- mice. At 6 hours post infection, VACV ΔE3 and VACV E3Δ37N had low levels of eIF2α-P. At 9 hours post infection, only VACV ΔE3 and VACV E3Δ37N had robust eIF2α-P. VACV E3Δ37N IBTR3, VACV E3Δ37N IBTR7, and MPXV did not lead to eIF2α-P. There was no eIF2α-P detected for any viral infection in the PKR -/- cells indicating that PKR is solely responsible for phosphorylation of eIF2α. These results indicate that reduction in dsRNA and elimination of free dsRNA can inhibit PKR recognition during VACV E3Δ37N infection.

We confirmed the MEF 129 results in HeLa cells infected with VACV WT, VACV ΔE3, VACV E3Δ37N, VACV E3Δ37N IBTR3, VACV E3Δ37N IBTR7, and MPXV at 6 or 9 hours post infection (Figure 2-3B). Only VACV ΔE3 starts to phosphorylate PKR at 6hpi. At 9hpi, VACV ΔE3 and VACV E3Δ37N leads to robust phosphorylation of PKR and some eIF2α phosphorylation. MPXV and VACV E3Δ37N IBTR3 do not have any detectable PKR-P, but VACV E3Δ37N IBTR7 has low levels of PKR-P. This demonstrates that reduction of dsRNA and subsequent elimination of free dsRNA also excludes detection of virus by HeLa PKR.

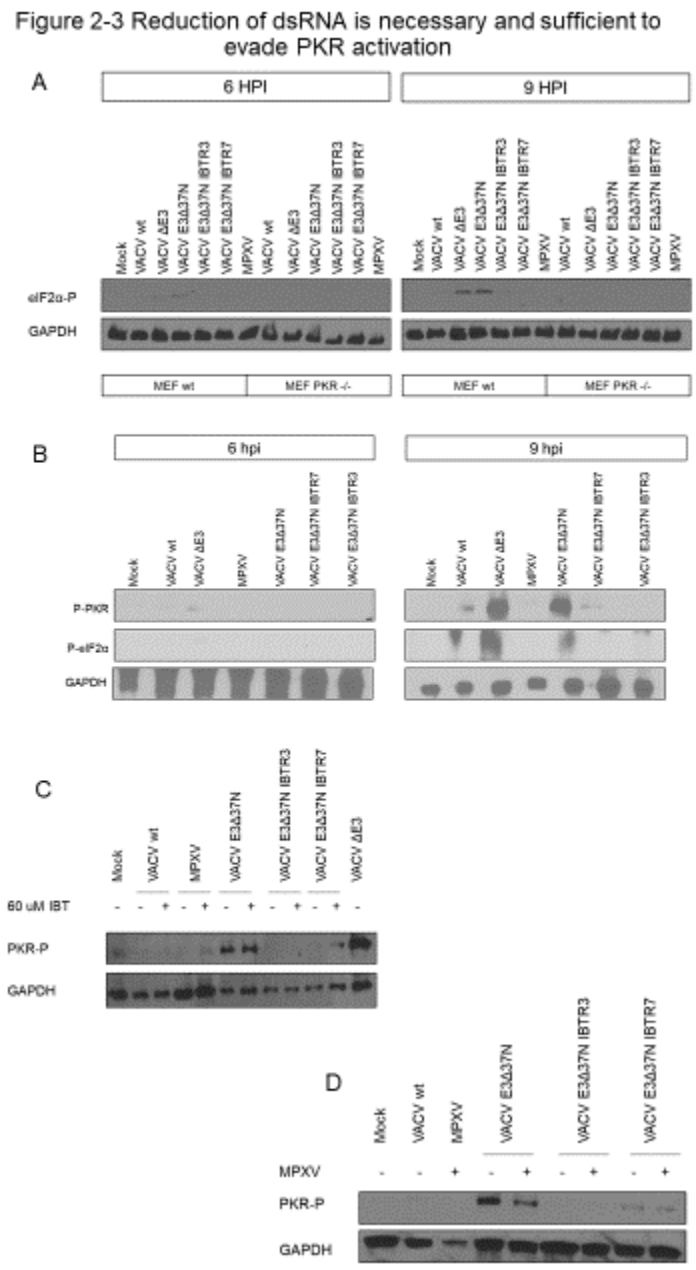

Figure 2-3: Reduction of dsRNA is Necessary and Sufficient to Evade PKR Activation

(A) MEF 129 cells from WT or PKR -/- mice were pre-treated for 18 hours with 1000 U IFNα. Cells were infected with VACV WT, VACV ΔE3, VACV E3Δ37N, VACV E3Δ37N IBTR3, VACV E3Δ37N IBTR7 and MPXV at an MOI 10 and harvested at either 6 or 9 hours post infection (HPI) as indicated. Lysates were harvested and analyzed on a Western blot probed for phosphorylated eIF2α (P-eIF2α) and GAPDH. (B) HeLa cells were infected at an MOI 5 with VACV WT, VACV ΔE3, VACV E3Δ37N, VACV E3Δ37N IBTR3, VACV E3Δ37N IBTR7 and MPXV and lysates were harvested at 6 or 9 hours post infection. Lysates were run on a western blot and probed for phosphorylated PKR (p-PKR), p-eIF2α, and GAPDH. (C) HeLa cells were treated with either 0 or 60 μM IBT and infected with VACV WT, VACV ΔE3, VACV E3Δ37N, VACV E3Δ37N IBTR3, VACV E3Δ37N IBTR7 and MPXV. Lysates were harvested at 9 hours, run on a Western blot and probed for P-PKR. (D) HeLa cells were infected with virus at a total MOI of 10 with VACV WT, MPXV, VACV E3Δ37N, VACV E3Δ37N IBTR3, and VACV E3Δ37N IBTR7. Cells were also co-infected by

combining MPXV (MOI 5) with VACV E3Δ37N (MOI 5), VACV E3Δ37N IBTR3 (MOI 5), or VACV E3Δ37N IBTR7 (MOI5) for a total MOI of 10.

In order to see if treatment with 60 µM of IBT could sufficiently increase dsRNA to overcome E3 in low dsRNA producing mutants, HeLa cells were treated with either 0 or 60 µM IBT and infected with VACV WT, VACV ΔE3, VACV E3Δ37N, VACV E3Δ37N IBTR3, VACV E3Δ37N IBTR7 and MPXV. In VACV E3Δ37N, PKR detects infection with or without IBT treatment. MPXV and VACV E3Δ37N IBTR3 fully inhibit PKR with or without IBT treatment. In VACV E3Δ37N IBTR7, PKR-P is faintly detectable indicating that increasing its dsRNA levels may be enough to overwhelm E3 (Figure 2-3C).

Finally in order to determine if MPXV compensates solely by producing low dsRNA or also has a redundant mechanism for inhibition of PKR during infection, we co-infected to see if MPXV could protect against PKR-P (Figure 2-3D). In single-virus infected cells, PKR was phosphorylated in VACV E3Δ37N and more faintly in VACV E3Δ37N IBTR7; no PKR-P was detected in VACV WT, MPXV, or VACV E3Δ37N IBTR3 infected cells. In MPXV:VACV E3Δ37N co-infected cells, there appears to be slightly less PKR-P than in VACV E3Δ37N alone. However in MPXV: VACV E3Δ37N IBTR7 cells, there is no reduction in PKR-P. This indicates a stoichiometric relationship between dsRNA and the E3 protein.

Reduction of dsRNA permits VACV E3Δ37N to grow in IFN treated MEF 129 cells. PKR solely restricts VACV E3Δ37N growth in IFN treated MEF 129, so we hypothesized that reduction of dsRNA would restore growth after IFN treatment (76). Previous research demonstrated that VACV E3Δ83N was restricted by type 1 IFN and recovered by PKR-/-, so we wanted to confirm that VACV E3Δ37N behaved similarly (76). MEF 129 cells from WT or PKR -/- mice were pre-treated IFNα and infected with VACV WT and VACV E3Δ37N virus for single-step growth curves (Figure 2-4A). While VACV WT grows 100-fold under all conditions, VACV E3Δ37N does not

grow in MEF 129 WT cells following IFN treatment. However, in the MEF129 PKR -/- cells, VACV E3Δ37N replicates in the presence and absence of IFN.

In order to determine if reduction of dsRNA could restore VACV E3Δ37N growth in IFN treated MEF 129 cells, WT cells were pretreated IFNα and infected with VACV WT, VACV ΔE3, VACV E3Δ37N, VACV E3Δ37N IBTR3, VACV E3Δ37N IBTR7, and MPXV viruses at an MOI of 10 (Figure 2-4B). Virus was harvested at 0 or 1 day post infection, titered in BSC 40. While VACV WT and MPXV grew between 10-100 fold under all conditions, VACV E3Δ37N was restricted in IFN treated cells with less virus harvested than in the input. Both VACV E3Δ37N IBTR3 and VACV E3Δ37N IBTR7 grew between 10-100 fold in IFN treated cells similar to VACV WT and MPXV growth in this cell line. This data demonstrates that reduction of dsRNA can overcome PKR-restriction of growth.

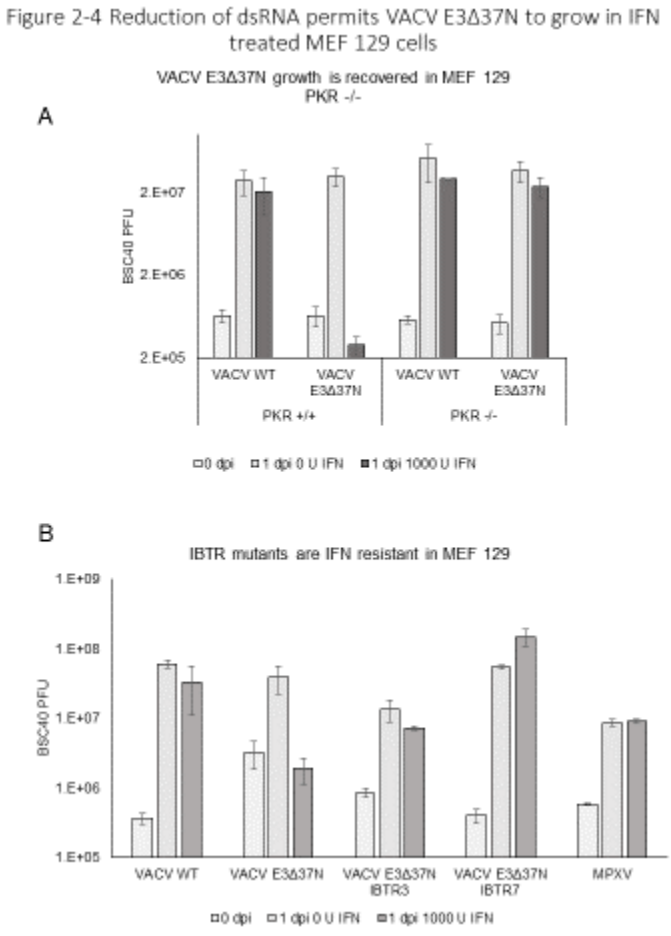

Figure 2-4: Reduction of dsRNA Permits VACV E3Δ37N to Grow in IFN Treated MEF 129 Cells

(A) MEF 129 cells from WT or PKR -/- mice were pre-treated with 0 or 1000 U IFNα. VACV WT and VACV E3Δ37N virus infected cells at an MOI of 10. Virus was harvested at 1 hour post infection (0 days) or 1 day post infection. Recovered virus was titered in BSC 40 and graphed. (B) MEF 129 WT cells were pretreated with 0 or 1000 U IFN α and infected with VACV WT, VACV ΔE3, VACV E3Δ37N, VACV E3Δ37N IBTR3,

VACV E3Δ37N IBTR7, and MPXV viruses at an MOI of 10. Virus was harvested at 0 or 1 day post infection, titered in BSC 40 and graphed. Error bars represent standard error.

Discussion

Previous research has demonstrated that PKR is activated in VACV E3 N-terminal truncation mutants in multiple cell lines and that this is sufficient to restrict virus growth in stabilized MEFs derived from 129S/v mice (76, 159). Further research demonstrated that despite having a truncated E3 homologue, MPXV evades detection by PKR (167). Additionally, MPXV also produces less dsRNA than VACV and VACV mutants for IBT resistance lead to low dsRNA (173, 186, 188). We built on these studies to demonstrate that MPXV evades PKR detection by producing less dsRNA than VACV.

First we were able to produce VACV E3Δ37N with lower dsRNA content by using methods previously described (Figure 2-1) (186). We demonstrated that these viruses produced lower total dsRNA and were less responsive to IBT (Figure 2-2 A-B). Additionally we determined that they produced less free dsRNA by flow cytometry (Figure 2-2C). The reduced dsRNA mutants of these viruses produced dsRNA levels comparable to MPXV infection. We anticipated that after addition of IBT, the VACV E3Δ37N IBTR mutants would be similar to VACV E3Δ37N, but they were still comparable to VACV WT. This might also be the reason we did not see PKR phosphorylation after treatment of IBT in Figure 2-3C. It was unexpected that VACV WT treated with µM IBT did not lead to PKR phosphorylation. Future experiments could expand the IBT concentrations used and test for free dsRNA and PKR-P with 90 and 120 µM IBT. Based on the IBT inhibition curve in BSC 40 (Figure 2-1B), we would expect to see some PKR phosphorylation at 90-120 µM IBT.

The eIF2α-P blot in MEF 129 and the PKR-P and eIF2α-P blot in HeLa results confirmed our hypothesis that reduction of dsRNA would prevent PKR from recognizing the infection (Figure 2-3 A-B). Because redundancies in inhibitory pathways are common in poxviruses, we wanted to see if MPXV made any other PKR inhibiting proteins. In order to test this, we co-infected VACV

E3Δ37N with MPXV, and found a small reduction in PKR phosphorylation. However, the co-infection with VACV E3Δ37 IBTR7 virus found no reduction in PKR phosphorylation. This argues that the most likely reason for the reduction in PKR phosphorylation in the MPXV: VACV E3Δ37N co-infection is mixing a high dsRNA producing virus with a low dsRNA producing virus and therefore reducing the ratio of E3 to dsRNA. If there was a second protein inhibiting PKR-P, we should have seen complete protection in the MPXV: VACV E3Δ37N IBTR7 co-infection where two low dsRNA viruses are together. Future experiments to confirm this could include co-infections with VACV WT and VACV E3Δ37N mutants to demonstrate that VACV WT can protect against PKR-P. Additionally, co-infections between VACV E3Δ37N and VACV E3Δ37N IBTR viruses to confirm that combining high dsRNA and low dsRNA VACV will result in reduction of PKR-P.

Finally, we wanted to show that PKR activation can lead to negative consequences for the virus necessitating it to evolve around its E3 N-terminal truncation. We confirmed earlier reports that MEF129 restricts VACV E3Δ83N infection solely through PKR and expanded on it to demonstrate that VACV E3Δ37N is similarly restricted (Figure 2-4A). We also demonstrated that producing less dsRNA allows VACV E3Δ37N to replicate in the presence of IFN (B). This demonstrates that in systems where PKR is the only restrictor of VACV E3Δ37N can evolve to produce less dsRNA to continue replication (Figure 2-5). This is especially important for design of attenuated viral vectors. Many poxvirus genes can mutate to become IBT resistant (186). This suggests that the virus could mutate quite easily to evade PKR.

Figure 2-5 MPXV prevents PKR activation by making less dsRNA

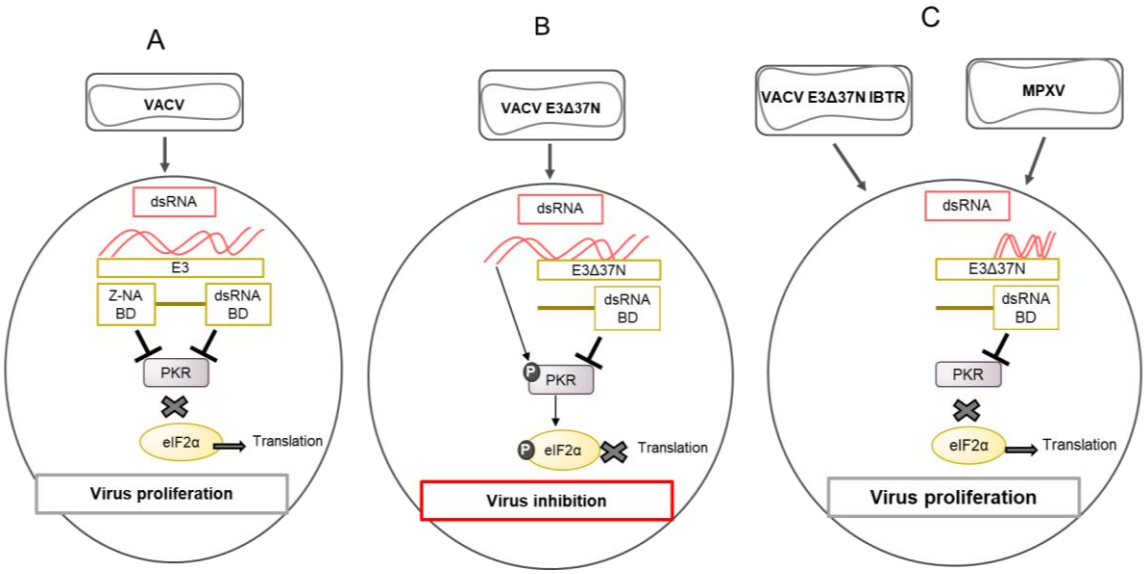

Figure 2-5: MPXV prevents PKR activation by making less dsRNA

In a normal VACV WT infection, dsRNA is generated at late times (A). VACV E3 then sequesters the viral dsRNA preventing recognition by PKR and allowing virus proliferation. However when the VACV E3 protein is truncated in the N-terminus, dsRNA builds up in the cells and eventually overtakes E3's ability to sequester it and activates PKR (B). This leads to total translation shut down and viral inhibition. In MPXV less dsRNA is produced leading to a manageable amount for the truncated E3 homologue (C). This prevents PKR activation and allows viral replication to proceed. This process can be replicated in VACV E3Δ37N by reducing total dsRNA through IBT selection.

CHAPTER 3

VACCINIA VIRUS E3 PREVENTS SENSING OF Z-RNA TO BLOCK 1 ZBP1-DEPENDENT NECROPTOSIS

Edited from the following publication:

Heather S. Koehler, Samantha Cotsmire, Ting Zhang, Siddharth Balachandran, Jason W. Upton, Jeffrey Langland, Daniel Kalman, Bertram L. Jacobs, Edward S Mocarski. Cell Host & Microbe, Volume 29, Issue 8, 2021, Pages 1266-1276.e5, ISSN 1931-3128, https://doi.org/10.1016/j.chom.2021.05.009.

Abstract

Necroptosis mediated by Z-nucleic acid binding protein (ZBP)1 (also called DAI or DLM1) contributes to innate host defense against viruses by triggering cell death to eliminate infected cells. During infection, vaccinia virus (VACV) protein E3 prevents death signaling by competing for Z-form RNA through an N-terminal Zα domain. In the absence of this E3 domain, Z-form RNA accumulates during the early phase of VACV infection, triggering ZBP1 to recruit receptor interacting protein kinase (RIPK)3 and execute necroptosis. The C-terminal E3 double strand RNA binding domain must be retained to observe accumulation of Z-form RNA and induction of necroptosis.

Substitutions of Zα from either ZBP1 or the RNA editing enzyme double-stranded RNA adenosine deaminase (ADAR)1 yields fully functional E3 capable of suppressing virus induced necroptosis. Overall, our evidence reveals the importance of Z-form RNA generated during VACV infection as a pathogen-associated molecular pattern (PAMP) unleashing ZBP1/RIPK3/MLKL-dependent necroptosis unless suppressed by viral E3.

Introduction

Necroptosis is an important host defense mechanism against viruses (Guo et al., 2018; Kaiser et al., 2013; Koehler et al., 2017; Mocarski et al., 2015; Nogusa et al., 2016; Shubina et al., 2020; Upton and Chan, 2014; Upton et al., 2010, 2012) that is mediated by receptor

interacting protein (RIP) kinase (RIPK)3 and mixed-lineage kinase-domain-like (MLKL), a pseudokinase that drives plasma membrane leakage (Sun et al., 2012). RIPK3 contains an Nterminal kinase domain and a C-terminal RIP homotypic interaction motif (RHIM). To trigger necroptosis, RIPK3 must first be recruited through RHIM-dependent interactions with RIPK1, TIR-domain-containing adapter-inducing interferon (IFN)β (TRIF) or Z-nucleic acid (NA) binding protein 1 (ZBP1). TNF-induced, RIPK1/RIPK3-dependent necroptosis (Cho et al., 2009) and virus-induced ZBP1/RIPK3-dependent necroptosis (Koehler et al 2017) act in concert against VACV as this virus replicates in the cytoplasm of infected cells.

The ZBP1/RIPK3 pathway of necroptosis kills cells during infection with E3 N-terminal deletion mutant VACV, E3Δ83N (Koehler et al 2017). This mutant completely lacks a Zα motifcontaining domain known to bind left-handed Z-form double-stranded (ds)NA (Z-NA) (Kim et al., 2004) but retains a C-terminal dsRNA binding domain (dsRBD) known to interact with conventional right-handed A-form dsRNA (Figure 1). The dsRBD is best known for preventing protein kinase R (PKR) activation (Chang et al., 1992). E3 must retain the ability to contact ZNA to preserve virulence and immunomodulation of inferferon signaling (Brandt et al., 2005; Kim et al., 2003; White and Jacobs, 2012). Notably, alanine substitutions replacing conserved amino acids, either P63 (E3P63A) or Y48 (E3Y48A) yield attenuated viruses that replicate poorly in mice similar to viruses with complete deletion of the N-terminal Zα motif-containing region. Given LD50 of Zα mutants are multiple orders of magnitude higher than wt VACV, E3 Z-NA binding contribution to VACV pathogenesis has been attributed to suppression of virus-induced necroptosis (Koehler et al 2017). The precise mechanisms through which E3 Zα promotes replication and Zα-deficient VACV triggers ZBP1-dependent necroptosis have not been explored.

ZBP1 has long been recognized as an interferon-inducible protein (called DLM-1) later implicated as a DNA-dependent activator of IFN regulatory factors (DAI) (Takaoka et al., 2007) as well as an inducer of NFκB-dependent transcription through RHIM interactions with RIPK1 and RIPK3 (Kaiser et al., 2008). Although ZBP1 contributes to IFN induction during infection with herpes simplex virus (HSV)1 (Pham et al., 2013) and human cytomegalovirus (HCMV) (DeFilippis

et al., 2010), this specialized pathogen sensor is best known for triggering virus induced death pathways (Mocarski et al., 2015; Upton and Chan, 2014). The characterization of murine cytomegalovirus (MCMV) mutants lacking the viral inhibitor of RIP activation (vIRA) brought to light RHIM signaling suppression to prevent recruitment and activation of RIPK3 during infection (Upton et al., 2010, 2012). In this setting, the viral inhibitor of caspase-8 activation (vICA) sensitizes cells to necroptosis (Kaiser et al., 2011; Mocarski et al., 2011) depending on the cell type that is infected (Daley-Bauer et al., 2017). HSV1 relies on a homologous RHIM suppressor to prevent activation of ZBP1 by newly synthesized RNA in human cells (Guo et al., 2018). During infection with viruses such as influenza A virus (IAV) that fail to suppress caspase-8, ZBP1 senses RNA and triggers combined apoptotic and necroptotic cell death pathways (Kuriakose et al., 2016; Nogusa et al., 2016; Thapa et al., 2016; Zhang et al., 2020). Combined death pathways are observed during infection with cell death suppressor mutants of either HSV1 (Guo et al., 2015) or MCMV (Daley-Bauer et al., 2017). In some settings, markers of inflammasome activation and pyroptosis are also observed, prompting the term PANoptosis (Samir et al., 2020). The combined activation of apoptosis and necroptosis by RIPK3 initially emerged from studies of kinase mutants and inhibitors (Mandal et al., 2014). The Z domain characteristic of the ZBP1/ADAR1 family has long been known to recognize either Zform DNA or RNA (Placido et al., 2007; Schwartz et al., 2001). Studies with IAV (Nogusa et al. 2016; Thapa et al., 2016; Zhang et al., 2020), MCMV (Maelfait et al., 2017; Sridharan et al., 2017) and HSV1 (Guo et al., 2018) have implicated ZBP1 as a natural sensor of newly transcribed RNA rather than DNA, extending and correcting earlier interpretations that had not considered the potential role for RNA (Pham et al., 2013; Takaoka et al., 2007). In each of these settings, dsRNA accumulates within infected cells as a pathogen-associated molecular pattern (PAMP) that is recognized by ZBP1 dependent on the presence of the Zα1 and/or Zα2. Most recently, restriction of VACV replication and pathogenesis by Zα-deficient E3Δ83N mutant virus (Figure 1A) was revealed to be dependent on ZBP1/RIPK3-dependent necroptosis (Koehler et al., 2017). Although E3 Zα appears to compete for Z-NA species produced in the course of virus infection,

evidence of Z-NA accumulation in VACV infected cells as well as the means through which ZBP1 becomes activated remain unresolved.

Here, we show that Z-form RNA accumulates during the early phase of Z-deficient VACV infection, triggering ZBP1 to initiate necroptosis. Z-RNA serves as the ZBP1-activating PAMP; however, distinct from observations with IAV defective interfering particles in the nucleus of infected cells (Zhang et al., 2020), this DNA virus promotes the accumulation of Z-RNA in the cytoplasm dependent on the viral E3 C-terminal dsRNA binding domain (dsRBD). Thus, expression of mutant E3 that retains dsRNA binding capacity but lacks Z-NA binding capacity leaves VACV susceptible to ZBP1-mediated sensing through the exposure of Z-RNA in the cytoplasm of infected cells. This scenario implicates the E3 dsRBD in promoting PAMP formation and the Z domain in suppressing ZBP1 activation during wt VACV infection.

Materials and methods

CELLS SVEC4-10 (CRL 2181) and SVEC-derived ZBP1-deficient clone29-11 cells and various ZBP1-transduced cells were previously generated (Sridharan et al., 2017), Cells were cultured in DMEM containing 4.5 g/ml glucose, 10% FBS (Peak Serum), 2 mM L-glutamine, 100 U penicillin/ml, and 100 U streptomycin/ml (Invitrogen). BHK21 (ATCC-CCL-10) and L929 (ATCC-CRL-6364) were cultured in MEM (GIBCO) supplemented with 5% FBS, 0.1 mM nonessential amino acid solution (GIBCO) and 50 µg gentamycin/ml. F2 HeLa cells (kind gift of George Pavlakis, NCI) were maintained in DMEM; (GIBCO) supplemented with 5% FBS (HyClone). Pkr−/− and wt MEFs (129/SV background) were generously provided by Lynda Morrison, Saint Louis University, and were maintained in DMEM with 10% FBS and 50 µg gentamicin/ml. RK-E3L (RK13) cells (ATCC CCL-37) have been stably transfected with a plasmid expressing the E3L gene under regulatory control of the Tet-Off system (Clontech) maintained in MEM (Cellgro) supplemented with 5% FBS. All cells were incubated at 37°C in the presence of 5% CO2.
VIRUS The Western Reserve (WR) strain was employed as parental wt VACV to generate E3 mutant viruses as previously described (Brandt and Jacobs, 2001; Chang et al., 1995; Kim et al.,

2003; Shors et al., 1997). E3 loss of function mutant viruses were previously generated by alanine substitution (Kim et al., 2003). Zα chimeric substitution viruses were previously generated by replacing nucleotides 61–261 (amino acids 1–67) of the vaccinia virus E3L gene with nucleotides 554–742 (Zα) from human ADAR1 or nucleotides 116–316 (Zα) from murine ZBP1 (Kim et al., 2003). We confirmed the identity of all recombinant viruses by sequencing a PCR product using E3L flanking primers. All experiments with these viruses were performed using an MOI of 5 unless specified otherwise.

Virus Stock Preparation. BHK21 cells were used to propagate wt and recombinant viruses except for ΔE3L which was propagated on RK-E3L cells. Cell culture medium was removed from the monolayers and virus infections were performed in MEM (GIBCO) supplemented with 2% FBS, 50 µg gentamycin/ml, and 0.1 mM nonessential amino acid solution (GIBCO). Cells were infected at a MOI of 0.01 at 37ºC with rocking every 10 min. After 1 hr adsorption, the inoculum was removed and cell culture medium was replaced. At 100% CPE, virus was released from cells by three rounds of freeze/thaw (–80ºC/37ºC) cycles followed by 30s sonication with a probe type sonicator on ice. Cell debris was removed by centrifugation (700 × g for 10 min at 4ºC) and supernatant was stored in aliquots at –80ºC. The virus titer in the supernatant was determined by plaque assay.

Spontaneous isatin-β-thiosemicarbazone (IBT)-resistant mutants were previously generated from parental E3Δ37N as described (Cresawn et al., 2007). After 1 hr incubation, inoculum was aspirated and replaced with fresh medium containing 45 µM IBT. 24 hr later, virus was collected as describe above. IBT-resistant progeny were isolated by plaque purification in the presence of 45 µM IBT.

Plaque reduction assays L929 cell monolayers were treated with 0 to 300 U/ml of mouse IFNα (Calbiochem) and then infected with 1 x 102 PFU of wt VACV or E3 mutant viruses (Koehler et al., 2017). Plaques were counted after fixation with 50% methanol and staining with crystal violet at 3 to 4 dpi. Percent plaque reduction was calculated by comparing the input PFU to the number of plaques formed in treated monolayers.

Cell viability Viability was assessed with a SYTOX nuclear stain exclusion assay or by a CellTiter-Glo Luminescent Cell Viability Assay (Promega). For SYTOX nuclear stain, Hoechst 33342 (2'-[4-ethoxyphenyl]-5-[4-methyl-1piperazinyl]-2,5'-bi-1H-benzimidazole) and SYTOX® were applied for 15 min prior to infection and throughout the time following infection. Cells were incubated at 37°C in the presence of 5% CO2 on an EVOS™ FL Auto Imaging System (Invitrogen) with onstage incubator system. An image was collected every 2 min for 5 hr. Sytox+ cells were considered dead, so the percentage of cells excluding this dye were determined in 10 fields at 100X magnification for each independent experiment (N=3). CellTiter-Glo® Luminescent Cell Viability Assay was performed at 12 hpi according to manufacturer's recommendations (Mandal et al., 2014).

Cell Extracts and Immunoblot. 50% confluent cell monolayers in 60 mm dishes infected with viruses at a MOI of 5 for various times were washed twice with PBS, scraped, pelleted and lysed in 100 µl of 100 mM Tris-Cl (pH 6.8) with 2% SDS and 100 mM 2-mercaptoethanol and 1X Halt Protease and Phosphatase Inhibitor Cocktail (Pierce Thermo Scientific). Cell lysates were further processed utilizing QIAshredder columns (Qiagen) according to manufacturer's recommendations. Boiled samples were subjected to denaturing SDSPAGE using 10% gels. Membranes were blocked in 3% skim milk in Trisbuffered saline with 0.1% Tween20 Detergent (TBST) for 1 hr and then incubated in primary antibody diluted 1:1000 in PBS overnight at 4°C. Membranes were then washed and incubated in secondary antibody (diluted 1:5000) for 2 hr at room temperature. Immunoreactive bands were visualized by chemiluminescence with horse radish peroxidase substrate.

Immune adsorption ZBP1-null 29-11 cell derivatives (Sridharan et al., 2017) were plated on 10 cm dishes at 50% confluency. At 24 hr post-seeding, cells were infected, incubated until 4 hpi, scraped and resuspended in ice cold Ca+2- and Mg+2-free 1X Hanks balanced salt solution (HBSS*) supplemented with 10 mM HEPES, pH 7.3 (Gibco), and irradiated on ice at 400 mJ/cm2 in a Spectrolinker XL-1500 to crosslink nucleic acids and proteins. Following crosslinking cells

were scraped, sedimented and lysed in 0.5 ml of ice-cold Ca+2- and Mg+2-free 1X phosphate-buffered saline (PBS) supplemented with 0.1% SDS, 0.5% deoxycholate, 0.5% Nonidet (N)P-40 (PXL buffer) with SUPERase•In RNase Inhibitor (Invitrogen) and 1X Halt Protease and Phosphatase Inhibitor Cocktail (Pierce Thermo Scientific) for 15 min and subjected to brief sedimentation at 10,000xg for 10 min to remove insoluble cell debris. 10% of lysates were reserved to assess total protein or RNA. Mouse monoclonal anti-Z-NA antibody Clone Z22 or mouse monoclonal E3 NR-4547 was incubated with anti-mouse IgG Dynabeads (Thermo). After washing unbound antibody, Dynabeadbound anti-Z-NA antibody was then added to lysates and incubated while rotating for 4 hr at 4°C, washed 3X in a magnetic stand in 1 ml of 1X PXL buffer followed by two washes with 50mM Tris-Cl, pH7.4, 10mM MgCl2 and 0.5% NP-40 (PNK+ buffer). For RNA bridging studies, beads were treated in between the two wash steps with DNase I with or without RNase T1 at 10 U/ml in 1 mM EDTA and 10 mM Tris-Cl, pH 7.8 (TE buffer). For RNA quantification beads were incubated in Trizol for 10 min then RNA was isolated according to manufacturer's instructions and quantified on a Nanodrop instrument. For protein association, beads were then incubated in 1X SDS lysis, heated at 95°C for 10 min and placed back on magnetic stand to remove the supernatant for SDS-PAGE using 4-20% gradient gels and immunoblotting after transfer to polyvinylidene difluoride (PVDF) membranes.

Live cell imaging L929 cells were seeded in 12-well CytoOne tissue culture treated plates (USA Scientific) and pre-treated with 100 U/ml of mouse IFNα (Calbiochem) for 18 hr prior to infection. Live cell nuclear stain Hoechst 33342 was applied 15 min prior to infection. Cells were infected and incubated for an additional 5 hr prior to evaluation of alterations in morphology with an EVOS™ FL Auto Imaging System (Invitrogen). For time-lapse imaging, cells were overlaid with MEM supplemented with 1 µM SYTOX Green NA stain (Thermo Fisher Scientific) and 5 µg/ml Hoechst 33342 (Thermo Fisher Scientific). Cells were incubated at 37°C supplemented with 5% CO2 on the EVOS™ System with onstage incubator system (Koehler et al., 2017). An image was taken every 2 min for 5 hr.

Cell treatments Cell death suppressor cocktail including GSK inhibitor composed of N-(6-

(Isopropylsulfonyl)quinolin-4-yl)benzo[d]thiazol-5-amine (GSK'872, GlaxoSmithKline) at 3 μM and zVAD fmk (Enzo Life Sciences) at 50 μM was applied to cells 1 hr prior to and during infection (Mandal et al., 2014). Mouse cells were treated with IFNα (Calbiochem) or mouse IFNβ (PBL assay). To induce TNF dependent necroptosis, cells were treated with 50 μM zVAD fmk (Enzo life sciences) for 1 hr then stimulated with 25 ng TNF/ml (PeproTech) and lysates were harvested 6 hr after addition of TNF (Koehler et al., 2017). Cells were then treated with increasing concentration of inhibitors throughout infection. Cytosine arabinoside (AraC) was used at 200 μg/ml, 400 μg/ml, 800 μg/ml and 1600 μg/ml starting at 1 hr prior to infection Cycloheximide (CHX) was used at 20 μg/ml, 40 μg/ml, 80 μg/ml, 900 and 120 μg/ml starting at 30 min after infection. Hydroxyurea (HU) was used at 5 μM, 10 μM, 20 μM and 40 μM starting 1 hr prior to infection Actinomycin D (ActD) treated throughout infection at 1 μg/ml, 2 μg/ml, 4 μg/ml, 8 μg/ml starting 1 hr prior to infection Sarracenia extract (Sar) made from an ethanol extract (Arndt et al., 2012) was used at 10 μl/ml, 30 μl/ml, 60 μl/ml, 120 μl/ml starting at 1 hr prior to infection. siRNA transfection: L929 cells were plated in 6-well dishes at 30% confluency, allowed to adhere for 24 hr and transfected with ON-TARGETplus siRNA (Dharmacon) or control siRNA using INTERFERin transfection reagent (Polyplus) according to manufacturer's recommendations. Following transfection, cells were incubated for 36 hr, either mock- or IFN□-treated for 18 hr and subjected to infection for times indicated.

Immunofluorescence imaging Cells were plated on 8-well glass slides (EMD Millipore), allowed to adhere for at least 24 hr and infected at a MOI of 5. Following infection, cells were fixed in 4% (w/v) paraformaldehyde, permeabilized in 0.2% (v/v) Triton X-100, blocked with MAXblock Blocking Medium (Active Motif), and incubated overnight in a humidified chamber with primary antibodies at 4°C. After three washes in PBS, slides were incubated with fluorophore-conjugated secondary antibodies for 1 hr at room temperature. Cells were then washed 3X in PBS, slides were mounted in ProLong Gold Antifade Reagent (Thermo Fisher Scientific) and imaged by confocal microscopy on a Leica SP8 instrument. Fluorescence intensity was quantified and subjected to statistical calculations using Leica LAS X software. In some experiments, cells were

subjected to additional treatments post fixation. Proteinase K treatment was performed with (0.008 U/ml) for 20 to 40 min at 37°C. RNase A (1 µg/ml) or DNase I (25 U/ml) was used for 1 hr at 37°C. Primary antibodies were used at the following dilutions Z-NA (Z22 clone Ab, 1:200), A-RNA (J2 clone, 1:50), E3 (rabbit polyclonal, 1:500).

Flow cytometry Z-RNA: Infected SVEC4-10-derived EV and wt ZBP1 29-11 cells were UV crosslinked at 4 hpi, stained with fixable viability 700 (BD Horizon) and permeabilized with CytoPerm/Fix kit (BD) for 20 min at 4°C. Following permeabilization and DNase I treatment, cells were blocked in FACS buffer (2% BSA, 0.9% sodium azide in PBS) with 10% normal rat serum and then probed with mouse monoclonal anti-Z-NA antibody clone Z22 at 1:100 in Permwash buffer (BD) for 30 min at 4°C then washed 3X with Permwash buffer followed by secondary anti-mouse-IgG 488 antibody (Invitrogen). Cells were evaluated by flow cytometry using a BD LSR Fortessa Cell Analyzer and gated on FlowJo9 software to exclude doublets and dead cells to determine the frequency and median fluorescence intensity of Z-NA+ cells. dsRNA (A-RNA): HeLa cells were mock- or virus-infected with either wt VACV, ΔE3, E3Δ37N, E3Δ37NIBTR-3, E3Δ37NIBTR-7, VACV-A24R-R1, or MPXV. At 6 hpi, cells were trypsinized and fixed with CytoPerm/Fix kit (BD). Cells were stained with rabbit anti-VACV (Abcam) and mouse anti-dsRNA (J2 clone, Scicons) overnight at 4°C. Cells were washed and stained with anti-rabbit-IgG Pacific Blue (BD) and anti-mouse-IgG 488 (Invirtogen) for 4 °C. Cells were washed, resuspended in FACS buffer (2% BSA, 0.9% sodium azide in PBS) and were analyzed by flow cytometry using a BD FACSymphony™ A3 Cell Analyzer and cells were gated to exclude doublet and non-viable cells.

QUANTIFICATION AND STATISTICAL ANALYSIS For all comparisons between mean values from mock, infected, control or treated samples, significance was determined by a nonparametric Mann-Whitney test using Graphpad Prism9 with $p \leq 0.05$ considered significant (*,$p \leq 0.05$,**, $p \leq 0.01$ ***, $p \leq 0.001$). Error bars represent SD with an $N \geq 3$ as indicated in the figure legends. All statistical analysis was performed using Prism 8 (Graphpad).

Results

Amino acids in the N-terminus of E3 that impart Z-NA binding are required to restrict VACV-induced necroptosis. As a virulence factor, E3 is known to confer type I IFN resistance on VACV (Brandt and Jacobs, 2001; Chang et al., 1992) through the action of its N-terminal Z domain together with its C-terminal dsRBD (Figure 3-1A). Both domains contribute to type I IFN resistance as well as to viral pathogenesis in mice (Brandt et al., 2005; Kim et al., 2003; White and Jacobs, 2012). The N-terminal domain suppresses virus-induced necroptosis (Koehler et al., 2017). Type I IFN priming boosts ZBP1 levels in L929 cells rendering these cells susceptible to necroptosis following infection with Z-deficient E3Δ83N. To determine more precisely whether E3 suppression of virus-induced necroptosis involves interaction with Z-NA, Z loss-of-function point mutants (Kim et al., 2003) generated by alanine substitution (E3Y48A or E3P63A) were evaluated in IFN-primed L929 cells along with wt VACV as well as control E3E42A (Figure 1A). When infected with either loss-of-function point mutant, L929 cells showed a pattern of compromised replication (Figure 3-1B), accompanied by loss of membrane integrity (Figure 3-1C), activated MLKL (Figure 3-1D) and necrotic morphology (Figure 3-1E). In contrast, E3E42A, like wt VACV, failed to trigger appreciable death of infected cells. These data demonstrate that the suppression of VACV-induced necroptosis depends on an E3 domain characterized for its ability to recognize Z-NA (Ha et al., 2004; Kim et al., 2004).

Figure 1.

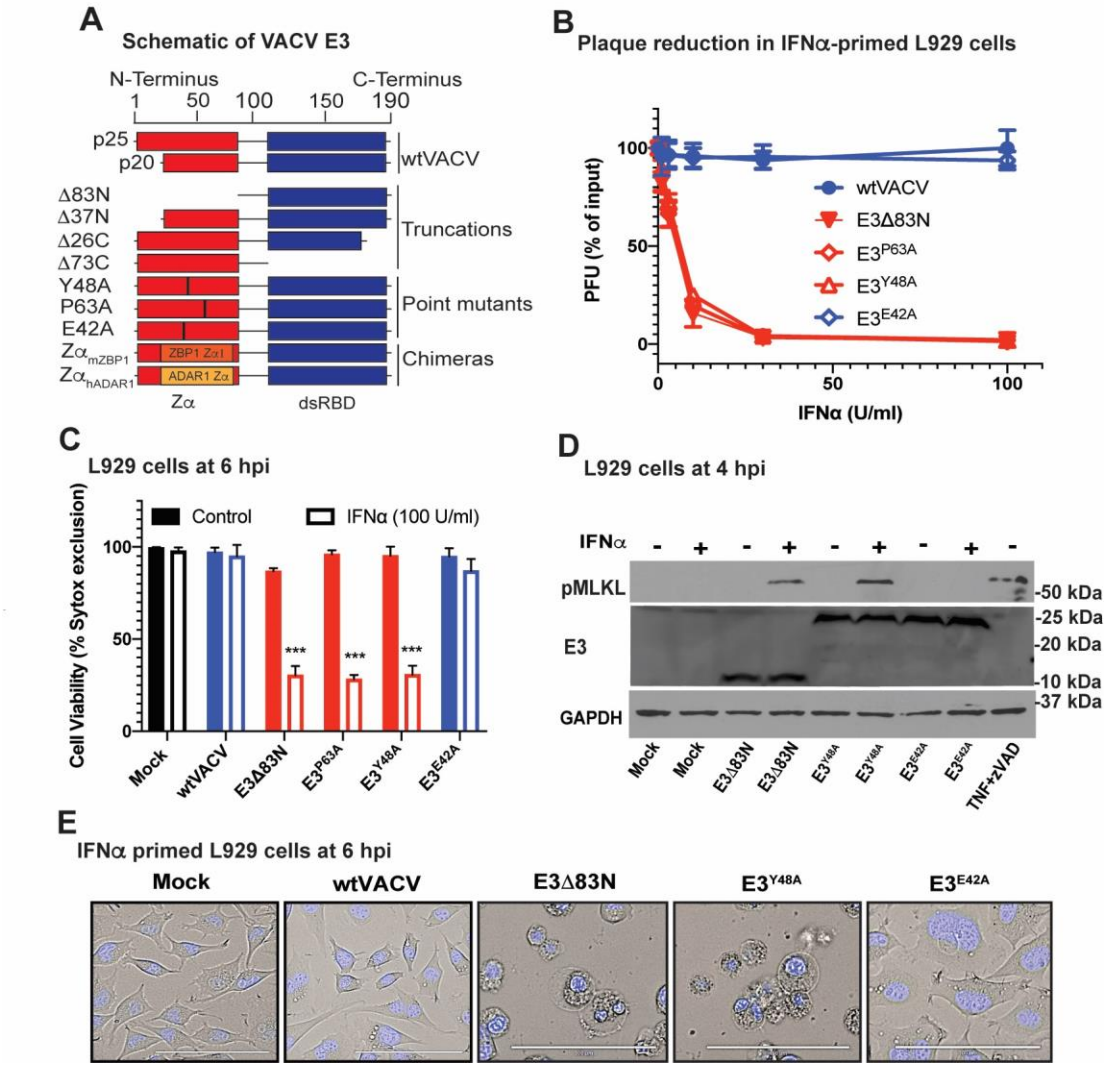

Figure 3-1 Amino Acids in the N-terminus of E3 that Impart Z-NA Binding are Required to Restrict VACV-Induced Necroptosis. (A) A schematic diagram of VACV E3 and E3 derivatives made previously (Kim et al., 2003) and used in this study, including truncation mutants (E3Δ83N, E3Δ37N, E3Δ26C, E3Δ73C), single amino acid substitution mutants (E3Y48A, E3P63A, E3E42A) and chimeric E3 with Zα substitutions (ZαhADAR1, ZαmZBP1). (B) Plaque reduction assay performed by pretreating L929 cells with increasing concentrations of mouse IFNα for 18 hr prior to infection. Percent reduction of PFU was calculated as a proportion of input PFU for each virus evaluated. E3Y48A and E3P63A point mutations disrupt Z-NA binding; whereas, E3E42A is

located outside of Zα so this protein retains Z-NA binding and is included as a control (Kim et al., 2003). (C) L929 cells either left untreated or treated with mouse IFNα (100 U/ml) for 18 hr and subsequently infected at a MOI of 5 with each of the viruses shown. Cell viability was determined by SYTOX dye exclusion by counting an average of 10 fields microscopically at 6 hpi in three individual experiments. (D) Immunoblot (IB) of L929 cell lysates either left untreated (-) or pretreated (+) with IFNα and prepared at 4 hpi (MOI of 5 with indicated viruses) for phospho-MLKL, total E3 levels and GAPDH (as a loading control) following separation by SDS-PAGE. Mock infected cells and cells induced into necroptosis by TNF at 25 ng/ml in the presence of 50 μM zVAD-fmk from 1 hr prior to TNF (Koehler et al., 2017) are included as a negative and positive controls, respectively. (E) Phase contrast micrographs showing the morphology of L929 cells pretreated with IFNα and left uninfected (Mock) or infected at a MOI of 5 with the indicated viruses before being stained at 6 hpi with cell-permeant Hoechst 33342 and visualized. Bar indicates 100μM. Error bars represent the standard deviation (SD). Figures are representative of three independent replicates, except panel B and C which compiles the results of the replicates. Statistical significance was determined by a nonparametric Mann-Whitney test using Graphpad Prism9 with $p \leq 0.05$ considered significant (*, $p \leq 0.05$,**, $p \leq 0.01$ ***, $p \leq 0.001$).

ZBP1 Zα2 domain senses VACV and triggers necroptosis. Necroptosis-sensitive L929 and SVEC4-10 cells were employed to investigate the contribution of type I IFN priming to cell death following E3 Z-deficient VACV infection. L929 cells required priming with IFNβ to exhibit robust MLKL phosphorylation (Figure 3-2A, left) and loss of viability (Figure 3-2B) indicative of necroptosis. In contrast, E3 mutant VACV triggered phosphorylation of MLKL (Figure 3-2A, left) and necroptosis (Figure 3-2B) in SVEC4-10 cells independently of priming, consistent with constitutive high ZBP1 levels independent of pretreatment (Figure 3-1A). SVEC4-10-derived ZBP1-null empty vector (EV) control cells (Sridharan et al., 2017) resisted death unless stably reconstituted with FLAG epitope tagged full-length wt ZBP1 (Figure 3-2A, middle, and 3-2B). Likewise, siRNA-mediated inhibition of ZBP1 expression in IFNβ-primed L929 cells prevented

VACV-induced necroptosis (Figure 3-2A, right, and 3-2B). Together, these data establish that type I IFN sensitizes cells to VACV-induced necroptosis by boosting ZBP1 levels as noted for other settings (Ingram et al., 2019; Kuriakose et al., 2016; Thapa et al., 2016; Yang et al., 2020). SVEC4-10 cells express constitutive levels of ZBP1 that support ZBP1-dependent necroptosis without a requirement for IFN priming consistent with previous observations (Upton et al., 2010, 2012).

In order to interrogate the contribution of ZBP1 Z-NA binding domains, cells expressing epitope tagged wt ZBP1 as well as Z1 and Z2 loss-of-function mutants (Sridharan et al., 2017) known to disrupt binding to Z-NA (Brown et al., 2000; Placido et al., 2007) were evaluated for susceptibility to VACV-induced necroptosis. SVEC4-10-derived ZBP1-null cells stably transduced with wt ZBP1 exhibited sensitivity to necroptosis compared to EV control (Figure 3-2C). Cells transduced with ZBP1 deletion mutant of Z1 together with Z2 (ZBP1ΔZα1/Zα2) or combined loss-of-function point mutants in Z1 (N46D/Y50A) together with Z2 (N122D/Y126A) (ZBP1mutZα1Zα2) resisted cell death. Mutation of Zα2 (ZBP1mutZα2) alone conferred resistance as well; whereas, mutation of Zα1 (ZBP1mutZα1) alone did not. Necroptosis-sensitive cells treated with a death suppressor cocktail composed of RIPK3-inhibitor GSK'872 and caspase inhibitor zVAD-fmk did not succumb to E3∆83N-induced death. These combined inhibitors preserved cell viability in all settings as expected from prior characterization of prominent RIPK3-dependent cell death pathways (Mandal et al., 2014). The dependence of VACV-induced necroptosis on ZBP1 Z2 was confirmed by immunoblots showing the absence of phosphorylated MLKL in ZBP1ΔZα1/Zα2, ZBP1mutZα2 and ZBP1mutZα1/Zα2 as well as EV control (Figure 3-2D). In contrast, cells transduced with either wt ZBP1 or ZBP1mutZα1 showed the expected activation of MLKL consistent with triggering necroptosis. Together, these results implicate ZBP1 Zα2 in sensing VACV to initiate necroptosis, results that are reminiscent of a requirement for Z2 in other characterized virus-induced death settings where ZBP1 has been implicated as the pathogen sensor (Guo et al., 2018; Kesavardhana et al., 2020; Sridharan et al., 2017; Thapa et al., 2016)

as well as settings where RIPK1-deficient cells have shown sensitivity to IFN-induced, ZBP1dependent necroptosis (Ingram et al., 2019; Yang et al., 2020).

Figure 2

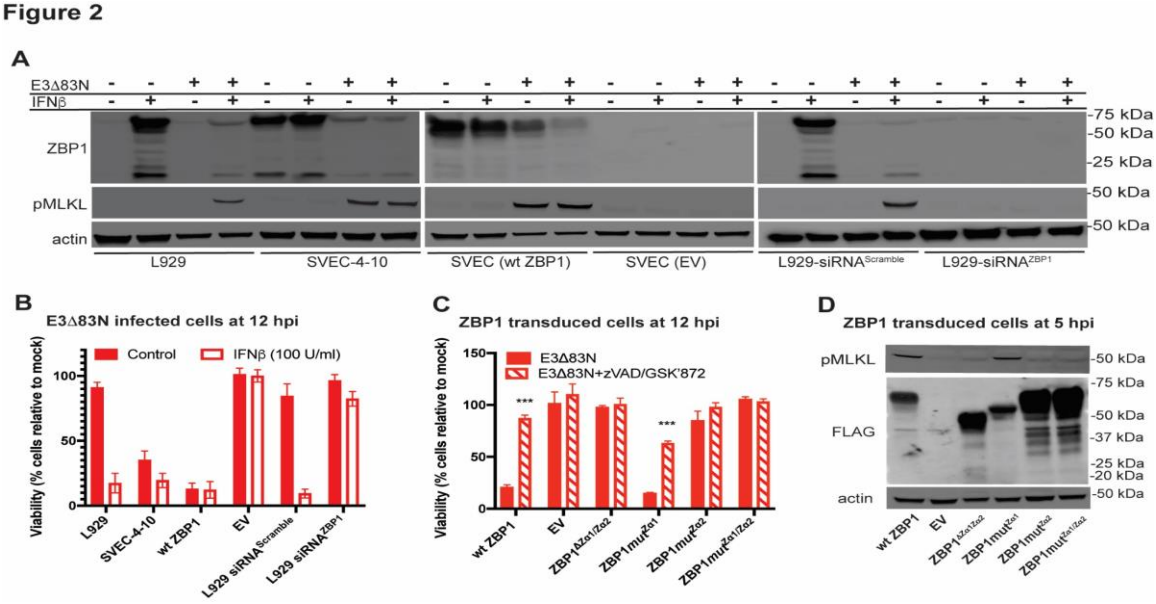

Figure 3-2 ZBP1 Requires Z2 to Sense VACV and Trigger Necroptosis. (A) IB of L929, SVEC4-10, FLAG-ZBP1-reconstituted SVEC (wt ZBP1) and ZBP1-null SVEC (EV) (Sridharan et al., 2017) cells either left untreated (-) or pretreated with 100 U/ml of mouse IFNβ for 18 hr (+) and either left uninfected (-) or infected at an MOI of 5 with E3Δ83N (+). L929 cells in rightmost panel were transfected with either a scrambled siRNA pool or an siRNA pool targeting ZBP1 for 36 hr prior to IFNβ treatment. Lysates were harvested at 4 hpi, and, following SDS-PAGE, evaluated for phospho-MLKL and ZBP1. (B) Viability of L929, SVEC4-10, wt ZBP1 or EV cells either untreated or pretreated with IFNβ and then infected at an MOI of 5 with E3Δ83N for 12 hr determined by measuring intracellular ATP levels with a Cell Titer-Glo Luminescent Cell Viability Assay kit. Rightmost bars show results from cells transfected with either a scrambled siRNA pool or an siRNA pool targeting ZBP1 as described in Panel A. CellTiter-Glo assay (Promega) (C) Viability of ZBP1-null SVEC29-11 cells reconstituted with indicated ZBP1 constructs infected with E3Δ83N either alone or in combination with zVAD-fmk plus GSK'872 assessed at 12 hpi by CellTiter-Glo assay as described in Panel B. (D) IB of ZBP1 reconstituted SVEC29-11 cells infected at a MOI of 5. Lysates were prepared as described in Panel A and evaluated for

phospho-MLKL and FLAG-ZBP1. Error bars represent the SD. Each set of data is representative of two replicates except for panel B and C which compiles the results of the replicates. Statistical significance was determined as described in Figure 3-1.

VACV E3 Z and dsRNA binding domains collaborate to regulate necroptosis. To further characterize the requirements for VACV-induced necroptosis, we evaluated E3 domain-specific mutants affecting the N-terminal Z-NA binding domain and/or C-terminal Aform-specific dsRBD (Chang and Jacobs, 1993). Infection with N-terminal deletion mutants E3Δ37N unleashed necroptosis with a pattern identical to E3□83N (Koehler et al., 2017), including loss of membrane integrity by 6 hpi (Figure 3-3A) subsequent to activation of MLKL (Figure 3-3B). Two different dsRBD mutants (E3Δ26C or E3Δ73C) resisted death, suggesting that A-RNA binding did not contribute to cell death suppression. Surprisingly, E3-deficient VACV (ΔE3L) resisted necroptosis. Thus, the E3 dsRBD must be retained in order for E3 Z-deficient virus to unleash necroptosis. To evaluate whether E3 dsRBD and Z domain function when expressed as separate proteins, IFN-primed L929 cells were simultaneously infected with VACV carrying the C and N terminal mutations such that both domains were expressed on separate E3 derivatives. As expected, wt VACV or E3Δ73C infections alone did not cause the death of cells and E3Δ37N induced death (Figure 3-3C) associated with activated MLKL (Figure 3-3D). There was no change in this pattern of necroptosis during coinfections of E3Δ37N, capable of binding dsRNA, together with E3Δ73C, capable of recognizing Z-NA. Thus, the E3 Z domain and the dsRBD must be retained on the same molecule to observe cell death suppression. These studies identify the E3 dsRNA binding as necessary to either sensitize cells to ZBP1dependent death or to prohibit other pathways on which necroptosis depends.

Figure 3

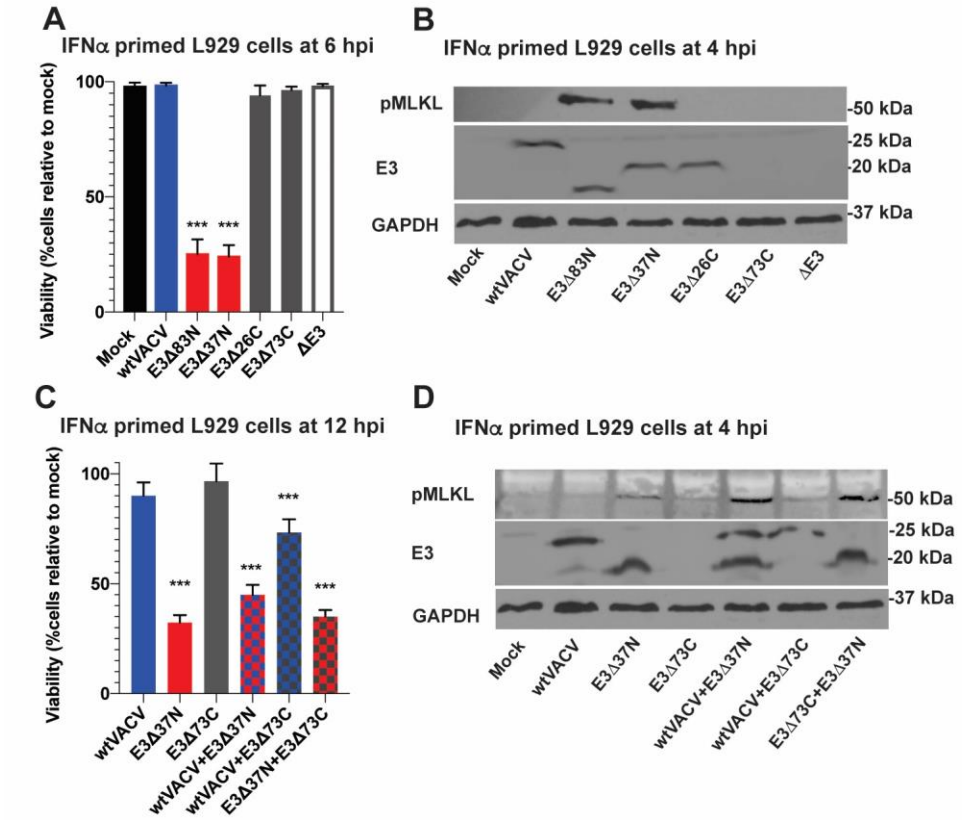

Figure 3-3 VACV E3 Zα Domain and dsRBD Collaborate to Regulate Cell Death. (A) Viability of L929 cells that were IFN-pretreated as described in Figure 1 and subsequently infected at an MOI of 5 with the indicated viruses. Cell viability was determined at 6 hpi by Sytox dye exclusion as described in Figure 1. (B) IB of L929 cells that were IFNα-pretreated as described in Figure 1 prior to infection at an MOI of 5 with the indicated viruses. Lysates were harvested at 4 hpi and, following SDS-PAGE, evaluated for phospho-MLKL. (C) Viability of IFNβ-pretreated L929 cells were infected with a single virus at an MOI of 10 or co-infected with two viruses each at an MOI of 5. Cell viability was determined at 12 hpi by CellTiter-Glo assay as described in Figure 2. (D) IB of IFNβ-primed L929 cells infected with single virus or coinfected with two viruses as described in Panel C. Lysates were harvested at 4 hpi and, following SDS-PAGE, evaluated for phospho-MLKL. Error bars represent the SD. Each set of data is representative of three replicates except

for panel A and C which compiles the results of the replicates. Statistical significance was determined as described in Figure 3-1.

VACV E3 ZBD suppresses transcription-dependent necroptosis independent of PKR. To determine the steps in viral replication necessary to trigger necroptosis, we utilized a series of chemical inhibitors known to block stages of VACV replication. We first showed that virus entry was necessary, given that UV-inactivated E3∆83N particles failed to activate MLKL (Figure 3-4A). E3∆83N-infected cells treated with inhibitors of protein synthesis (cytosine arabinoside or cycloheximide) or DNA synthesis (hydroxyurea) supported activation of MLKL; whereas, a general inhibitor of RNA transcription (Actinomycin D) or specific inhibitor of VACV transcription (Sarrsina) (Arndt et al., 2012) blocked MLKL phosphorylation (Figure 3-4B). These data reveal a role for early transcription prior to viral DNA replication in the induction of necroptosis reminiscent of the requirement for transcription in other settings where virus induced ZBP1 activation initiates a cell death cascade (Guo et al., 2018; Kesavardhana et al., 2020; Sridharan et al., 2017; Thapa et al., 2016).

Given the importance of the E3 dsRBD in PKR activation as well as the early activation of PKR following infection with ∆E3L virus (Chang et al., 1992) we sought to characterize the accumulation of A-RNA in infected cells. A-RNA accumulated in L929 cells within the first 4 hpi based on immunofluorescent imaging with conventional dsRNA-specific J2 antibody, as observed previously (Schonborn et al., 1991; Weber et al., 2006). A-RNA accumulated to equivalent levels in wt and E3 Z-deficient VACV-infected cells by this time (Figure 3-4C-D). Thus, dsRNA accumulates in VACV-infected cells independently of the E3 Z domain. In order to determine whether IFN-responsive A-RNA sensor PKR contributes to virus-induced necroptosis, we compared the susceptibility of PKR-deficient (Pkr-/-) and wt MEFs. When MEFs were primed with IFN and subsequently infected with E3Δ83N, necroptosis remained robust in Pkr-/- cells (Figure 3-4E-F) indicating that PKR does not contribute to activation or suppression of VACV-induced, ZBP1-mediated necroptosis.

Figure 4

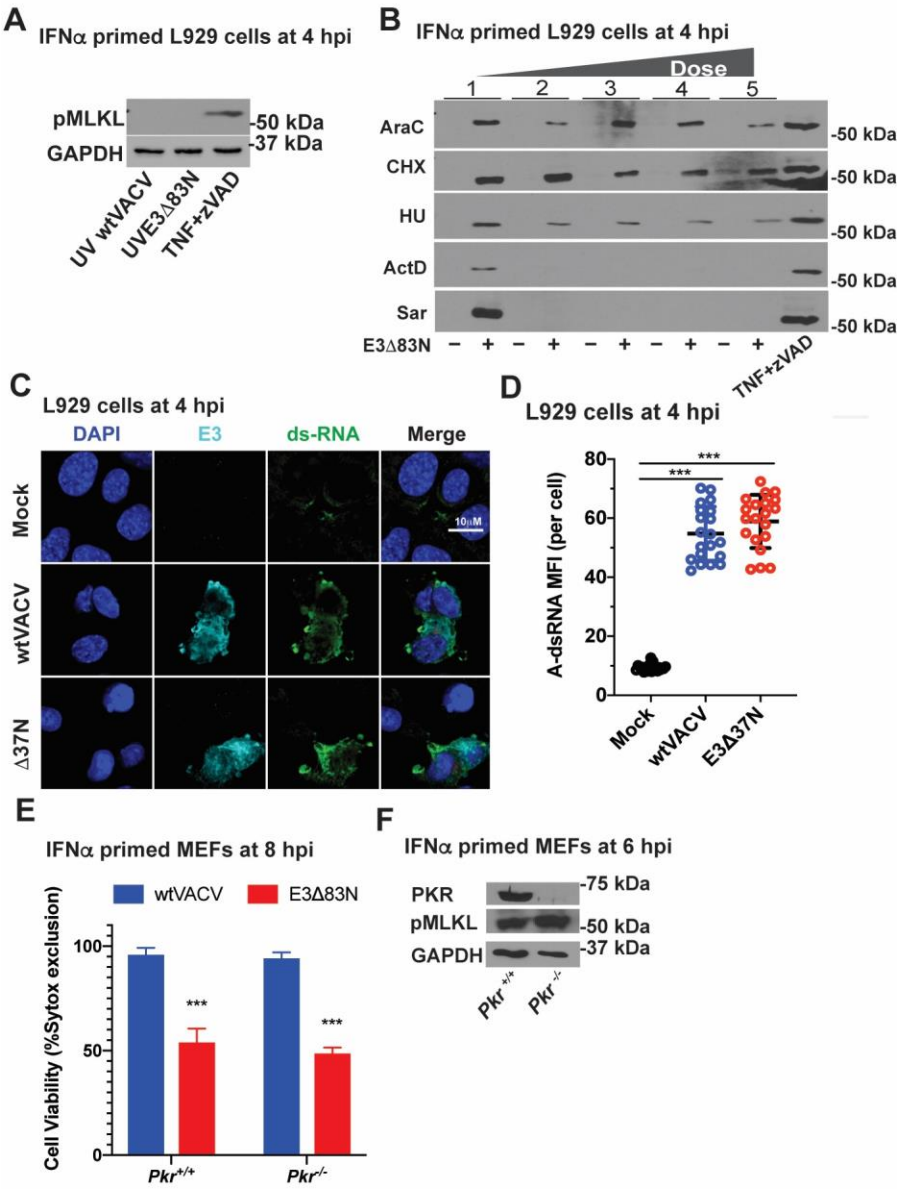

Figure 3-4 VACV E3 Zα Regulates Transcription-Dependent Induction of Necroptosis without Any Contribution of PKR. (A) IB of L929 cells that were IFNα-pretreated as described in Figure 1 and then infected with an equivalent MOI of 5 using UV-inactivated viral particles. TNF plus zVAD-fmk is shown as a positive control as described in Figure 1. Lysates were harvested at 4 hpi and, following SDSPAGE, evaluated for phospho-MLKL. (B) IB of L929 cells that were IFNα-pretreated as described in Figure 1 and then treated with increasing doses of the following

inhibitors: cytosine arabinoside (AraC), at 200, 400, 800 and 1600 mg/ml; cycloheximide (CHX) at 20, 40, 80 and120 mg/ml; hydroxyurea (HU) at 5, 10, 20 and 40 mM: Actinomycin D (ActD) at 1, 2, 4 and 8 mg/ml; and, Sarracenia extract (Sar) at 10, 30, 60 and 120 µl/ml. Treatment with AraC, HU, ActD and Sar started 1 hr prior to infection and continued throughout infection. Treatment with CHX started 30 min post-adsorption and continued throughout infection. Positive control TNF plus zVAD-fmk is described in Figure 1. Lysates were harvested at 4 hpi and, following SDS-PAGE, evaluated for phospho-MLKL. (C) Confocal immunofluorescent micrographs of L929 cells either uninfected (Mock) or virus infected at a MOI of 5 with wt VACV or E3Δ37N, fixed and permeabilized then subsequently stained with J2 anti-A-RNA (green), anti-E3 (cyan) and DAPI nuclear dye (blue). Bar represents 10µM (D) Quantification of the median fluorescence intensity of A-form dsRNA specific staining by J2 antibody analyzed with Leica LAS X software to generate mean fluorescence intensity of 20 individual cells with mean indicated. (E) Viability of IFN-primed Pkr+/+ and Pkr -/- MEFs infected at a MOI of 5 with wt VACV or E3Δ83N. Cell viability was determined at 8 hpi by Sytox dye exclusion as described in Figure 1. (F) IB of Pkr+/+ and Pkr -/- MEFs primed with IFN for 18h and then infected with E3Δ83N as in Panel E. Lysates were harvested at 6 hpi and, following SDS-PAGE, evaluated for PKR, phospho-MLKL or GAPDH. Error bars represent SD. Statistical significance was determined as described in Figure 1. Each set of data is representative of two replicates except for panel F which compiles the results of the replicates. Statistical significance was determined as described in Figure 3-1.

VACV terminates early transcription at precise sites but is imprecise in the termination of intermediate and late transcripts, resulting in the generation of overlapping transcripts that form dsRNA species, particularly at late times of infection (Duesberg and Colby, 1969). In order to evaluate the impact of accumulating A-RNA levels on the induction of necroptosis, we utilized isatin beta-thiosemicarbazone (IBT), an agent known to enhance processivity of the VACV intermediate/late RNA polymerase and increase the abundance of viral A-RNA (Condit and Niles, 2002). IBT-resistant (IBTR) mutants (E3Δ37NIBTR3 and E3Δ37NIBTR7) produced less A-RNA

than parental virus (Figure S2A) and failed to activate PKR (Figure S2B) similar to viruses previously characterized to be IBTR, such as monkeypox virus (MPXV) or VACV mutant A24R1R carrying a mutation in the viral RNA polymerase (Arndt et al., 2016). Nevertheless, IBTR E3∆37N derivatives showed patterns of growth sensitivity (Figure S2C), cell death (Figure S2D) and activated MLKL (Figure S2E) similar to the IBT-sensitive parental virus. Thus, increased dsRNA character of intermediate and late transcripts did not influence the induction of necroptosis.

Z-RNA accumulates during VACV infection. Given that accumulating A-RNA did not appear to dictate necroptosis outcomes, we next asked whether Z-NA accumulated during VACV infection. To this end, infected cells were fixed and stained at 4 hpi with monoclonal antibody (clone Z22) raised against Z-DNA (Staiano-Coico et al., 1985) and recently employed to characterize Z-RNA (Zhang et al., 2020). Z-NA was present in the cytoplasm of either E3∆37N or wt VACV-infected cells but was absent from mock-infected cells (Figure 3-5A and S2A). The mean fluorescence intensity appeared to be significantly greater in the absence the E3 Z domain (Figure 3-5B). Importantly, this signal resisted DNase I treatment but was sensitive to RNase A treatment (Figure 3-5C and S2B) suggesting accumulation of cytoplasmic Z-RNA within infected cells. The Z-RNA-specific signal was significantly more intense in cells infected with the Z-deficient virus (E3∆83N) compared to either wt VACV or E3-null virus (∆E3), indicating that the accumulation of Z-RNA depended on E3 dsRBD function as well as the absence of the E3 Z domain (Figure S2C). Furthermore, Proteinase K treatment reduced the Z-NA-specific signal intensity in E3Δ37N-infected cells (Figure 3-5A-B and S2A), consistent with a contribution of protein to the Z-RNA signal within infected cells. This result contrasts the Z-NA signal attributed to defective viral dsRNA in the nucleus of IAV-infected cells (Zhang et al., 2020). In VACV-infected cells, the most robust cytoplasmic Z-RNA signal occurs in the presence of Z-deficient E3 that has retained the ability to bind A-RNA. Once induced to form, this Z-RNA may recruit ZBP1, resulting in RIPK3mediated activation of MLKL and execution of necroptosis.

Figure 5

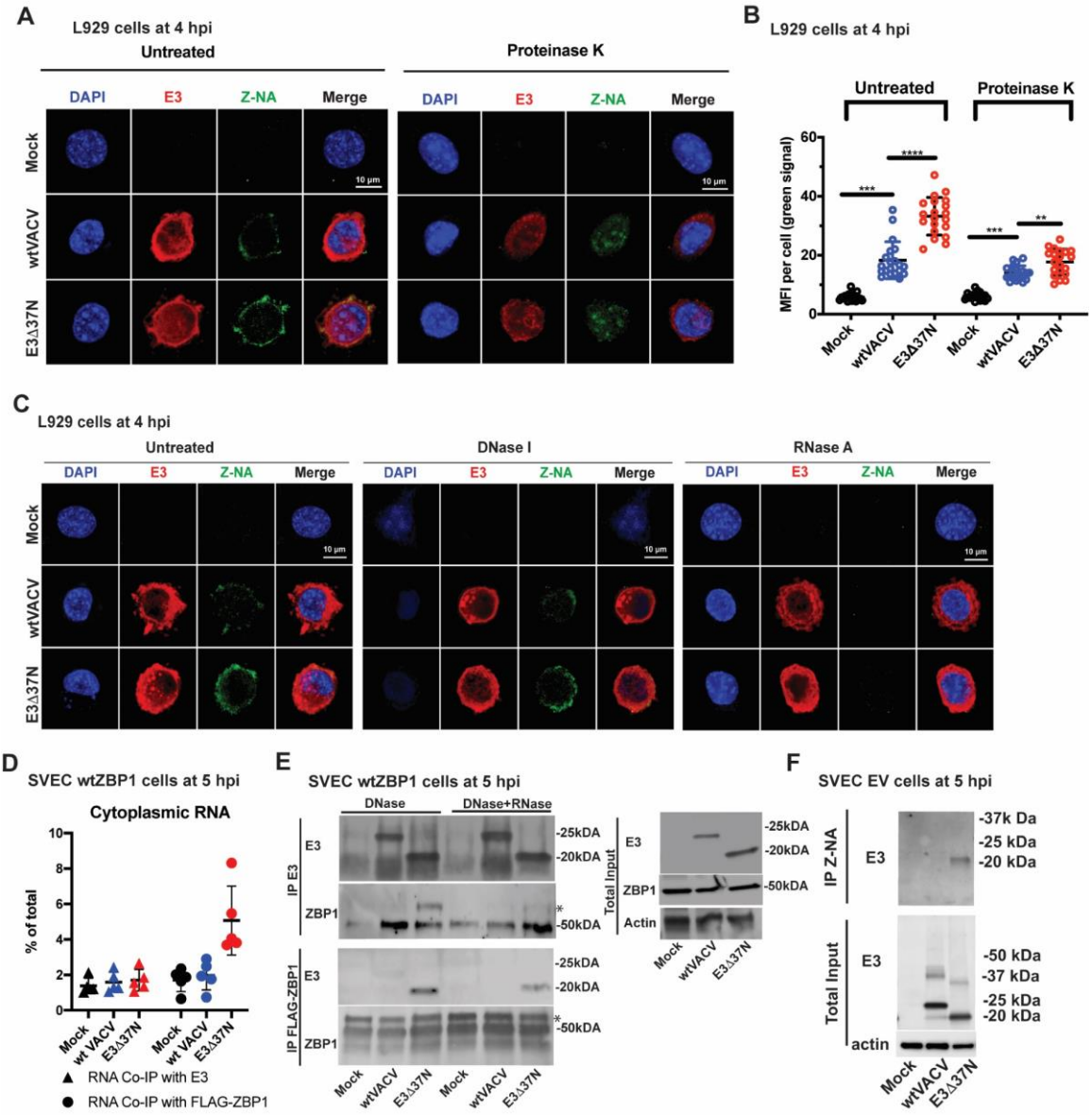

Figure 3-5. E3 Sequesters Z-RNA that Accumulates during VACV Infection. (A) Confocal immunofluorescent micrographs of single L929 cells at 4 hpi. Cells were either uninfected (Mock) or infected with the indicated viruses at an MOI of 5, fixed and permeabilized prior to staining with anti-Z-NA antibody (green), anti-E3 antibody (red) and DAPI nuclear dye (blue). Bar indicates 10 μM. (B) Quantification of the median florescence intensity (MFI) of Z-NA specific monoclonal antibody staining in individual L929 cells using Leica LAS X software. Each point represents an individual cell and mean represents the average intensity from 20 cells. (C) Confocal

immunofluorescent micrographs of single L929 cells at 4 hpi. Cells were either uninfected (Mock) or infected with the indicated viruses at an MOI of 5 and fixed and permeabilized then subsequently left untreated or digested with DNase I or RNase A. Cells were stained as described in Panel A. (D) Coimmunoprecipitation (Co-IP) of RNA bound to E3 or ZBP1. SVEC-derived wt ZBP1 cells were left uninfected (Mock) or infected with indicated viruses at an MOI of 5. At 5 hpi cells were UV crosslinked, lysed and either ZBP1- or E3-associated RNA was isolated by coimmunoprecipitation with E3-specific antibody (triangles) or FLAG-specific antibody. RNA associates with either of these immunoprecipitates was isolated by Trizol, quantified by Nanodrop and the proportion recovered was compared to total cytoplasmic RNA. (E) Coimmunoprecipitation of E3 and ZBP1. SVEC-derived wt ZBP1 cells were either left uninfected (Mock) or infected at an MOI of 5 with wt VACV (expresses p20 and p25) or E3Δ37N (expresses only p20). Cells were UV-crosslinked at 5 hpi, lysed and cell lysates were subjected to immunoprecipitation with either mouse anti-E3-specific antibody (BEI) or rabbit anti-FLAG antibody (Cell signaling) specific for ZBP1 here). Immunoprecipitates were treated with DNase I alone or in combination with RNase T1 and subsequently washed to remove unbound proteins. Total lysates (right panel) and immunoprecipitates were subjected to SDS-PAGE and evaluated for ZBP1 with a mouse anti-ZBP1 antibody (Adipogen) or for E3 with rabbit polyclonal anti-E3 antibody. * indicated specific bands (F) Coimmunoprecipitation of E3 with anti-Z-NA antibody. SVEC EV cells were either left uninfected (Mock) or infected at an MOI of 5 with wt VACV or E3Δ37N. Cells were UV crosslinked at 6 hpi and treated with DNase I. Z-NA was immunoprecipitated from whole cell lysates and total lysates and immunoprecipitated samples were subjected to SDS-PAGE and IB evaluation with rabbit polyclonal anti-E3 antibody. Error bars represent the SD. Each set of data is representative of three replicates. Statistical significance was determined as described in Figure 3-1.

E3 dsRBD promotes formation of Z-RNA and recruitment of ZBP1. The E3L gene naturally encodes a full-length 190 amino acid protein, p25, and a shorter protein, p20, arising from

translation initiation at M38 (Chang et al., 1992). E3□37N encodes only the Z-deficient shorter protein (Figure 3-1A) that retains the ability to bind A-RNA via its C-terminal dsRBD with an affinity similar to full-length p25 (Chang and Jacobs, 1993). To determine how these E3 isoforms impacted the association of cytoplasmic RNA with ZBP1, we infected FLAGZBP1-reconstituted SVEC cells with either wt VACV or E3Δ37N, and, at 5 hpi, subjected cells to UV crosslinking and lysis. After E3- or FLAG-ZBP1-associated RNA was isolated by immunoprecipitation with anti-E3 or anti-FLAG antibody, respectively, RNA was subsequently recovered, purified and quantified by Nanodrop. Overall, similar proportions of E3-associated RNA were detected in wt VACV- and E3Δ37N-infected cells (Figure 3-5D and S2H). However, more RNA was associated with FLAG-ZBP1 in E3Δ37N-infected cells compared to wt VACV infected cells. To determine whether Z-deficient E3 p20 promoted bridging to ZBP1 via RNA, FLAG-ZBP1 reconstituted cells were infected and subjected to UV crosslinking, lysis and incubation with either anti-E3 or anti-FLAG antibody immobilized on beads. Following incubation, antibody:bead complexes were washed and then either left untreated or RNase treated for 15 min. After additional washing, bound proteins were recovered, separated and subjected to immunoblot evaluation. Whereas full-length E3 p25 did not associate with ZBP1, E3Δ37N-encoded p20 and ZBP1 clearly associated in reciprocal immunoprecipitation assays (Figure 3-5E). This interaction was substantially reduced when antibody:bead complexes were treated with RNase T1, consistent with an RNA bridge between Z-deficient E3 and ZBP1. Finally, the failure to detect any bridging between E3 p25 and ZBP1 during wt VACV infection appeared to reflect efficient Z-mediated competition by E3 for Z-RNA thereby preventing recognition by ZBP1.

We next sought to evaluate whether the RNA bound to Z-deficient E3 exhibited Z-form character by employing Z-NA-specific antibody for immunoprecipitation on DNase-treated cytoplasmic lysates. E3Δ37N-encoded p20 was expressed at levels similar to p25 by wt VACV (Figure 3-5F). Z-NA-specific antibody immunoprecipitated E3Δ37N-encoded p20 but not wt VACV-encoded p25 or the smaller amounts of p20 made during wt VACV infection. Although Z-deficient E3 consistently bound Z-RNA, full-length E3 either failed to bind or was bound to Z-

RNA in a way that prevented access by Z-NA-specific antibody. To distinguish between these possibilities, we utilized flow cytometry to detect free Z-RNA in permeabilized DNase-treated SVEC4-10 cells that were either deficient in ZBP1 (EV), or reconstituted with wt ZBP1 or ZBP1mut Z1/Z2 (Sridharan et al., 2017). These experiments revealed an increase in fluorescent signal following infection with E3-Z-deficient mutant virus, but only in ZBP1mutZ1/Z2 cells (Figure S2E-G). Both frequency of Z-RNA-positive cells and median fluorescence intensity were reduced in ZBP1-expressing cells, suggesting that wt VACV-encoded E3 or cellular ZBP1 occlude access of anti-Z-NA-specific antibody depending on Z function. Most importantly, these data strongly reinforce a mechanism where Z-deficient E3 binds to dsRNA, exposing ZRNA that promotes recruitment of ZBP1 to trigger virus-induced necroptosis.

Equivalence of Z-NA binding family Z substitutions in suppressing necroptosis. A conserved structure is characteristic of the Z family consisting of a helix-turn-helix motif with an additional β-sheet (Rich and Zhang, 2003) even though minimal sequence identity is retained outside of amino acids that make contact with Z-NA (Figure 3-6A). Given evidence that E3 Z sequestered Z-RNA from ZBP1, we sought to determine the capacity of Z from other family members to substitute for E3 Z. Prior studies revealed substitution of E3 Z with either Z1 from murine ZBP1 or Z from human ADAR1 fully complemented pathogenesis (Brandt et al., 2005; Kim et al., 2003; White and Jacobs, 2012). Virulence correlated with the ability of E3 to bind Z-NA (Kim et al., 2003). Here, substitution of mouse ZBP1 Z1 (E3ZmZBP1) or human ADAR1 Z (E3ZhADAR1) restored type I IFN resistance (Figure 3-6B), restricted loss of viability (Figure 3-6C) and blocked MLKL activation (Figure 3-6D). These data further implicate the function of Z within E3 as a competitor and critical suppressor of VACV-induced necroptosis.

Figure 6

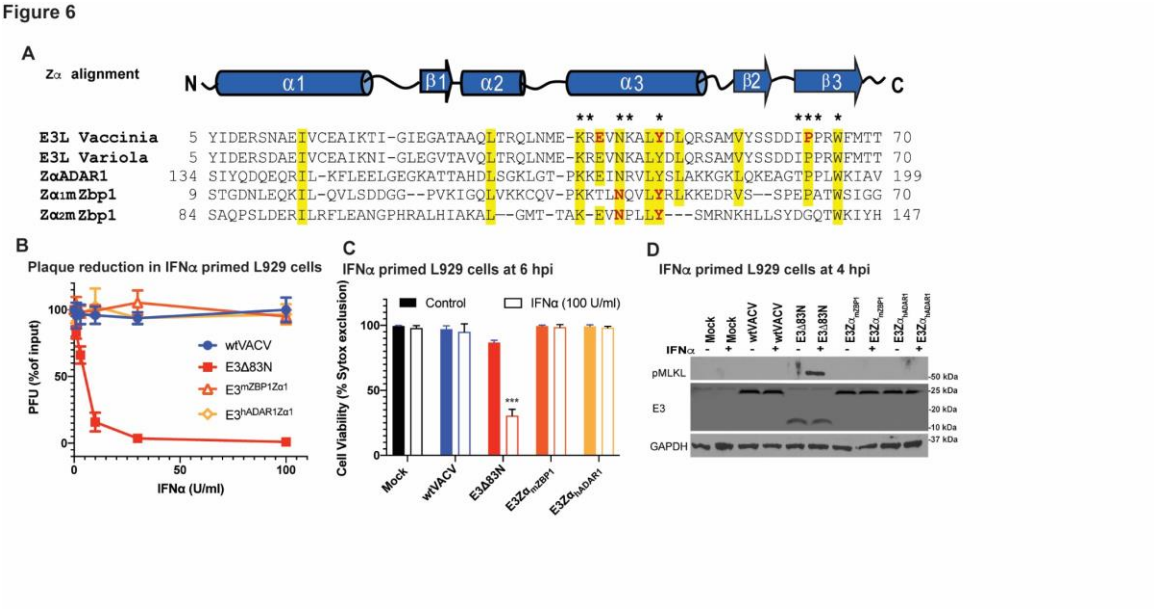

Figure 3-6. Equivalence of Z-NA Binding Family Z Substitutions in Suppressing Necroptosis. (A) Sequence alignment of the Za of VACV E3, variola E3, hADAR1 and mouse Z1 and Z2. Yellow signifies >70% sequence identity, amino acids with an asterisk above are known to be required for ZNA binding and those in red have been targeted by point mutations (Kim et al., 2004; Kim et al., 2003). The GenBank accession numbers for the various sequences are as follows: AAA02759 (vaccinia virus); NP_042088 (variola virus); ADAR 1 (Homo sapiens): AAB06697; ZBP1 (Mus musculus): NP_067369 (B) Plaque reduction assays using Z chimeric viruses were performed on IFNα-primed L929 cells as described in Figure 1. (C) L929 cells left untreated or treated with IFN for 18hr and subsequently infected at a MOI of 5 with the indicated viruses. Cell viability was determined at 6 hpi using by Sytox dye exclusion as described in Figure 1. (D) IB of L929 cell lysates from cells either left untreated or IFNα-pretreated as described in Figure 1 and then infected with a MOI of 5 with the indicated viruses. Lysates were harvested at 4 hpi, subjected to SDS-PAGE and evaluated for phospho-MLKL. Error bars represent the SD. Statistical significance was determined as described in Figure 1. Each set of data is representative of three replicates except for panel B and C which compiles the results of the replicates. Statistical significance was determined as described in Figure 3-1.

Discussion

ZBP1-dependent necroptosis is a critical antiviral pathway that plays out against DNA viruses as well as the dsRNA virus IAV. Suppression of virus-induced necroptosis provides a survival advantage for replicating VACV and supports pathogenesis in mice. The importance of blocking cell death pathways during poxvirus infection first emerged from studies showing the caspase inhibitor B13R sensitizes to TNF-dependent necroptosis (Chan et al., 2003; Cho et al., 2009; Li and Beg, 2000) as well as an earlier report suggesting that dsRNA triggers apoptosis during infections with E3-deficient VACV (Kibler et al., 1997). Upon detailed study, virus lacking the E3 Z-NA binding domain (Koehler et al., 2017) revealed the importance of virus-induced necroptosis (ZBP1& RIPK3 & MLKL) during VACV infection. Here, we have shown this pathway relies on ZBP1 sensing of Z-RNA in infected cells and requires the E3 dsRBD. Both the N terminal Z-NA and C-terminal A-RNA binding domains are retained and clearly important to the biology of a wide range of orthopoxviruses, including the human smallpox virus, variola, in addition to vaccinia strains. Suppression of PKR is also important in all of these poxviruses; however, suppression of necroptosis proceeds independently of PKR. VACV E3 suppresses virus-induced necroptosis by competing with ZBP1 sensing of virus-induced Z-RNA. E3 has no impact on TNF-induced necroptosis (TNF, TNFR1, RIPK1, RIPK3, MLKL). As with other virus-induced death settings (Guo et al., 2018; Kaiser et al., 2013; Koehler et al., 2017; Nogusa et al., 2016; Shubina et al., 2020; Upton and Chan, 2014; Upton et al., 2010, 2012), ZBP1dependent necroptosis does not require either TNF signaling or RIPK1 (Koehler et al., 2017).

VACV E3 has long been recognized as a suppressor of PKR and other dsRNA-dependent antiviral mediators via its C-terminal dsRBD (Jacobs et al., 2009; Rahman and McFadden, 2020). Here, E3 emerges as a promiscuous RNA binding protein, relying on its A-RNA interaction dictated by the C-terminal region as well as an N-terminal Z domain to interact with Z-RNA and prevent activation of ZBP1. Induction of necroptosis in the absence of E3 Z appears to hinge upon recruitment of the host-encoded sensor ZBP1 via Z2 sensing of newly

transcribed Z-RNA that accumulates shortly after infection. The process depends on the interaction of the E3 dsRBD with A-form RNA in a way that promotes Z-RNA character that is recognized as a PAMP by ZBP1. While a complete understanding will require structural studies, this scenario is supported by our demonstration of an RNA bridge between Z-deficient E3 and ZBP1 prior to induction of necroptosis as well as the reduction of cytosolic Z-RNA signal following protease treatment of fixed infected cells. The presence of E3 Z-deficient p20:Z-RNA complexes in E3 Z mutant-infected cells, but not in wt VACV-infected cells, supports a model where the A-RNA:protein complex promotes formation of the appropriate Z-NA-character PAMP. Full-length E3 seems to rely on its Z-NA binding domain to prevent ZBP1 access. In this way, competitive binding via Z motifs in E3 and ZBP1 apparently dictate Z-RNA accessibility and VACV-associated death or survival outcomes. A-RNA binding proteins, several of which inhibit PKR like E3, are expressed by many DNA viruses as well as IAV and may be involved in the induction of Z-RNA that triggers this pathway in other systems.

The mechanism described here, as previously (Koehler et al., 2017), relied on necroptosis sensitive cells as well as infections of mice. Many common cell lines that have been employed for VACV lack necroptosis machinery present in mice as well as in cell lines used in our studies. While the possible consequences of E3:ZBP1 competition has been evident in mouse pathogenesis studies (Brandt et al., 2005; Brandt and Jacobs, 2001; White and Jacobs, 2012), a focus on modulation of PKR function prevailed because this activity predominates in necroptosis-insensitive cells (Jacobs et al., 2009; Rahman and McFadden, 2020). The Nterminal, Z-function long recognized as biologically significant from in vivo studies of virulence in mice can now be attributed to suppression of necroptosis. When cells are competent, ZBP1dependent cell death predominates as an early event in the virus replication cycle, proceeding in a PKR-independent manner. Some cell types, like SVEC4-10 endothelial cells, express constitutive ZBP1; whereas, other cell types, such as the L929 fibroblasts, require IFN-priming to induce sufficient ZBP1 to support the necroptotic pathway. It is likely that both are important in the physiological response to virus infection against viruses but as likely to vary between viruses. For

example, the type I IFN response does not impact the restriction of MCMV replication through unleashed necroptosis (Upton et al., 2010, 2012); whereas, IFN has been central to the observations with IAV (Samir et al., 2020). Our work emphasizes both the importance of the Z-RNA sensing pathway and the crucial contribution made by a viral competitor of Z-RNA PAMP recognition. The importance of this PAMP in a growing number of DNA and RNA viruses combined with the various mechanisms that DNA viruses have adopted to suppress sensing, signaling and execution of cell death pathways reinforce the importance of this innate immune pathway in host defense.

E3 suppression of necroptosis is critical to VACV infection. ZBP1 represents a potent host defense pathway poised to cut short infection by driving the death of cells early in infection. ZRNA-triggered, ZBP1-mediated cell death described here for E3 mutant VACV has been observed in other viruses, including herpesviruses and IAV (Guo et al., 2018; Kesavardhana et al., 2020; Maelfait et al., 2017; Sridharan et al., 2017; Zhang et al., 2020). ZBP1 has also been implicated as a trigger of broad cell death outcomes in nonviral IFN-stimulated settings such as in RIPK1-deficient cells (Ingram et al., 2019; Yang et al., 2020). Orthopoxvirus E3 suppresses virus-induced necroptosis through a competition for the PAMP rather than by RHIM-signaling suppression characterized in herpesviruses (Guo et al., 2018; Upton et al., 2010). Recently the viral inducer of RIPK3 degradation (vIRD) was identified in coxpox and was shown to regulate virus-induced inflammation and pathogenesis (Liu et al., 2021). Other poxviruses that typically lack E3 institute a block to this same pathway at the downstream execution stage of MLKL activation (Petrie et al., 2019). Thus, poxviruses have evolved several distinct mechanisms to escape the consequences of necroptosis and other programmed death pathways.

It has long been known from genetic studies that VACV E3 Z confers type I IFN resistance as well as virulence in mice (Brandt et al., 2005; Brandt and Jacobs, 2001; White and Jacobs, 2012). Similarly, this capacity has been tied to Z-NA binding (Kim et al., 2003). We now recognize that Z-NA binding by E3 is crucial for prevention of necroptosis, a mechanism that involves competition with type I IFN-regulated ZBP1. Unquestionably, our data demonstrate that

the induction of necroptosis by Z-deficient mutants of VACV relies on a mechanism where the dsRBD associates with newly transcribed RNA, inducing Z-NA character that acts as a PAMP to recruit and bridge to ZBP1. In the course of this recruitment, ZBP1 triggers RIPK3 to mediate the activation of MLKL followed by execution of cell death.

Acknowledgments

We thank Liliana Hongyan Guo, Ph.D. and Hernandez-Villalobos for assistance as well as other laboratory members for helpful discussions. PHS grants from NIH supported this work (R01 AI095394 to BLJ, R01 AI135025 to SB, R01 AI020211 to ESM, 2R56DK074731-08A1 and R01DK074731 to DK). This research was supported by the Emory University School of Medicine Flow Cytometry Core and by NIH Cancer Center Support Grant P30CA006927 awarded to Fox-Chase Cancer Center.

References

1. Arndt, W., Mitnik, C., Denzler, K.L., White, S., Waters, R., Jacobs, B.L., Rochon, Y., Olson, V.A., Damon, I.K., and Langland, J.O. (2012). In vitro characterization of a nineteenth-century therapy for smallpox. PLoS One 7, e32610.
2. Arndt, W.D., White, S.D., Johnson, B.P., Huynh, T., Liao, J., Harrington, H., Cotsmire, S., Kibler, K.V., Langland, J., and Jacobs, B.L. (2016). Monkeypox virus induces the synthesis of less dsRNA than vaccinia virus, and is more resistant to the anti-poxvirus drug, IBT, than vaccinia virus. Virology 497, 125-135.
3. Brandt, T., Heck, M.C., Vijaysri, S., Jentarra, G.M., Cameron, J.M., and Jacobs, B.L. (2005). The N-terminal domain of the vaccinia virus E3L-protein is required for neurovirulence, but not induction of a protective immune response. Virology 333, 263-270.

4. Brandt, T.A., and Jacobs, B.L. (2001). Both carboxy- and amino-terminal domains of the vaccinia virus interferon resistance gene, E3L, are required for pathogenesis in a mouse model. J Virol 75, 850-856.

5. Brown, B.A., 2nd, Lowenhaupt, K., Wilbert, C.M., Hanlon, E.B., and Rich, A. (2000). The Zalpha domain of the editing enzyme dsRNA adenosine deaminase binds left-handed Z-RNA as well as Z-DNA. Proc Natl Acad Sci U S A 97, 13532-13536.

6. Chan, F.K., Shisler, J., Bixby, J.G., Felices, M., Zheng, L., Appel, M., Orenstein, J., Moss, B., and Lenardo, M.J. (2003). A role for tumor necrosis factor receptor-2 and receptor-interacting protein in programmed necrosis and antiviral responses. J Biol Chem 278, 51613-51621. Chang, H.W., and Jacobs, B.L. (1993). Identification of a conserved motif that is necessary for binding of the vaccinia virus E3L gene products to double-stranded RNA. Virology 194, 537547.

7. Chang, H.W., Uribe, L.H., and Jacobs, B.L. (1995). Rescue of vaccinia virus lacking the E3L gene by mutants of E3L. J Virol 69, 6605-6608.

8. Chang, H.W., Watson, J.C., and Jacobs, B.L. (1992). The E3L gene of vaccinia virus encodes an inhibitor of the interferon-induced, double-stranded RNA-dependent protein kinase. Proc Natl Acad Sci U S A 89, 4825-4829.

9. Cho, Y.S., Challa, S., Moquin, D., Genga, R., Ray, T.D., Guildford, M., and Chan, F.K. (2009). Phosphorylation-driven assembly of the RIP1-RIP3 complex regulates programmed necrosis and virus-induced inflammation. Cell 137, 1112-1123.

10. Condit, R.C., and Niles, E.G. (2002). Regulation of viral transcription elongation and termination during vaccinia virus infection. Biochim Biophys Acta 1577, 325-336.

11. Cresawn, S.G., Prins, C., Latner, D.R., and Condit, R.C. (2007). Mapping and phenotypic analysis of spontaneous isatin-beta-thiosemicarbazone resistant mutants of vaccinia virus. Virology 363, 319-332.

12. Daley-Bauer, L.P., Roback, L., Crosby, L.N., McCormick, A.L., Feng, Y., Kaiser, W.J., and Mocarski, E.S. (2017). Mouse cytomegalovirus M36 and M45 death suppressors

cooperate to prevent inflammation resulting from antiviral programmed cell death pathways. Proc Natl Acad Sci U S A 114, E2786-E2795.

13. DeFilippis, V.R., Alvarado, D., Sali, T., Rothenburg, S., and Fruh, K. (2010). Human cytomegalovirus induces the interferon response via the DNA sensor ZBP1. J Virol 84, 585-598.

14. Duesberg, P.H., and Colby, C. (1969). On the biosynthesis and structure of double-stranded RNA in vaccinia virus-infected cells. Proc Natl Acad Sci U S A 64, 396-403.

15. Guo, H., Gilley, R.P., Fisher, A., Lane, R., Landsteiner, V.J., Ragan, K.B., Dovey, C.M., Carette,

16. J.E., Upton, J.W., Mocarski, E.S., et al. (2018). Species-independent contribution of ZBP1/DAI/DLM-1-triggered necroptosis in host defense against HSV1. Cell Death Dis 9, 816.

17. Guo, H., Omoto, S., Harris, P.A., Finger, J.N., Bertin, J., Gough, P.J., Kaiser, W.J., and Mocarski, E.S. (2015). Herpes simplex virus suppresses necroptosis in human cells. Cell Host & Microbe 17, 243-251.

18. Ha, S.C., Lokanath, N.K., Van Quyen, D., Wu, C.A., Lowenhaupt, K., Rich, A., Kim, Y.G., and Kim, K.K. (2004). A poxvirus protein forms a complex with left-handed Z-DNA: crystal structure of a Yatapoxvirus Zalpha bound to DNA. Proc Natl Acad Sci U S A 101, 14367-14372.

19. Ingram, J.P., Thapa, R.J., Fisher, A., Tummers, B., Zhang, T., Yin, C., Rodriguez, D.A., Guo, H., Lane, R., Williams, R., et al. (2019). ZBP1/DAI drives RIPK3-mediated cell death induced by IFNs in the absence of RIPK1. J Immunol 203, 1348-1355.

20. Jacobs, B.L., Langland, J.O., Kibler, K.V., Denzler, K.L., White, S.D., Holechek, S.A., Wong, S., Huynh, T., and Baskin, C.R. (2009). Vaccinia virus vaccines: past, present and future. Antiviral Res 84, 1-13.

21. Kaiser, W.J., Upton, J.W., Long, A.B., Livingston-Rosanoff, D., Daley-Bauer, L.P., Hakem, R., Caspary, T., and Mocarski, E.S. (2011). RIP3 mediates the embryonic lethality of caspase-8deficient mice. Nature 471, 368-372.

22. Kaiser, W.J., Upton, J.W., and Mocarski, E.S. (2008). Receptor-interacting protein homotypic interaction motif-dependent control of NF-kappa B activation via the DNA-dependent activator of IFN regulatory factors. J Immunol 181, 6427-6434.

23. Kaiser, W.J., Upton, J.W., and Mocarski, E.S. (2013). Viral modulation of programmed necrosis. Cur Opin Virol 3, 296-306.

24. Kesavardhana, S., Malireddi, R.K.S., Burton, A.R., Porter, S.N., Vogel, P., Pruett-Miller, S.M., and Kanneganti, T.D. (2020). The Zalpha2 domain of ZBP1 is a molecular switch regulating influenza-induced PANoptosis and perinatal lethality during development. J Biol Chem 295, 8325-8330.

25. Kibler, K.V., Shors, T., Perkins, K.B., Zeman, C.C., Banaszak, M.P., Biesterfeldt, J., Langland, J.O., and Jacobs, B.L. (1997). Double-stranded RNA is a trigger for apoptosis in vaccinia virusinfected cells. J Virol 71, 1992-2003.

26. Kim, Y.G., Lowenhaupt, K., Oh, D.B., Kim, K.K., and Rich, A. (2004). Evidence that vaccinia virulence factor E3L binds to Z-DNA in vivo: Implications for development of a therapy for poxvirus infection. Proc Natl Acad Sci U S A 101, 1514-1518.

27. Kim, Y.G., Muralinath, M., Brandt, T., Pearcy, M., Hauns, K., Lowenhaupt, K., Jacobs, B.L., and Rich, A. (2003). A role for Z-DNA binding in vaccinia virus pathogenesis. Proc Natl Acad Sci U S A 100, 6974-6979.

28. Koehler, H., Cotsmire, S., Langland, J., Kibler, K.V., Kalman, D., Upton, J.W., Mocarski, E.S., and Jacobs, B.L. (2017). Inhibition of DAI-dependent necroptosis by the Z-DNA binding domain of the vaccinia virus innate immune evasion protein, E3. Proc Natl Acad Sci U S A 114, 1150611511.

29. Kuriakose, T., Man, S.M., Malireddi, R.K., Karki, R., Kesavardhana, S., Place, D.E., Neale, G., Vogel, P., and Kanneganti, T.D. (2016). ZBP1/DAI is an innate sensor of

influenza virus triggering the NLRP3 inflammasome and programmed cell death pathways. Sci Immunol 1. Li, M., and Beg, A.A. (2000). Induction of necrotic-like cell death by tumor necrosis factor alpha and caspase inhibitors: novel mechanism for killing virus-infected cells. J Virol 74, 7470-7477.

30. Liu, Z., Nailwal, H., Rector, J., Rahman, M.M., Sam, R., McFadden, G., and Chan, F.K. (2021). A class of viral inducer of degradation of the necroptosis adaptor RIPK3 regulates virus-induced inflammation. Immunity 54, 247-258 e247.

31. Maelfait, J., Liverpool, L., Bridgeman, A., Ragan, K.B., Upton, J.W., and Rehwinkel, J. (2017). Sensing of viral and endogenous RNA by ZBP1/DAI induces necroptosis. EMBO J 36, 25292543.

32. Mandal, P., Berger, S.B., Pillay, S., Moriwaki, K., Huang, C., Guo, H., Lich, J.D., Finger, J., Kasparcova, V., Votta, B., et al. (2014). RIP3 induces apoptosis independent of pronecrotic kinase activity. Mol Cell 56, 481-495.

33. Mocarski, E.S., Guo, H., and Kaiser, W.J. (2015). Necroptosis: The Trojan horse in cell autonomous antiviral host defense. Virology 479-480, 160-166.

34. Mocarski, E.S., Upton, J.W., and Kaiser, W.J. (2011). Viral infection and the evolution of caspase 8-regulated apoptotic and necrotic death pathways. Nat Rev Immunol 12, 79-88.

35. Nogusa, S., Thapa, R.J., Dillon, C.P., Liedmann, S., Oguin, T.H., 3rd, Ingram, J.P., Rodriguez,

36. D.A., Kosoff, R., Sharma, S., Sturm, O., et al. (2016). RIPK3 activates parallel pathways of MLKL-driven necroptosis and FADD-mediated apoptosis to protect against Influenza A Virus. Cell host & microbe 20, 13-24.

37. Petrie, E.J., Sandow, J.J., Lehmann, W.I.L., Liang, L.Y., Coursier, D., Young, S.N., Kersten, W.J.A., Fitzgibbon, C., Samson, A.L., Jacobsen, A.V., et al. (2019). Viral MLKL homologs subvert necroptotic cell death by sequestering cellular RIPK3. Cell Rep 28, 3309-3319 e3305.

38. Pham, T.H., Kwon, K.M., Kim, Y.E., Kim, K.K., and Ahn, J.H. (2013). DNA sensing-independent inhibition of herpes simplex virus 1 replication by DAI/ZBP1. J Virol 87, 3076-3086. Placido, D., Brown, B.A., 2nd, Lowenhaupt, K., Rich, A., and Athanasiadis, A. (2007). A lefthanded RNA double helix bound by the Zalpha domain of the RNA-editing enzyme ADAR1. Structure 15, 395-404.

39. Rahman, M.M., and McFadden, G. (2020). Myxoma virus-encoded host range protein M029: A multifunctional antagonist targeting multiple host antiviral and innate immune pathways. Vaccines (Basel) 8, 244.

40. Rich, A., and Zhang, S. (2003). Timeline: Z-DNA: the long road to biological function. Nat Rev Genet 4, 566-572.

41. Samir, P., Malireddi, R.K.S., and Kanneganti, T.D. (2020). The PANoptosome: A deadly protein complex driving pyroptosis, apoptosis, and necroptosis (PANoptosis). Front Cell Infect Microbiol 10, 238.

42. Schonborn, J., Oberstrass, J., Breyel, E., Tittgen, J., Schumacher, J., and Lukacs, N. (1991). Monoclonal antibodies to double-stranded RNA as probes of RNA structure in crude nucleic acid extracts. Nucleic Acids Res 19, 2993-3000.

43. Schwartz, T., Behlke, J., Lowenhaupt, K., Heinemann, U., and Rich, A. (2001). Structure of the DLM-1-Z-DNA complex reveals a conserved family of Z-DNA-binding proteins. Nat Struct Biol 8, 761-765.

44. Shors, T., Kibler, K.V., Perkins, K.B., Seidler-Wulff, R., Banaszak, M.P., and Jacobs, B.L. (1997). Complementation of vaccinia virus deleted of the E3L gene by mutants of E3L. Virology 239, 269-276.

45. Shubina, M., Tummers, B., Boyd, D.F., Zhang, T., Yin, C., Gautam, A., Guo, X.J., Rodriguez, D.A., Kaiser, W.J., Vogel, P., et al. (2020). Necroptosis restricts influenza A virus as a standalone cell death mechanism. J Exp Med 217, e20191259.

46. Sridharan, H., Ragan, K.B., Guo, H., Gilley, R.P., Landsteiner, V.J., Kaiser, W.J., and Upton, J.W. (2017). Murine cytomegalovirus IE3-dependent transcription is required for DAI/ZBP1mediated necroptosis. EMBO Rep 18, 1429-1441.

47. Staiano-Coico, L., Stollar, B.D., Darzynkiewicz, Z., Dutkowski, R., and Weksler, M.E. (1985). Binding of anti-Z-DNA antibodies in quiescent and activated lymphocytes: relationship to cell cycle progression and chromatin changes. Mol Cell Biol 5, 3270-3273.

48. Sun, L., Wang, H., Wang, Z., He, S., Chen, S., Liao, D., Wang, L., Yan, J., Liu, W., Lei, X., et al. (2012). Mixed lineage kinase domain-like protein mediates necrosis signaling downstream of RIP3 kinase. Cell 148, 213-227.

49. Takaoka, A., Wang, Z., Choi, M.K., Yanai, H., Negishi, H., Ban, T., Lu, Y., Miyagishi, M., Kodama, T., Honda, K., et al. (2007). DAI (DLM-1/ZBP1) is a cytosolic DNA sensor and an activator of innate immune response. Nature 448, 501-505.

50. Thapa, R.J., Ingram, J.P., Ragan, K.B., Nogusa, S., Boyd, D.F., Benitez, A.A., Sridharan, H., Kosoff, R., Shubina, M., Landsteiner, V.J., et al. (2016). DAI senses influenza A virus genomic RNA and activates RIPK3-dependent cell death. Cell Host Microbe 20, 674-681.

51. Upton, J.W., and Chan, F.K. (2014). Staying alive: cell death in antiviral immunity. Mol Cell 54, 273-280.

52. Upton, J.W., Kaiser, W.J., and Mocarski, E.S. (2010). Virus inhibition of RIP3-dependent necrosis. Cell Host Microbe 7, 302-313.

53. Upton, J.W., Kaiser, W.J., and Mocarski, E.S. (2012). DAI/ZBP1/DLM-1 complexes with RIP3 to mediate virus-induced programmed necrosis that is targeted by murine cytomegalovirus vIRA. Cell Host Microbe 11, 290-297.

54. Weber, F., Wagner, V., Rasmussen, S.B., Hartmann, R., and Paludan, S.R. (2006). Doublestranded RNA is produced by positive-strand RNA viruses and DNA viruses but not in detectable amounts by negative-strand RNA viruses. J Virol 80, 5059-5064.

55. White, S.D., and Jacobs, B.L. (2012). The amino terminus of the vaccinia virus E3 protein is necessary to inhibit the interferon response. J Virol 86, 5895-5904.

56. Yang, D., Liang, Y., Zhao, S., Ding, Y., Zhuang, Q., Shi, Q., Ai, T., Wu, S.Q., and Han, J. (2020). ZBP1 mediates interferon-induced necroptosis. Cell Mol Immunol 17, 356-368.

57. Zhang, T., Yin, C., Boyd, D.F., Quarato, G., Ingram, J.P., Shubina, M., Ragan, K.B., Ishizuka, T., Crawford, J.C., Tummers, B., et al. (2020). Influenza virus Z-RNAs induce ZBP1-mediated necroptosis. Cell 180, 1115-1129 e1113.

CHAPTER 4

E3 MUST INHIBIT DSRNA AND ZRNA FOR VACV TO BE PATHOGENIC IN ANIMAL MODELS AND COMPLEX CELLS

Abstract

Poxviruses such as vaccinia virus (VACV) or monkeypoxvirus (MPXV) make double-stranded RNA (dsRNA) as part of their lifecycle. In order to protect against immune recognition of dsRNA, poxviruses produce the E3 protein which has a C-terminal dsRNA binding domain and a N-terminal Z-form nucleic acid (ZNA) binding domain. The N-terminal ZBD is necessary for pathogenesis *in vivo* by intranasal and intracranial infection. It has been implicated in inhibition of PKR recognition of dsRNA and subsequent eIF2α deactivation. It has also been associated with obstruction of DAI detection of ZNA leading to necroptosis. This study examines how the roles of dsRNA and ZNA inhibition interact in complex cell lines. Furthermore, it studies what nucleic acids might be triggering the innate immune response in animal models after intracranial and intranasal infections.

Introduction

Poxviruses have a broad animal host range and often cause disease in humans. They replicate their large double-stranded DNA genomes in the cytoplasm of infected host cells and produces a double-stranded RNA (dsRNA) byproduct at late times post infection (49, 50). Because dsRNA can be readily detected by the innate immune system, poxviruses evolved means to evade detection. Vaccinia virus (VACV) produces the protein E3 which is necessary for type 1 Interferon (IFN) resistance in cells and animal models (162, 178). Host cells can be primed with IFN to up-regulate innate immune proteins that detect viral nucleic acids (181). The E3 protein has two nucleic acid binding domains, a dsRNA binding domain in the C-terminus and a Z-form nucleic acid binding domain (ZBD) in the N-terminus (158, 170). The C-terminus indispensably conceals dsRNA from detection by the host cells both *in vitro* and *in vivo* (160, 189).

Monkeypox (MPXV), an emerging orthopox virus, has a naturally occurring N-terminal truncation of its VACV E3 homologue protein, F3 (167). Despite this mutation, it is highly transmissible and can cause severe disease in humans and small rodents like prairie dogs (175, 190). In order to understand how the virus may be pathogenic in humans despite this mutation, MPXV was compared to VACV E3 N-terminal deletion mutants. Vaccinia E3's N-terminus must remain in-tact for pathogenesis by intranasal and intracranial injections in wild-type mouse models (160, 191). Pathogenesis of N-terminal deletion VACV mutants was restored in mice with the IFN receptor knocked out demonstrating that the N-terminus is also involved in IFN resistance (76). Mechanistic studies in HeLa cells and demonstrated that an interferon-induced dsRNA binding protein, protein kinase receptor (PKR), was activated during infection with VACV mutants deleted of E3's N-terminus (189). Additionally, in mouse embryonic fibroblasts (MEFs) PKR was necessary to inhibit viral replication of VACV E3 N-terminal mutants after stimulating the cells with IFN (76). However, unlike in the IFN receptor knock out mice, in mice with PKR knocked replication of VACV N-terminal deletion mutants was attenuated compared to wild-type (76). MPXV does not lead to produces less dsRNA than VACV (173). Reduction of dsRNA in VACV E3 N-terminal deletion mutants was sufficient to rescue growth in cells with PKR-dependent inhibition (Chapter 2).

More recently, data has emerged implicating the cell death pathway necroptosis in inhibition of VACV E3 N-terminal deletion viruses (130). Necroptosis is a rapid, inflammatory cell death that occurs when the mixed lineage kinase domain like protein (MLKL) forms holes in the cell membrane (124, 126). MLKL activation follows activation of proteins containing RIP homotypic interaction motif (RHIM) domains such as RIP1 and RIP3 (192, 193). In VACV E3 N-terminal deletion viruses, DNA-induced activator of IFN (DAI) activates RIP3 through their RHIM domains leading to necroptosis (130). Like VACV's E3 protein, DAI contains a ZBD, and further studies demonstrated that ZNA not dsRNA is the nucleic acid responsible for its activation (131, 170).

These studies reveal that the N-terminus may be involved in the masking of multiple nucleic acids throughout the course of a VACV infection. MPXV can evade detection by PKR but not by DAI (10, Chapter 3). Previous studies show MPXV produces less dsRNA than VACV (15). Like MPXV, reduction of dsRNA in VACV E3 N-terminal deletion mutants was sufficient to rescue growth in cells with PKR-dependent inhibition, but not in cells with necroptosis-dependent inhibition (Chapter 2 & Chapter 3). Because of these conflicting phenotypes, we hypothesized that in complex cells and animal models both pathways must be inhibited for VACV E3 N-terminal deletion mutants to grow. In this study we compared the phenotypes of the cells involved in these studies and looked at pathogenesis *in vivo* to further elucidate what may be happening with MPXV.

Materials and Methods

Cells. L929 cells were maintained in Eagle's Minimal Essential Medium (MEM, Cellgro) supplemented with 5% fetal bovine serum (FBS, HyClone). BSC 40 cells were maintained in Dulbecco's Modified-Minimal Essential Medium (DMEM, Cellgro) supplemented with 5% FBS. MEFs (129/SV background) were generated from embryos as previously described (76) and were maintained in DMEM supplemented with 10% heat-inactivated FBS (HI FBS). FBS was heat-inactivated by incubation at 56°C for 30 minutes. JC (murine adenocarcinoma) cells were maintained in Roswell Park Memorial Institute medium (RPMI, ATCC) supplemented with 10% HI FBS. All cells were incubated at 37°C in the presence of 5% CO_2.

Small molecules. For IFN treatment, cells were pre-treated with 1000 units of recombinant mouse α-interferon at 37°C for 18 hours. Chemical induction of necroptosis was conducted by pre-treating cells for 1 hour with zVAD-FMK (ZVD) (ApexBio) at 50 μM followed by addition of mouse TNF-α (Sigma) at 20 ng/mL as previously described (106, 147). Inhibition of RIP3 or RIP1 was accomplished though treatment with 10μM GSK 872 or 10μM GSK 963 respectively for 1 hour prior to infection or treatment and with media overlay (127, 147). Istatin β-

thiosemicarbazome (IBT) was used to increase dsRNA made by VACV and select for low dsRNA producing mutants as previously described (186, 187).

Viruses. The vaccinia virus Western Reserve strain (VACV) was used throughout this study with the unmodified virus designated VACV WT. VACV containing a 37 amino acid N-terminal truncation of E3 (VACV E3Δ37N) was generated as previously described (162). VACV E3Δ37N with reduced dsRNA were generated by picking plaques in the presence of IBT and propagating virus. Viruses confirmed to have reduced dsRNA were designated VACV E3Δ37N IBTR3 and VACV E3Δ37N IBTR7. VACV with a wild-type E3 and mutation in the A24R gene confirmed to give low dsRNA (VACV mutA24) were a generous gift from Richard Condit's lab (186, 187). Monkeypox virus Walter Reed 267 strain (MPXV), was used in this study. VACV where the E3 protein has been replaced with its MPXV homologue, F3 (VACV ΔE3::MPXV F3), was generated as previously described (167).

Growth kinetics. Cells were seeded in 12 well plates to be 80% confluent at the time of infection. For multi-step kinetics, cells were infected with an MOI of 0.01 of the indicated virus for 1 hour then washed 3 times with warm media before the overlay with growth medium. Infected cells were incubated under normal growth conditions until they were harvested by scraping into media at the indicated times. After subjecting samples to three freeze-thaw cycles, the titers of VACV, the VACV recombinants, and MPXV were determined by plaquing in the permissive cell line, BSC 40. Single-step kinetics were done using the same protocol except that an MOI of 5 was used. When necroptosis inhibitor GSK 872 was used, cells were pre-treated by adding inhibitor to a final concentration of 10μM for 1 hour prior to infection. The media overlay included 10μM GSK 872 where indicated.

Cell death assays. Cell death assays were conducted using propidium iodide exclusion measured by fluorescence imaging or CellTiter-Glo (CTG, Promega). For both assays, cells were plated to 80% confluency before treatment or infection. Cells were infected for 1 hour at MOI 5 before overlay with media. Lysates for CellTiter-Glo were harvested at 18 hours post-infection or 18 hours post-treatment and measured using the manufacturer's protocol. For dye exclusion,

Hoechst 33342 {2′-[4-ethoxyphenyl]-5-[4-methyl-1-piperazinyl]-2,5′-bi-1H-benzimidazole} was used as the nuclear stain and propidium iodide as the excluded stain. Fluorescent images were recorded and counted at the indicated times as previously described (147).

MLKL phosphorylation. Cells were plated to be at 80% confluency at time of infection and infected at MOI 5. Lysates were harvested and the western blot was performed as previously described (147).

RT-PCR Methods. RNA was isolated from mock- or IFN-treated cells at 18 h post-treatment using Qiagen's Rneasy Mini Kit. RNA was then reverse transcribed into cDNA using PrimeScript RT reagent kit (Takara). Samples were amplified using PrimeTime Gene Expression Master Mix (IDT) on a CFX Connect Real-Time PCR detection system (BioRad). Primer sets were purchased from IDT.

Mice and *in vivo* infections. Wild-type C57BL/6J were purchased from Jackson Laboratories and were bred and housed by the Arizona State University Department of Animal Care and Technologies (DACT). MLKL KO were received from Dr. Jiahuai at State Key Laboratory of Cellular Stress Biology, School of Life Sciences, Xiamen University. Anesthesia, intracranial, and intranasal infections were carried out according to university Institutional Animal Care and Use Committee (IACUC) regulations as previously described (160). Mice were anesthetized with a 1 µL/kg body weight intraperitoneal injection of ketamine cocktail (KXA) containing 37.5 mg/ml ketamine, 7.5 mg/ml xylazine, and 2.5 mg/ml acepromazine maleate. Before infection, tubes of VACV were blinded by a third party. All MPXV *in vivo* experiments were conducted under BSL3 conditions. For intranasal infections, the left nostril of 5 week old mice were injected with 5(10^5) PFU virus resuspended to10 µL with PBS using a Pipetman and protein loading tip. For intracranial infections, four week old mice were injected in the cranium just left of center with 5(10^4) PFU virus resuspended to 5 µL in PBS using a 30-gauge hypodermic needle with a stopper to normalize needle depth to 3 mm and a 50 µl syringe. All mice were monitored for clinical symptoms on a scale of 0-3 from low to high severity including weight loss, infection of either eye, rapid breathing, hunching, ruffling of fur, sneezing, and malaise. For intracranial

infections, twitching or seizing were also monitored as neurological symptoms. Loss of 10-20% of original weight was scored as 1, 20-30% of original weight lost was scored as 2, and mice who lost more than 30% of weight were euthanized. Clinical score as reported was a total of all categories, and mice who scored higher than 17 were euthanized.

Tissue spread. Tissues were harvested from infected mice euthanized by asphyxiation with CO2 at 65days post infection and frozen rapidly in liquid nitrogen. Tissues were brought to a l0% (wt/vol) suspension with RPMI supplemented with anti-anti (Thermo Fisher Scientific). The samples were homogenized on ice by a mechanical hand homogenizer. Virus was released by two additional cycles of freeze-thaws at -80°C and sonicated. Virus titers were determined by a standard plaque assay using BSC 40 cells.

Statistics. Error bars displayed indicated standard error. Statistical significance was calculated in Excel using a two tailed, unpaired, student's T test. P values are as reported in figures.

Results

Monkeypox's E3 homologue, F3, is naturally truncated at the N-terminus. The E3 homologues of orthopox viruses were aligned using Clustal Omega as shown in Figure 4-1A. The N-terminus is highly conserved among these proteins with the exception of MPXV. MPXV's homologue, F3, has a naturally occurring mutation in its start codon shifting the translated region to the next Methionine codon (M38). This results in a protein truncated by the first 37 amino acids. In order to compare the homologue proteins made by VACV and MPXV, VACV constructs were made by either deleting the first 37 amino acids from E3 (VACV E3Δ37N) or by replacing the entire E3 protein with the MPXV F3 protein (VACV ΔE3::MPXV F3) as shown in Figure 4-1B. We also made VACV more MPXV-like by selecting VACV E3Δ37N for low dsRNA producing mutants (VACV E3Δ37N IBTR3, VACV E3Δ37N IBTR7) (Chapter 2). These viruses were used throughout this study and compared to the controls VACV WT (wild-type virus), MPXV, and VACV mutA24R (VACV mutant with a wild-type E3 locus and mutated A24 protein which produces less dsRNA) whose phenotypes are outlined in Table 4-1.

Figure 4-1: Viruses used in this study

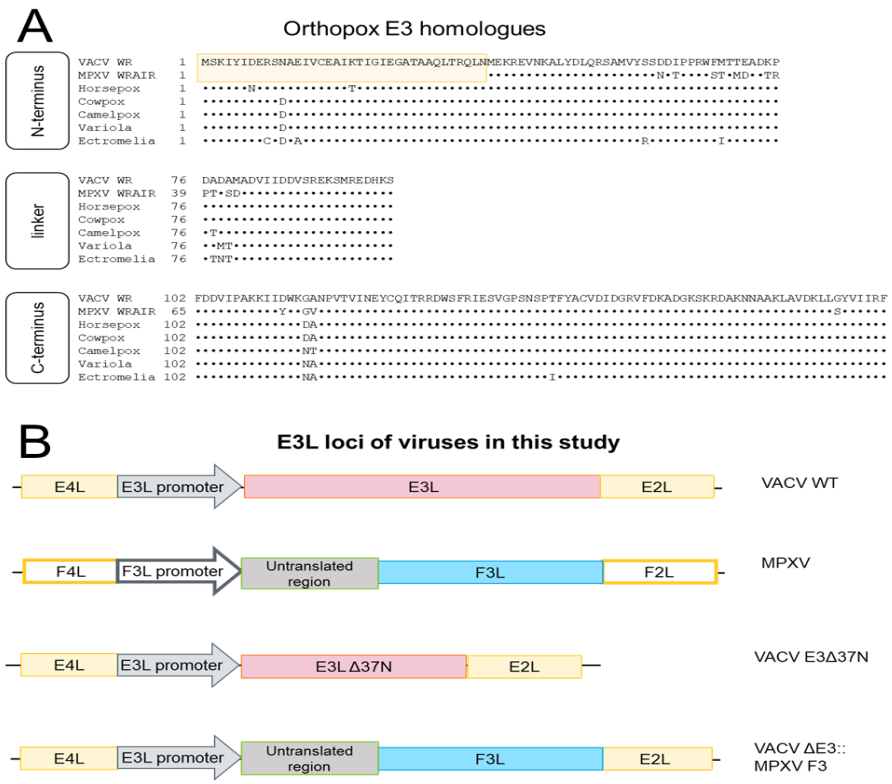

Figure 4-1 Viruses Used in this Study. (A) Alignment of VACV E3 homologues from various orthopox viruses using Clustal Omega. (B) This schematic shows how the E3L gene was deleted from VACV and the MPXV F3L including the naturally occurring untranslated region was added in its place.

Table 4-1 Viruses Used in this Study

	E3 locus	dsRNA produced
VACV WT	WT	High
VACV mutA24	WT	Low
VACV E3Δ37N	N-terminal deletion	High
VACV E3Δ37N IBTR3	N-terminal deletion	Low
VACV E3Δ37N IBTR7	N-terminal deletion	Intermediate
MPXV	N-terminal deficient	Intermediate
VACV ΔE3::MPXV F3	N-terminal deficient	High

VACV E3 N-terminal deficient viruses do not grow in JC cells, but MPXV does. Relative titers of VACV WT, VACV E3Δ37N, and MPXV in BSC 40 (African green monkey kidney cells) and JC (murine mammary adenocarcinoma) cells were determined by plaque assay as demonstrated in Figure 4-2A. JC cells were less permissive than BSC 40 for all viruses, but especially for VACV E3Δ37N. VACV WT had a 10 fold difference in plaquing efficiency and MPXV had a 40 fold difference in plaquing efficiency. On the other hand, VACV E3Δ37N had about a 50,000 fold difference in plaquing efficiency. While relative MPXV titers were slightly lower than VACV WT in JC, this may be due in part to MPXV producing smaller plaques which are more difficult to count. In order to determine if VACV E3Δ37N or MPXV was actually restricted in JC cells, detailed multi-step growth kinetics were assayed in multiple cell lines. Cells were infected with an MOI of 0.01 before harvesting at the indicated times and plaqued in BSC 40 cells because they are permissive for all viruses. Figure 4-2B shows that all viruses grow well in BSC 40. We also assessed VACV ΔE3::MPXV F3 to confirm that MPXV's homologue does not have any gain of function mutations in JC (Figure 4-2C). VACV WT and MPXV both 3 logs, but VACV E3Δ37N and VACV ΔE3::MPXV F3 did not grow. Thus we determined that VACV growth was restricted in E3 N-terminal deficient viruses but not MPXV or VACV WT viruses and that recovery of MPXV growth was not due to unexpected activity of the F3 protein.

Figure 4-2 VACV E3 N-terminal deletion mutants do not grow in JC, but MPXV does

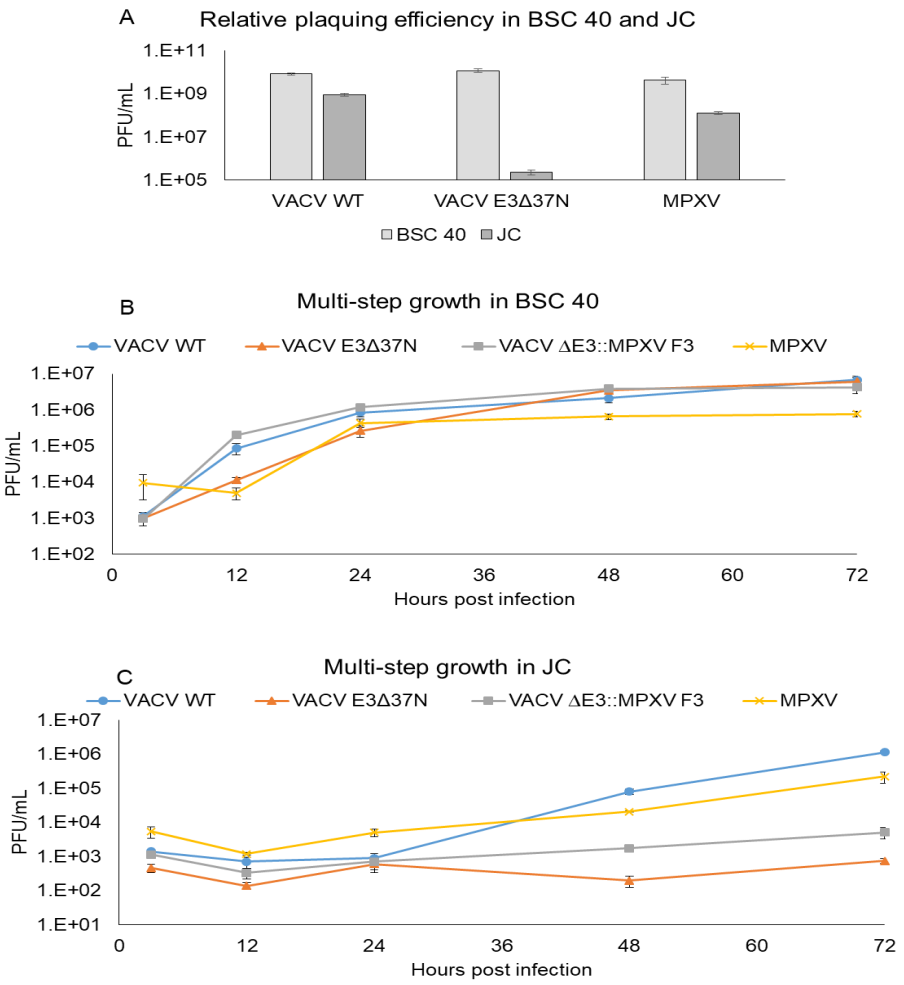

Figure 4-2 VACV E3 N-terminal Deletion Mutants Do Not Grow in JC, but MPXV Does. (A) The relative plaquing efficiency of VACV WT, VACV E3Δ37N, and MPXV in BSC 40 and JC was determined by standard plaque assay using the same titration tubes. (B & C) Multi-step growth curves were conducted by infecting either BSC 40 (B) or JC (C) cells at an MOI of 0.01 with VACV WT, VACV E3Δ37N, VACV ΔE3::MPXV F3, or MPXV and harvesting at 3, 12, 24, 48, and 72 hours post infection. Viruses were titered using BSC 40 since they are permissive for all mutants.

Reduction of dsRNA in VACV E3 N-terminal deletion mutants does not recover growth in JC. Next we sought to determine if VACV E3Δ37N mutants which produce less dsRNA will grow in JC cells as was described in MEF 129 in Chapter 2. First, end-point multi-step growth was analyzed by infecting BSC 40 cells or JC cells with MOI 0.01 of VACV WT, VACV E3Δ37N, VACV E3Δ37N IBTR3 (very low dsRNA) or VACV E3Δ37N IBTR7 (low dsRNA). Viruses were harvested at 3 hours post infection to normalize input and at 72 hours post infection to look for growth by

plaquing in BSC40. While the VACV WT grew about 5 logs in both cell lines, none of the VACV E3Δ37N viruses grew in JC cells regardless of how much dsRNA they produced (Figure 4-3A). All viruses grew well in BSC 40 cells demonstrating the mutations resulting in less production of dsRNA do not substantially affect virus growth kinetics in these cells. Detailed growth kinetics in JC cells were conducted for single-step (Figure 4-3B) and multi-step (Figure 4-3C) growth. In addition to VACV WT, VACV E3Δ37N, and VACV E3Δ37N IBTR (3 and 7) viruses, MPXV and VACV mutA24 were also studied. VACV mutA24 expresses WT E3 while producing very low levels of dsRNA and grows 3 logs in JC cells single-step growth similarly to VACV WT. MPXV grew 3 logs in the single-step growth curve, but took longer, only starting to plateau at 72 hpi and 3 logs of growth.

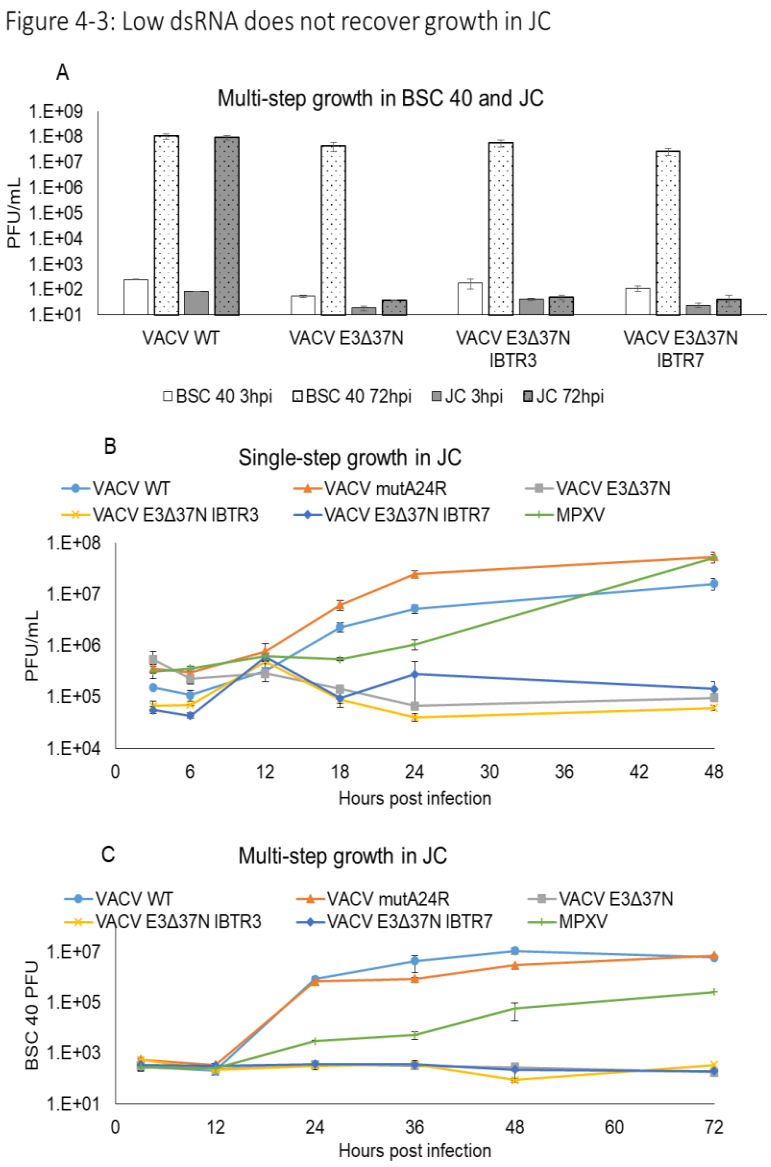

Figure 4-3 Low dsRNA Does Not Recover Growth in JC. (A) BSC 40 or JC cells were infected with VACV WT, VACV E3Δ37N, VACV E3Δ37N IBTR3, or VACV E3Δ37N IBTR7 at an MOI of 0.01 and harvested at 3 or 72 hours post infection (HPI) and titered in BSC 40 cells. (B & C) Detailed JC growth kinetics were assayed for VACV WT, VACV mutA24, VACV E3Δ37N, VACV E3Δ37N IBTR3, VACV E3Δ37N IBTR7, and MPXV with titers measured in BSC 40. For single-step growth kinetics (B), cells were infected with an MOI of 5 and harvested at 3, 6 12, 18, 24, or 48 HPI. For multi-step growth kinetics (C), cells were infected with an MOI of 0.01 and harvested at 3, 12, 24, 36, 48, or 72 HPI.

JC cells produce mRNA necessary for required necroptosis genes and make DAI mRNA constitutively. In order to begin to compare JC, MEF 129, and L929 to determine why there are three different phenotypes for restriction of VACV E3 N-terminal deficient viruses and MPXV, we measured mRNA expression of candidate genes for cellular restriction. Cells were treated with

recombinant mouse interferon-α (IFN) for 18 hours before harvesting RNA for cDNA conversion. Figure 4-4A demonstrates that JC cells and MEF 129 cells constitutively express DAI while it is IFN-dependent in L929. Additionally, MEF 129 only produce PKR when pre-treated with 1000 U IFN whereas JC and L929 express some PKR constitutively express low levels of PKR that are increased with 100 U IFN. All three cell lines produced similar levels of RIP1 and MLKL relative to housekeeping mRNAs, but RIP3 was one log lower in MEF 129 than L929 or JC cells (Figure 4-4B). Unexpectedly, the Western blot for RIP3 expression demonstrated that despite having a lower copy number of mRNA, it is still produced in MEF 129 (Figure 4-4C).

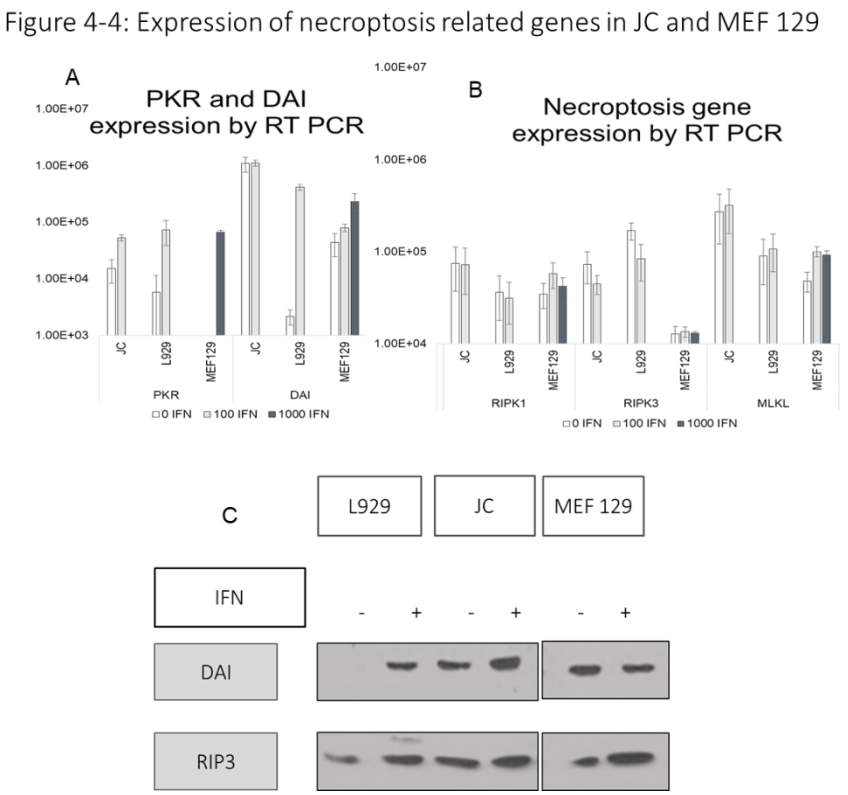

Figure 4-4 Expression of Necroptosis Related Genes in JC and MEF 129. (A & B) RNA was harvested from one million cells 18 hours post treatment with 0, 100, or 1000 units of IFNα. RNA was then converted to cDNA and probed for genes of interest. GAPDH, actin, Ppia, and TBP were used as housekeeping genes and averaged before normalization. Data is shown in relative units. (C) Cells were harvested at 18 hours post treatment with 0 or 1000 U IFNα and proteins were harvested in SDS buffer. Lysates were run on a Western blot and probed for DAI and RIP3.

MEF 129 are not sensitive to cell death by necroptosis inducers or virus. Based on the low RIP3 mRNA profile of MEF 129, we wanted to see if these cells could undergo necroptosis. Cells were pre-treated with 1000 U of IFN 18 hours pre-infection and infected with virus at an MOI 5 and stained with Hoescht and propidium iodide (PI) to look for cell death (Figure 4-5A). There was no detectable death at 12 hours post-infection. Cells were also stimulated with chemical inducers of necroptosis TNF/ZVD and necroptosis inhibitors GSK 872 and GSK 961 and either assayed for mitochondrial activity at 18 hours post-treatment or stained with Hoescht and PI at 36 hours post-treatment with no loss in viability (Figures 4-5B & 4-5C). These data demonstrate that PKR does not restrict growth of VACV E3∆37N through rapid cell death in MEF 129. Additionally, they indicate that MEF 129 may be impervious to cell death.

Figure 4-5 MEF 129 are not sensitive to cell death

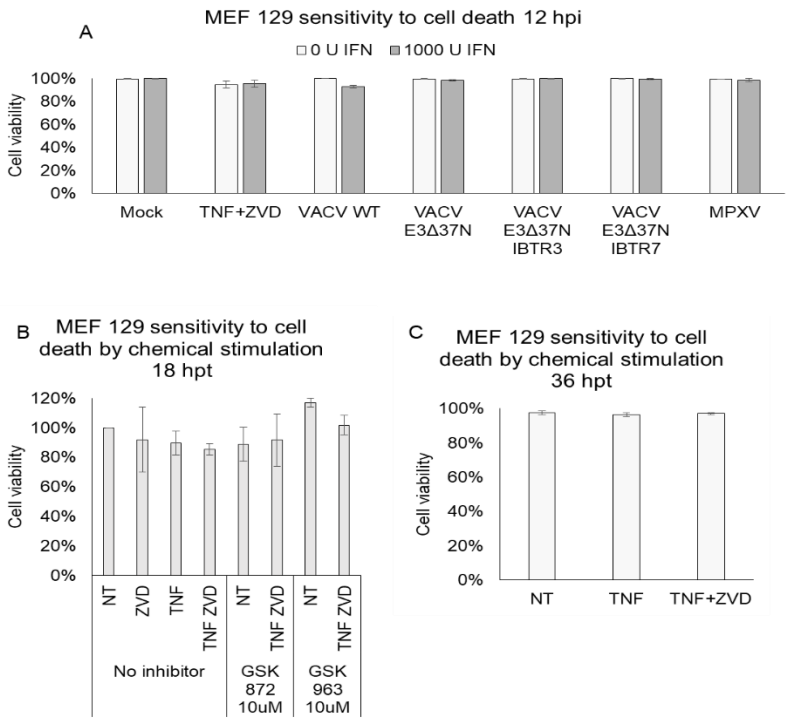

Figure 4-5 MEF 129 are Not Sensitive to Cell Death. (A) MEF cells were either untreated or stimulated with recombinant mouse interferon-α (IFN) at 18 hours before infection. Cells were then infected with VACV WT, VACV E3∆37N, VACV E3∆37N IBTR3, VACV E3∆37N IBTR7, or MPXV at an MOI of 5 or treated with 50 µM ZVD and 20ng/µL mouse TNFα. Cells were stained with Hoescht and propidium iodide (PI) and imaged at 12 hours post infection /treatment. Total cells were measured by Hoescht staining,

and dead cells were measured by PI staining. (B) Cells were stimulated with 50 µM ZVD and 20ng/µL mouse TNFα as indicated. Cells were also treated with 10 µM RIP 1 inhibitor GSK 963 or 10 µM RIP 3 inhibitor GSK 872 as indicated. At 18 hours post treatment, cells were assayed using CellTiter-Glo. (C) Cells were treated with 50 µM ZVD and 20ng/µL mouse TNFα as indicated. Total cells were measured by Hoescht staining, and dead cells were measured by PI staining at 36 hours post treatment.

JC can undergo necroptosis but do so differently than the L929. To determine if the JC cells would be more similar to L929 or MEF129, we tested for cell death after chemical and viral stimulation. JC cells were stimulated with chemical inducers of necroptosis TNF/ZVD and necroptosis inhibitors GSK 872 (RIP3) and GSK 961 (RIP1) and assayed for mitochondrial activity at 18 hours post-treatment using CellTiter-Glo (Figure 4-6A). JC cells were susceptible to cell death that was recovered by using RIP1 or RIP3 inhibitors. JC cells died after treatment of caspase inhibitor ZVD alone which is unusual because most cells require ZVD and TNF treatment for cell death. JC viability after infection was measured by dye exclusion using staining for Hoescht and PI at 12 hours post infection (Figure 4-6B). Cells were either mock or pretreated with GSK 872 one hour prior to infection with an MOI of 5. Like L929, VACV E3Δ37N infection lead to RIP3-dependent loss of cell viability compared to VACV WT. Unlike what was reported in chapter 3 for L929, MPXV and VACV E3Δ37N low dsRNA mutants do not reduce viability of JC cells. This indicates that the RIP3-dependent death may be different than what we see in L929. To determine if these cells were undergoing necroptosis or if RIP3 was inducing a different cell death pathway, lysates were harvested from JC cells infected with an MOI of 5 for 6 hours. A western blot was done and probed with antibody toward phosphorylated MLKL, the executor of necroptosis (Figure 4-6C). VACV E3Δ37N does undergo MLKL phosphorylation but MPXV and low dsRNA VACV E3Δ37N viruses did not have detectable phospho-MLKL. The western blot and cell viability data indicate that unlike L929, in JC reduction of dsRNA is sufficient to inhibit necroptosis.

Figure 4-6: JC cells are sensitive to necroptosis by viral infection and chemical stimulation.

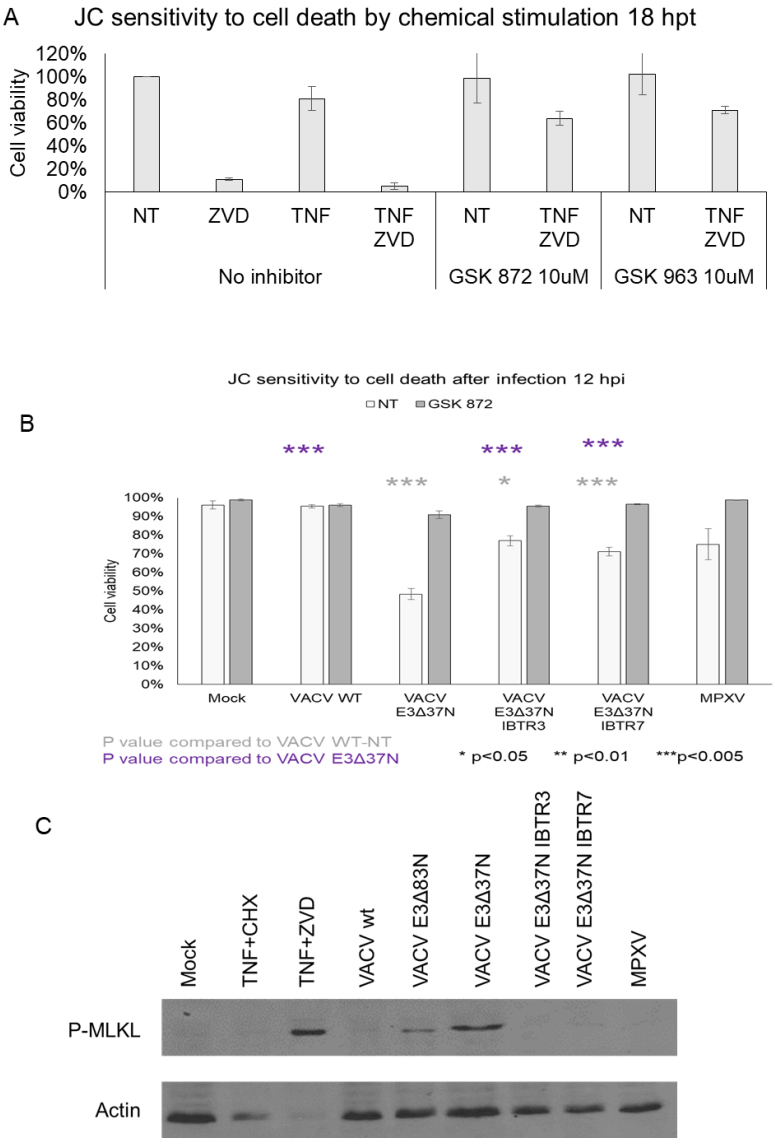

Figure 4-6 JC cells are Sensitive to Necroptosis by Viral Infection and Chemical Stimulation. (A) JC cells were treated with 50 µM ZVD and 20ng/µL mouse TNFα and assayed at 18 hours post treatment using CellTiter-Glo. Cells were also treated with 10 µM RIP 1 inhibitor GSK 963 or 10 µM RIP 3 inhibitor GSK 872 as indicated. (B) JC cells were pre-treated with mock or GSK 872 (10 µM) then infected with VACV WT, VACV E3∆37N, VACV E3∆37N IBTR3, VACV E3∆37N IBTR7, or MPXV at an MOI of 5 or treated with 50 µM ZVD and 20ng/µL mouse TNFα. Total cells were measured by Hoescht staining, and dead cells were measured by PI staining at 12 hours post treatment. (C) JC cells were infected with VACV WT, VACV E3∆83N, VACV E3∆37N, VACV E3∆37N IBTR3, VACV E3∆37N IBTR7, or MPXV at an MOI of 5 or treated with 50 µM ZVD and 20ng/µL mouse TNFα. At 12 HPI, lysates were

harvested and western blots were conducted to determine if MLKL was phosphorylated. Actin staining was used as the loading control.

Inhibition of RIP3 and reduction of dsRNA are both required to recover growth in JC cells. To determine if viral growth could be recovered by RIP3 inhibition or dsRNA reduction, JC cells were treated with the RIP3 inhibitor GSK 872 or mock treated before infection (Figure 4-7). VACV WT and MPXV both grew one log in the presence and absence of GSK 872. VACV E3Δ37N lost recoverable virus at 24 hours post infection in untreated cells, but in GSK 872 treatment allowed four-fold growth. The low dsRNA VACV E3Δ37N viruses grew one log only in the presence of GSK 872. When considered with the data that these viruses are not phosphorylating MLKL or dying, this suggests that RIP3 is inhibiting virus growth through means other than necroptosis in JC cells.

Figure 4-7: Both reduction of dsRNA and inhibition of RIP3 are needed to recover growth of N-terminal deletion mutants in JC cells.

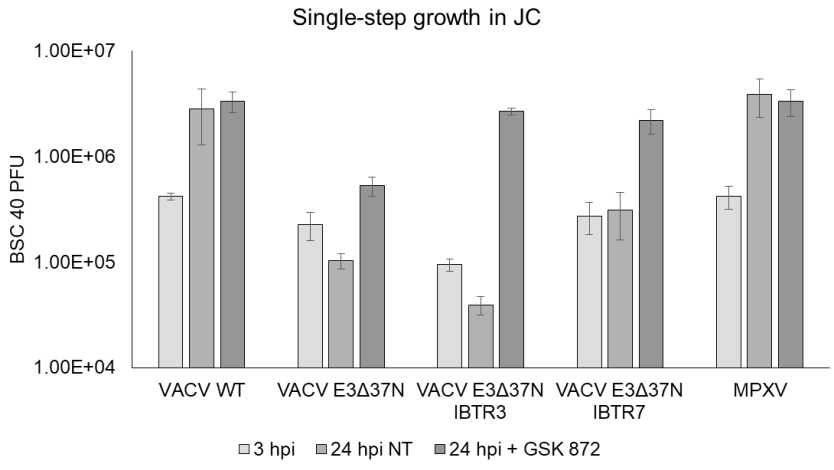

Figure 4-7 Both Reduction of dsRNA and Inhibition of RIP3 are Needed to Recover Growth of N-terminal Deletion Mutants in JC Cells. JC cells were either mock or pre-treated with 10 μM RIP 3 inhibitor GSK 872. Cells were then infected with VACV WT, VACV E3Δ37N, VACV E3Δ37N IBTR3, VACV E3Δ37N IBTR7, or MPXV at an MOI of 5. Viruses were harvested at 0 or 24 hours post-infection (HPI) and titered using BSC 40 cells.

Intracranial pathogenesis in mice is not fully recovered by MLKL knockout or reduction of viral dsRNA. Because replication in JC cells has been correlated to intracranial infections, C57/Bl6 mice were given intracranial infections with the VACV E3Δ37N IC LD_{50} and monitored for clinical symptoms. In WT mice (Figure 4-8A), VACV WT caused severe symptoms ranked greater than 15 between day 4 and day 5 necessitating the conclusion of the experiment at day 5. In MLKL-/- mice (Figure 4-8B), symptoms from VACV WT mice appeared more slowly between day 4 and day 6 when animals were euthanized. MPXV, VACV E3Δ37N, and low dsRNA VACV E3Δ37N all showed some recovery in MLKL -/- mice compared to WT mice, but that could be because the mice were euthanized a day later.

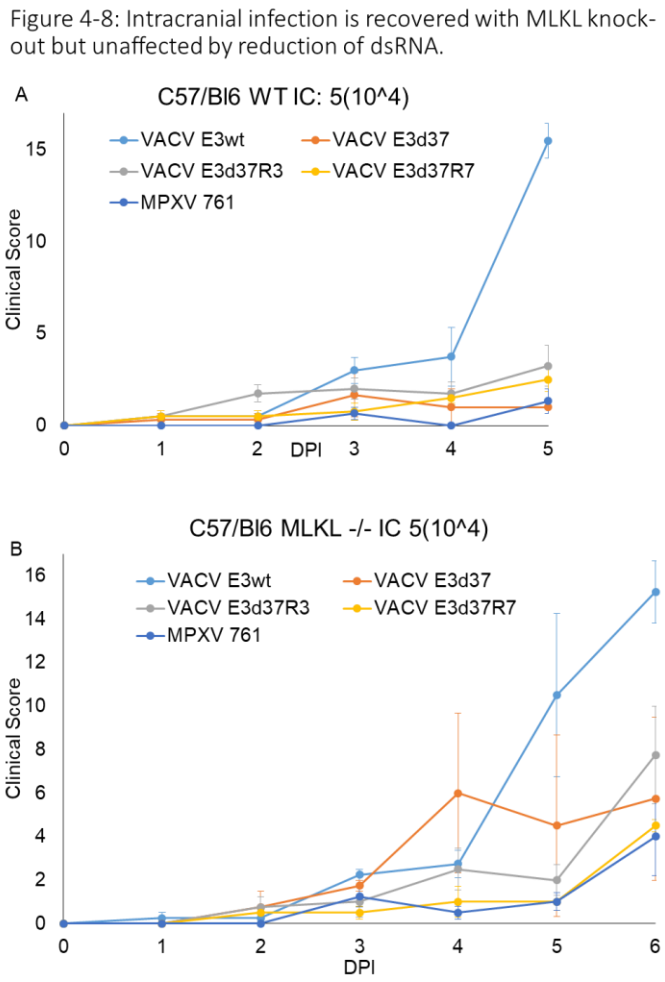

Figure 4-8 Intracranial Infection is Recovered with MLKL Knock-out but Unaffected by Reduction of dsRNA. Mice received intracranial injections of VACV WT, VACV E3Δ37N, VACV E3Δ37N IBTR3, VACV E3Δ37N IBTR7, or MPXV at the VACV E3Δ37N LD50 of $5(10^4)$ PFU. Clinical scores were determined each day post-infection. Wild-type C57/Bl6 mice (A) were euthanized at 5 days post-infection. MLKL -/- C57/Bl6 mice (B) were euthanized at 6 days post-infection.

Intranasal pathogenesis is not recovered by reduction of dsRNA in VACV E3Δ37N. In order to determine if dsRNA signaling played a role in intranasal pathogenesis, C57/Bl6 mice were injected with the VACV E3Δ37N IN LD_{50} through the intranasal route and monitored for weight loss (Figure 4-9A) and symptoms (Figure 4-9B). Mice infected with VACV WT, VACV E3Δ37N, and VACV E3Δ37N IBTR7 all lost a large percentage of their starting weight and had high clinical scores. VACV mutA24 and VACV E3Δ37N IBTR3 did not experience weight loss or develop severe symptoms of infection. We suspect that the loss of A24 function is sufficient to prevent pathogenesis in the mouse regardless of the E3 locus. There did not appear to be any recovery of pathogenesis in VACV E3Δ37N due to reduction of dsRNA.

Figure 4-9: Intranasal infection is not recovered by reduction of dsRNA.

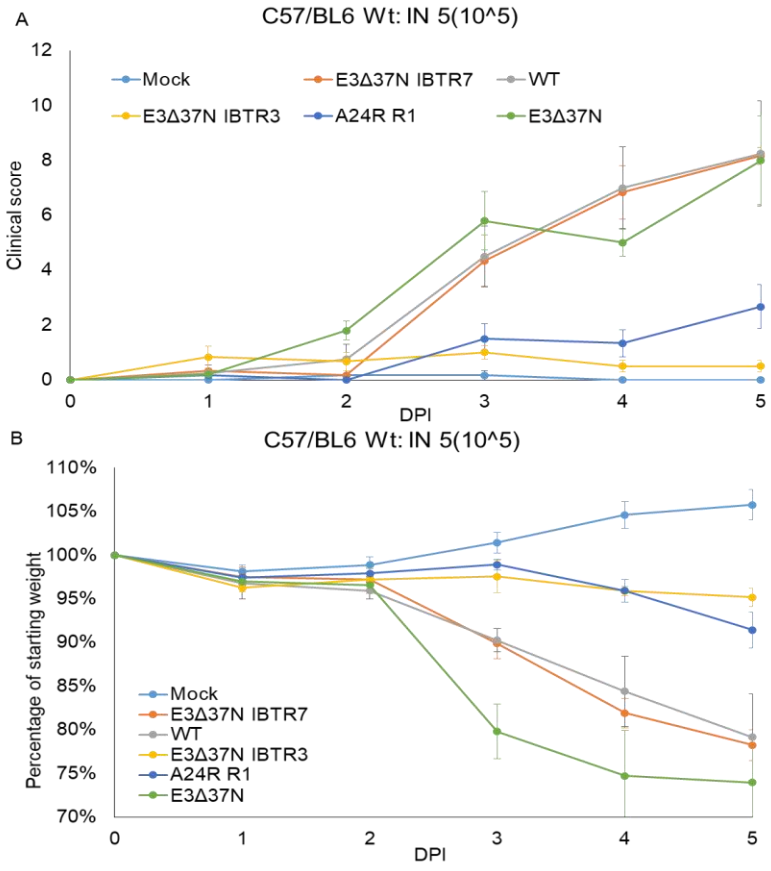

Figure 4-9 Intranasal Infection is not Recovered by Reduction of dsRNA. Wild type C57/Bl6 mice received intranasal injections with VACV WT, VACV E3Δ37N, VACV E3Δ37N IBTR3, or VACV E3Δ37N IBTR7 at the VACV E3Δ37N LD50 of 5(10^5) PFU. Clinical scores (A) and weight loss (B) were determined each day post-infection. Mice were euthanized at 5 days post-infection.

Reduction of dsRNA in VACV E3∆37N recovered replication in spleens. In order to determine if reduction of dsRNA increased spread to organs other than the lung. Mice were subjected to the VACV E3Δ37N LD_{50} by intranasal infections and euthanized for tissue harvest on day 5 when mice reached severe disease. There was no statistically significant difference among recovered virus in the nose which we used as input (Figure 4-10A). However, VACV E3∆37N growth was restricted in spleens by one log compared to VACV WT (Figure 4-10B). Both of the reduced dsRNA VACV E3∆37N viruses increased replication in spleens by one log compared to VACV E3∆37N. This indicated that reducing dsRNA in VACV E3Δ37N infections increased spread to spleen.

Figure 4-10: Spread to spleen is recovered by reduction of dsRNA in intranasal infections.

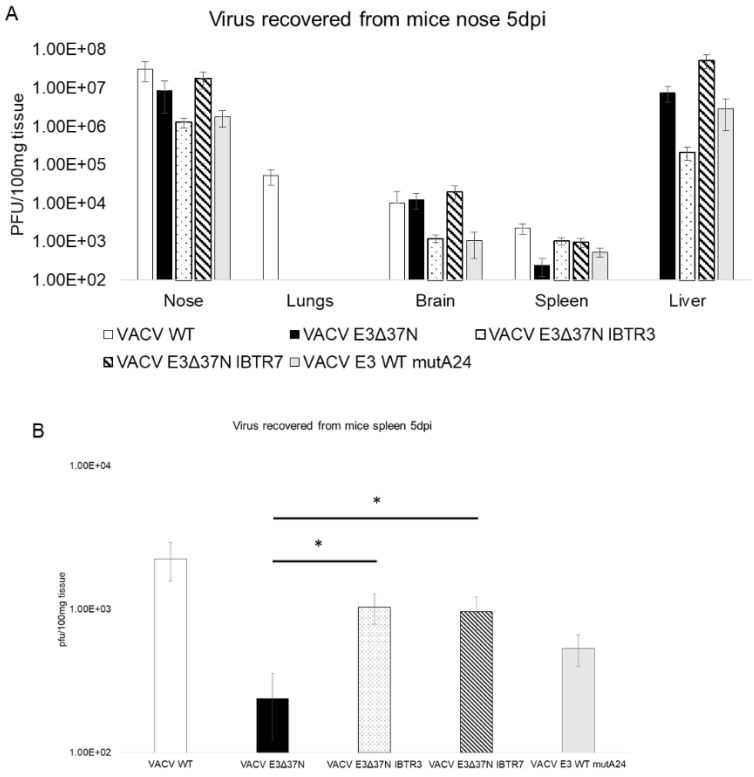

Figure 4-10 Spread to Spleen is Recovered by Reduction of dsRNA in Intranasal Infections. Wild type C57/Bl6 mice received intranasal injections with VACV WT, VACV E3∆37N, VACV E3∆37N IBTR3, or VACV E3∆37N IBTR7 at the VACV E3∆37N LD50 of 5(10^5) PFU. Organs were harvested at 5 days post-infection. Noses (A) were ground in liquid nitrogen with a mortar and pestle and titered in BSC 40. Spleens (B) were homogenized and titered in BSC 40.

Discussion

The full function of the VACV E3 N-terminus has been elusive for some time. While previous studies have taken place in cell lines where either dsRNA inhibition or necroptosis dominated restricting virus growth, we have demonstrated that in both JC cells and in mouse infections there seems to be a combined effect (76, 130, 189). This is especially important for MPXV which has evolved to overcome both inhibitory pathways to be pathogenic in humans despite its E3 homologue, F3 not having a functional N-terminus (167). We demonstrated that the MPXV F3 protein is not responsible for recovering growth in JC cells despite growing well in BSC 40s. Compared to MPXV and VACV WT which each grew approximately 3 logs in JCs over 3 days, VACV ΔE3::MPXV F3 and VACV E3Δ37N had no measurable increase in recovered virus (Figure 4-2). This demonstrated that MPXV has a different means of proliferating in JC cells.

We then hypothesized that it was possible that JCs like MEF 129 cells might restrict growth through PKR. We then screened IBT resistant VACV E3Δ37N for growth in JCs. None of these low dsRNA VACV E3Δ37N viruses grew in JC cells (Figure 4-3). Because JC cells did not fit into the MEF 129 category, we suspected they would act like L929 cells. In order to determine why these cell lines were so different, we tested gene expression by RT PCR and Western blot (Figure 4-4). PKR transcripts were only detected in MEF 129 after treatment with 1000 U IFN whereas JC and L929 both had some detectable transcripts even before IFN treatment. Conversely, DAI was primarily IFN inducible in L929 cells but seemed to have constitutive expression in JC and MEF 129. Furthermore, when the expression of necroptosis executor genes are assayed all the cells have expression of RIPK1, RIPK3, and MLKL. The only exception is MEF 129 cells which seemed to have lower RIPK3 expression than JC and L929 cells. Surprisingly, by Western blot analysis, RIP3 was expressed in MEF 129 cells. Most of what we know about RIP3 regulation suggests it is regulated during transcription by methylation, so the protein expression data was rather unexpected (194, 195).

Because the protein expression data suggested that all three cell lines would be able to undergo necroptosis, we wanted to confirm that. We have already shown that L929 cells undergo

necroptosis in chapter 3, so we focused on MEF 129 and JC cells (130, 196). Although MEF 129 cells express the genes necessary for necroptosis, they did not undergo necroptotic cell death after viral infection or chemical stimulation (Figure 4-5). This argues that either the proteins have mutated to become inactive or something is inhibiting them. Conversely, JC cells died in a RIP3-inhibitable manner after chemical stimulation and viral infection (Figure 4-6). Noticeably, unlike L929 cells where dsRNA levels were irrelevant to necroptosis, in JC cells, VACV E3Δ37N IBTR mutants had intermediate levels of cell death. In both VACV E3Δ37N IBTR3 and VACV E3Δ37N IBTR7, the percentage cell death was statistically different than in VACV WT and VACV E3Δ37N infected cells. Additionally by western blot analysis, they did not lead to early phosphorylation of MLKL indicating that they are inhibited some other way. Furthermore, also unlike L929, in single-step growth curves, GSK 872 is insufficient to rescue VACV E3Δ37N replication in JC (Figure 4-7). It can however rescue VACV E3Δ37N IBTR growth of both mutants. This demonstrates that unlike MEF 129 and L929 cells, JCs do not inhibit VACV E3Δ37N through one single simple pathway.

We wanted to compare how all of these data are relevant to animal models so we infected mice first intracranially in WT and MLKL -/- mice (Figure 4-8). All infections progressed more quickly in the WT mice than in the MLKL -/- mice. At 5 days post infection (dpi), one group of mice (VACV WT) reached our clinical score threshold for euthanasia. Because we blinded our experiment, we did not know which infection that was and chose to euthanize all WT mice that day. In the MLKL -/- mice, VACV WT reached the clinical score threshold for euthanasia at 6 days post infection and we chose to euthanize all mice at this time. In the WT mice, VACV E3Δ37N and VACV E3Δ37N IBTR mutants do not get sick as measured by clinical score. However in the MLKL -/- mice they begin to develop symptoms after 6 days post infection. This indicates that intracranially, loss of MLKL can recover VACV E3Δ37N growth and is consistent with previously published data (157). We did not observe an increase in clinical score of VACV E3Δ37N IBTR mutants compared to VACV E3Δ37N in either mouse line. This indicates that intracranially, necroptosis singularly inhibits VACV E3Δ37N infection.

We infected mice intranasally with the VACV E3Δ37N LD50 virus concentration to look for growth in different organs. In these infections, we observed high clinical scores for both VACV WT and VACV E3Δ37N (Figure 4-9). None of these scores reached the point where the mice would need to be euthanized by 5 dpi. We saw this same phenomenon with weight loss where both VACV WT and VACV E3Δ37N lost substantial amounts of weight. We were surprised by the restriction of VACV mutA24R and VACV E3Δ37N IBTR3. Both of these viruses have low clinical scores and weight loss. This indicates that IBTR mutants of VACV can lead to poor pathogenesis in animals. Previous studies of IBT resistance have not tested the virus in animals, so this was surprising. Based on the data from this experiment, we cannot conclude that VACV E3Δ37N IBTR mutants recover pathogenesis in IN models of infection. We also wanted to see if IBTR could recover spread of the virus within the host, so we titered virus from mouse noses and spleens (Figure 4-10). In noses, all viruses grew well as we expected. However, in spleens harvested from infected mice, VACV E3Δ37N is restricted compared to WT. In spleen, VACV E3Δ37N IBTR was present at up to one log more higher levels than VACV E3Δ37N. These data suggest that in animal models, the inhibitory pathways can be murky like in JCs.

The data from these studies often seems conflicting or difficult to keep straight, so we sought to come up with a hypothesis for how VACV E3Δ37N growth can be restricted in animals and complex cell lines (Figure 4-11). We ended up settling between two alternative hypotheses. The first is that JC cells inhibit VACV E3Δ37N growth in a two-step system. Early DAI-based detection of ZRNA initiates necroptosis of infected cells unless either DAI cannot recognize the infection, or if critical downstream regulators of necroptosis are inhibited. In this case, the virus proceeds to late stages of infection where dsRNA accumulates in the cell overwhelming the truncated E3 protein. Then PKR can recognize virus infection and proceed to inhibit viral growth. This hypothesis is strongly supported by Figure 4-7 which demonstrates that RIP3 inhibition and IBTR are both necessary for VACV E3Δ37N to grow in JCs. However, it does not explain the cell death assays in Figure 4-6 where IBTR mutants had less cell death than VACV E3Δ37N. This data could better be explained by the second hypothesis which suggests that there could also be

a combined effect where proteins recognizing ZRNA and dsRNA co-operate to direct RIP3 activity towards necroptosis or an alternative viral inhibitory pathway. RIP3 can play complex roles after viral infection, leading cells down different paths than just necroptosis (115). This hypothesis is consistent with the growth data in Figure 4-7, and with the cell death assays in Figure 4-6. Future experiments will focus on determining which hypothesis might be correct and expanding on our knowledge of how viruses interact with their host cells.

Figure 4-11 Alternate hypotheses explaining JC inhibition of VACV E3Δ37N

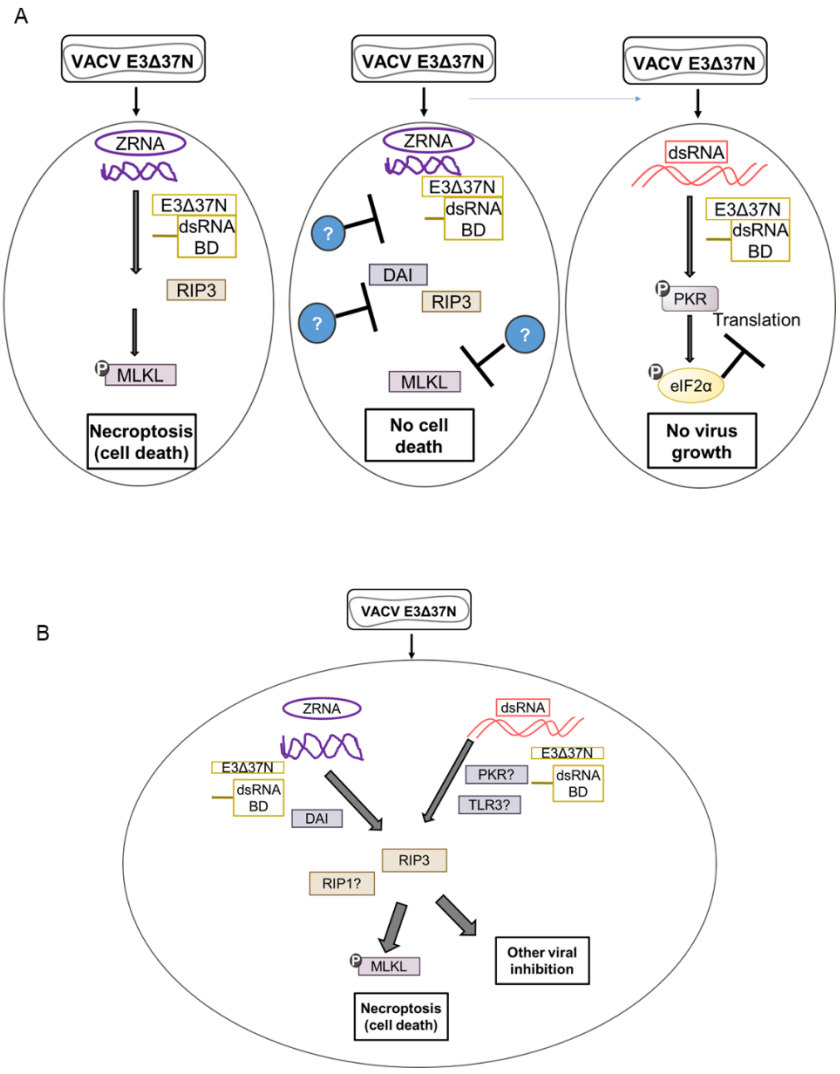

Figure 4-11 Alternate hypotheses explaining JC inhibition of VACV E3Δ37N. (A) One hypothesis for how JC cells inhibit VACV E3Δ37N growth is that it works in a two-step system. First early detection of ZRNA allows DAI to recognize the infection and initiate cell death. However, if for some reason either DAI cannot recognize the infection, or if critical downstream regulators of necroptosis are inhibited, the virus proceeds to late stages of infection. During late stages of infection, dsRNA accumulates in the cell overwhelming the truncated E3 protein, PKR can recognize virus infection and proceeds to inhibit viral growth. (B) Alternatively, there could also be a combined effect where proteins recognizing ZRNA and dsRNA co-operate to direct RIP3 activity towards necroptosis or an alternative viral inhibitory pathway.

CHAPTER 5

DETECTING NECROPTOSIS IN VIRUS-INFECTED CELLS

Edited from the following publication:

Cotsmire S.M., Szczerba M., Jacobs B.L. (2021) Detecting Necroptosis in Virus-Infected Cells. In: Lucas A.R. (eds) Viruses as Therapeutics. Methods in Molecular Biology, vol 2225. Humana, New York, NY. https://doi.org/10.1007/978-1-0716-1012-1_11

Abstract

Necroptosis has been implicated as a critical cell death pathway in cancers, Alzheimer's and other neurodegenerative diseases, and virus-infected cells. Necroptosis occurs when mixed-lineage kinase domain-like protein (MLKL) punctures the cytoplasmic membrane allowing a rapid influx of water leading to a loss of cellular integrity. As its role in human disease becomes apparent, methods identifying necroptosis will need to be further developed and optimized. Here we describe identification of necroptosis through quantifying cell death with pathway inhibitors and using western blots to identify end points of MLKL activation and protein-protein interactions leading to it.

Introduction

Necroptosis is a relatively newly identified form of programmed cell death that, unlike apoptosis and pyroptosis, is independent of caspases [1, 2]. Necroptotic cell death has been implicated in the response to infection, death receptor activation, and activation of toll-like receptors 3 and 4 (TLR 3 and TLR 4). Viruses have evolved necroptotic inhibitor proteins to retain pathogenesis during infection [3, 4]. Additionally, necroptosis has been detected in brains of patients with Alzheimer's disease and Parkinson's disease and has been implicated in age-related macular degeneration and in skin inflammation [5–7]. Additionally, a key regulator of necroptosis, receptor-interacting protein kinase 3 (RIPK3), has been implicated in tumor invasion during colorectal cancers and in response to chemotherapeutic agents [8, 9]. While necroptosis inhibits

viral pathogenesis in animal models, its involvement in human cancers and neurological diseases has not been elucidated. By studying the regulation of necroptosis during viral infection and other human diseases, we hope to identify targets for oncolytic viruses and viral protein therapies. While independent of caspase activation, necroptosis is dependent on the serine/threonine protein kinase, define RIPK RIPK3. In fact, active caspase 8, one key initiator caspase for apoptosis, can inhibit necroptosis by cleaving RIPK3 [10]. Once activated RIPK3 can phosphorylate define MLKL mixed-lineage kinase domain like pseudokinase (MLKL), the executioner of necroptosis [11]. Phosphorylation of MLKL on serine 358 in humans and S345 in mice is necessary but not sufficient to induce necroptotic cell death [12, 13]. A second step, trimerization, is dependent on highly phosphorylated inositol phosphates and on tyrosine phosphorylation (T357) of MLKL by the define TAM tyro3-Axl-Myr (TAM) kinases [14–16]. There are three sensors, define receptor interacting serine/threonine protein kinase 1 (RIPK1), DNA-dependent activator of interferon-regulatory factors (DAI), and TIR-domaincontaining adapter-inducing interferon-β (TRIF) pls RIPK1, DAI and TRIF, that act upstream of RIPK3 that can lead to RIPK3 activation. RIPK1 senses activation of death receptors [17]. DAI senses Z-form nucleic acid, associated with viral infection, while TRIF senses signaling by TRL3 and TLR4 [18, 19]. RIPK1, DAI, and TRIF can bind to RIPK3 through interaction of mutual RIP homotypic interaction motifs, define RIP homotypic intercation motif (RHIM) RHIMs, leading to RIPK3 phosphorylation and activation [20]. Once activated RIPK3 can phosphorylate MLKL, initiating the pathway leading to necroptotic cell death. In this manuscript, we describe methods to detect cell death and determine if the cell death is RIPK3-kinase dependent and associated with MLKL-serine and -tyrosine phosphorylation and MLKL trimerization (see Figure 5-1). While the requirement for RIPK1 kinase activity can be evaluated using RIPK1-specific kinase inhibitors and RIPK1 phospho-specific antiserum, no similar reagents are available to evaluate activation of DAI or TRIF. However, co-immune precipitation can be used to ask if DAI and TRIF are bound to RIPK3, which is presumed to be necessary for DAI- and TRIF-dependent activation of RIPK3. We have also recently shown that DAI-dependent necroptosis is associated with formation of large

cross-linkable complexes that contain DAI and RIPK3 [21]. Cross-linking can be done in living cells and in tissue from experimental animals and necropsy tissue from humans. Thus, cross-linking can be used to determine if DAI activation is associated with disease.

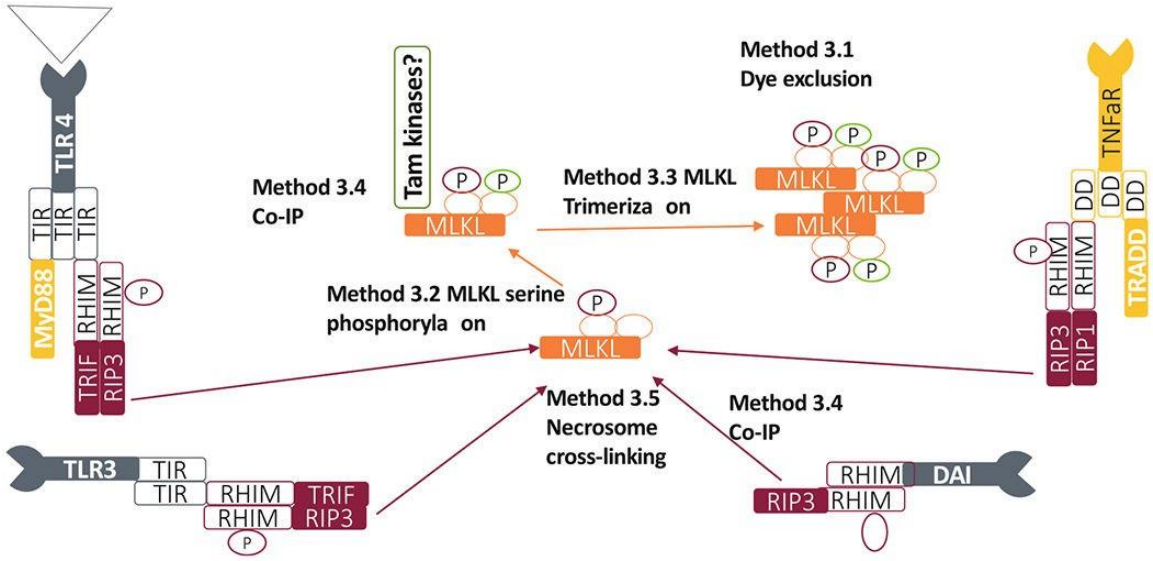

Figure 5-1 Necroptosis Overview

Overview showing how necroptosis can be induced and detected. This chapter describes how to detect the different stages of necroptotic death. We can detect initiation of RIPK3 activation with CoIP (see Subheading 3.4). Then we can detect RIPK3 induction of the necrosome with cross-linking (see Subheading 3.5). Next, we can detect MLKL serine phosphorylation (see Subheading 3.2) and tyrosine phosphorylation (see Subheading 3.5).

We also describe detection of MLKL trimerization (see Subheading 3.2) and cell death (see Subheading 3.1). The inhibitors we have described in Subheading 3.1 are critical for determining how the cells are dying

Materials

Cell Viability by Dye Exclusion with Inhibitors

Prepare all inhibitor stocks in sterile DMSO or water, as indicated. Dilute into the working concentration in warm medium. There are many alternative live/dead nucleic acid stains, but these are our preference due to cost and availability.

1. Hoechst: Allows for nuclear staining in blue fluorescent channels. Prepare stock solution at 1 mM dimethyl sulfoxide (DMSO), storing at −20 C until use at 1 µM.
2. Propidium iodide (PI): Stains nucleic acids, but is excluded from living cells. Detectable in the red channel. Prepare stock at 1 mg/mL in water and use at 1 µg/mL.
3. Fluorescent microscope or cell counter with red fluorescent protein (RFP) and 4′,6-diamidino-2-phenylindole (DAPI) channels.
4. RIPK3: While lack of RIPK3 involvement can rule out necroptosis, it has been shown to be involved in other death pathways and cannot be used to conclusively confirm it.
5. Prepare RIPK3 phospho-inhibitor stock at 10 mM in DMSO (store at −80 C) and use at working concentration depends on cell line but generally between 1 uM and 10 µM. Inhibits RIPK3 kinase activity in both human and mouse cells (we use Glaxo Smith Kline (GSK) compound 872).
6. RIPK1: Much like RIPK3, RIPK1 is involved in other cell death pathways and cannot solely be used to determine if necroptosis is occurring. Unlike RIPK3, RIPK1-independent necroptosis can still occur.
    a) GSK 963: Prepare stock 10 mM in DMSO, aliquot, and store at −80C. Thaw and dilute to working concentration at 1–10 µM in cell media. Inhibits kinase activity of both human and mouse RIPK1.
    b) Necrostatin-1 s (Nec-1 s): Prepare 10 mM solution in DMSO and store at −20 C for up to 1 month. Fully bring to room temperature before using at a concentration of 100 µM. Validated in human cells, mouse cells, and murine models.

7. MLKL: At the cell membrane MLKL executes necroptosis by forming pores allowing for unregulated ion transfer. It requires serine phosphorylation, homologous trimerization, cell membrane relocation, and a tyrosine phosphorylation before executing necroptosis. Inhibition of MLKL can be used to positively determine that necroptosis occurred.
8. Necrosulfonamide (NSA) inhibits only human MLKL after serine phosphorylation but before pore formation. Prepare a stock solution of 10 mM in DMSO and store at −20 C. Thaw and use at 1–10 μM.

MLKL Serine Phosphorylation

1. Approximately 1 × 106 cells per sample to be tested.
2. Halt™ Protease and Phosphatase Inhibitor Cocktail (100×) (we use 78446, Thermo Fisher or equivalent).
3. Dithiothreitol (DTT) prepared at 500 mM in DMSO and stored at −20 C.
4. Triton-X lysis buffer: Prepare a Triton-X lysis buffer to the following final concentrations in sterile water: 5 mM Ethylenediaminetetraacetic acid (EDTA), 10 mM Tris (hydroxymethyl) aminomethane-Cl (Tris–Cl) pH 8.0, 50 mM NaCl, 1% (v/v) Triton-X 100 (see Note 1).
5. 4× Sodium dodecyl sulfate-polyacrylamide gel electrophoresis (SDS-PAGE) loading buffer: Prepare the loading buffer to the following concentrations: 0.24% SDS, 0.2% bromophenol blue, 20% glycerol in sterile water (see Note 2).
6. 10% Polyacrylamide gels can be purchased or prepared.
7. Nitrocellulose membranes.
8. CAPS transfer buffer: Resuspend 10 mM CAPS (3-(cyclohexylamino)-1-propane sulfonic acid) in sterile water and adjust pH to 11. Just before use add 20% v/v methanol.
9. Tris-buffered saline with Tween (TBST): Dissolve NaCl (137 mM), KCl (2.7 mM), and Tris base (19 mM) in sterile water. Titrate pH to 7.4 and add Tween-20 to 0.05% (v/v).
10. Membrane-blocking buffer (MBB): Nonfat milk (NFM) diluted to 5% (w/v) in TBST.
11. BSA dilution buffer (BDB): 3% (v/v) Bovine serum albumin (BSA) in TBST.
12. Antibody dilution buffer (ADB): Nonfat milk (NFM) diluted to 3% (w/v) in TBST.

13. Reagents for detecting secondary antibodies.

14. Stripping buffer: 7.25 mM Tris-Cl, 0.1% sodium dodecyl sulfate, with 0.1% (v/v) β-mercaptoethanol added just before use.

15. Primary and secondary antibodies (see Note 3).

MLKL Trimerization

1. Approximately 1 × 106 cells per sample to be tested.

2. Halt™ Protease and Phosphatase Inhibitor Cocktail (100×) (we use 78446, Thermo Fisher or equivalent).

3. DTT prepared at 500 mM in DMSO and stored at −20 C.

4. 4× SDS-PAGE loading buffer (see Note 2).

5. 7.5% Polyacrylamide gels can be purchased or prepared.

6. Nitrocellulose membranes.

7. CAPS transfer buffer.

8. TBST.

9. Primary and secondary antibodies and appropriate buffers (see Note 3).

10. Reagents for detecting secondary antibodies.

11. Stripping buffer.

Co-Immunoprecipitation

1. Approximately 1 × 106 cells per sample to be tested.

2. Halt™ Protease and Phosphatase Inhibitor Cocktail (100×) (we use 78446, Thermo Fisher or equivalent).

DTT prepared at 500 mM in DMSO and stored at −20 C.

[1.] Just before lysing cells add protease and phosphatase inhibitors.

[2.] Just before denaturing protein, add DTT to 4× loading buffer to a final concentration of 4 mM.

3. Non-denaturing lysis buffer (NDB): Dilute Tris–HCl, pH = 7.5 to 10 mM, MgCl2 to 2 mM, KCl to 50 mM, and Triton X-100 to 1% (v/v) in sterile water (see Note 1).

4. Buffer I: Prepare Tris–HCl, pH = 7.5 at 20 mM, NaCl at 0.4 mM, EDTA at 1 mM Triton X-100 at 1% (v/v), glycerol at 20%(v/v), and Na3VO1 at 2 mM in sterile water.

5. Protein A/G PLUS-Agarose (Santa Cruz, sc-2003), 40 µL of 50% slurry/sample (20 µL for lysate pre-clearing and 20 µL for immunoprecipitation).

6. Primary antibody to pull down protein complexes (see Note 3).

7. 10% Polyacrylamide gels can be purchased or prepared.

8. Nitrocellulose membranes.

9. CAPS transfer buffer.

10. TBST.

11. Primary and secondary antibodies and appropriate buffers (see Note 3).

12. Reagents for detecting secondary antibodies.

13. Stripping buffer.

Table 5-1 Antibodies Used in these Protocols

Protein	Antibody clone	Species detected	Assays	Blocking buffer	Concentration	Dilution buffer
DAI	Zippy-1 AG-20B-0010-C100	Mouse, human	WB	MBB	500 ng/mL (1:2000)	ADB
			Co-IP		5 ng/µL	Buffer I
IPK3	CST D4G2A	Mouse	WB	MBB	85 ng/mL (1:2000)	ADB
Phospho-tyrosine	Sigma 05–321×		Co-IP		2.5 ng/µL	Buffer I
MLKL (serine phospho)	CST D6E3G	Mouse	WB	MBB	28 ng/mL (1:1000)	BDB
MLKL (total)	CST D6W1K	Mouse	WB	BDB	313 ng/mL (1:1000)	BDB

[3] Table 5-1 contains information on the antibodies we used for these protocols.

[4] DSP is very moisture sensitive and must be stored desiccated at 4C and be equilibrated to room temperature before opening. Because the NHS-ester moiety readily hydrolyzes and becomes nonreactive, prepare each use fresh and discarding any unused solution.

Necrosome Cross-Linking

1. Approximately 1 × 10^6 cells or 5–25 mg of animal tissue per sample to be tested.
2. Dithiobis[succinimidyl propionate] (DSP) crosslinker (we use 22585, Thermo Scientific): Prepare 100 µL of 25 mM DSP, by resuspending 1 mg of DSP in 100 µL DMSO (see Note 4).
3. Halt™ Protease and Phosphatase Inhibitor Cocktail (100×) (we use 78446, Thermo Fisher or equivalent).
4. Radioimmunoprecipitation assay buffer (RIPA) lysis buffer: 1% NP40, 0.1% SDS, 0.5% sodiumdeoxycholate, DTT prepared at 500 mM in DMSO and stored at −20C.
5. 4× SDS-PAGE loading buffer. DO NOT ADD DTT.
6. 10% Polyacrylamide gels can be purchased or prepared.
7. Nitrocellulose membranes.
8. CAPS transfer buffer.
9. TBST.
10. Primary and secondary antibodies and appropriate buffers (see Note 3).
11. Reagents for detecting secondary antibodies.
12. Stripping buffer.

Methods

Cell Viability by Dye Exclusion

Cell viability and dye exclusion can only be used to identify necroptosis in conjunction with necroptosis inhibitors. It is critical to set up inhibitors for this experiment according to their use as described in the Subheading 2.1 and demonstrated in Figure5-2. Furthermore, establishing the time of membrane disruption as indicated by dye exclusion makes determining the timelines for Subheadings 3.2, 3.3, 3.4, and 3.5 much simpler (see Note 5 for more information).

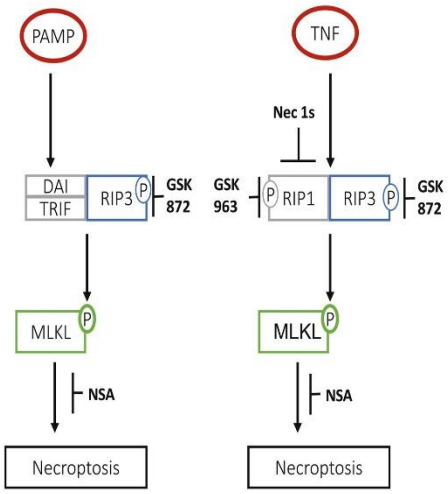

Figure 5-2 Necroptosis Inhibitors

Inhibitors used to determine mechanism of cell death. Membrane permeabilization is the final step before cell death. Detecting membrane permeabilization in the presence of kinase inhibitors of different proteins involved in necroptotic death is a critical first step for determining whether or not necroptosis might be involved and how long it takes for cells to die. Nec-1 s and GSK 963 both inhibit RIPK1 kinase activity. GSK 872 inhibits RIPK3 kinase activity. Necrosulfonamide (NSA) inhibits MLKL post-serine phosphorylation, and ZVAD inhibits pan-caspase activity.

1. One day prior to testing, plate cells in a tissue culture dish suitable for fluorescent imaging.
2. Prepare working concentrations of Hoechst dye and inhibitors of the necroptosis pathway by diluting into cell growth media. Pretreat cells by aspirating media and replacing with dye and inhibitors and incubating for 1 h under normal cell growth conditions (i.e., 37 °C, 5% CO2). All samples should have Hoechst dye; inhibitors should be used as appropriate.
3. Begin the experiment by aspirating dye media and adding a chemical death inducer or infecting with virus. If using inhibitors, include them in death inducer and viral preparations (see Note 6).
4. Prepare 10× PI in cell growth media and add to cells (1/10 v/v) at least 15 min before first time point. Gently swirl cells to allow dispersion of dye. PI can be left on cells for the course of the experiment.
5. Image cells using DAPI channel (Hoechst) and RFP channel (PI). Phase contrast can also be used for qualitative analysis of cell morphology.
6. Count all cells (blue) and dead cells (red).

Table 5-2 Optimal Time Points (in Hours Post-treatment) for these Assays in L929 Cells

Subheading	Assay	TNF + ZVD	VACV E3Δ83N
3.1	Dye exclusion	4–6	6–8
3.2	MLKL serine phosphorylation	2–4	4–5
3.3	MLKL trimerization	4	5–6
3.4	Tyrosine phospho-MLKL co-IP	4	4–5
3.4	DAI-RIP3 co-IP	N/A	1–3
3.5	Necrosome aggregation	1–3	1–3

MLKL Serine Phosphorylation

MLKL serine phosphorylation is the first step of MLKL activation by RIPK3. MLKL is also phosphorylated on a tyrosine residue, but at the time of this writing there are no commercially available antibodies specific to this phosphorylation site. To look at subsequent activation, Subheading 3.1 Cell death by dye exclusion, Subheading 3.3 MLKL Trimerization, and Subheading 3.4 Co-immunoprecipitation (with anti-tyrosine phospho antibody) can be used, for time points (see Note 5).

1. Prepare 1 × 10^6 cells by infecting or treating with chemical reagents suspected of inducing necroptosis (see Note 6).
2. At various time points scrape cells into media using the blunt end of a P1000 pipette tip.
3. Centrifuge @ 1000 × g for 10′ and gently remove media from pellet (see Note 7).
4. Resuspend pellet thoroughly in 60 µL of Triton-X lysis buffer with protease and phosphatase inhibitors.
5. Incubate cells on ice for 5′.
6. Centrifuge cells for 15′ at max speed at 4 °C.

---

[5] Once necroptosis is initiated, cells die very quickly. As such the time points used to harvest protein to study these phenomena are critical. Each time a new cell line or treatment will be studied, the first step is to establish a timeline. The fastest way to do this is to use Subheading 3.1 dye exclusion to take images of the cells at 30-min intervals to determine the time of membrane rupture. Table 5-2 contains data from our observations on the best times to perform these assays in L929 cells.

7. Keep the supernatant and add to 4× MLKL loading buffer + DTT (see Note 8).

8. Heat all samples for at least 10′ at 95 °C.

9. Load onto a 10% polyacrylamide gel (see Note 9).

10. Run slowly (70 V) until the ladder is in the separating gel. After this, the speed can be increased to 100 V until the 50 kDa marker is 2/3 of the way down the gel.

11. Transfer to nitrocellulose membrane in 1× CAPS transfer buffer with added methanol for 1 h at 100 V.

12. Block for 1 h with MBB. Rinse with TBST until no longer cloudy.

13. Wash with TBST 3× at RT for 5 min.

14. Add secondary antibody and incubate for 2 h at RT in ADB.

15. Wash with TBST 3× at RT for 15 min.

16. Expose and image blot.

17. Strip the blot by incubating in stripping buffer (see Note 10) for 15 min at 56 °C.

18. Block with MBB for 1 h at RT. Rinse with TBST until no longer cloudy.

19. Add primary MLKL antibody overnight at 4 °C (see Note 3).

20. Rinse 3× with TBST at RT for 5 min.

21. Add primary antibody (serine phospho-MLKL) overnight at 4 °C, and rinse 1 × with TBST (see Note 3).

22. Add secondary antibody. Incubate for 2 h at RT in ADB.

---

6. If infecting cells with virus, follow virus-specific infection protocols to infect >99% of cells and grow under standard culture conditions until desired time point.

7. Dead volumes of 10–50 µL should be left on pellets to avoid disturbing fragile cells.

8. The samples for this experiment do not freeze well. Upon thawing phosphorylated MLKL will barely be distinguishable between positive and negative controls. Have the gel ready to run the same day as the experiment is conducted.

23. Wash with TBST 3× at RT for 5 min.

24. Expose and image blot.

MLKL Trimerization

MLKL trimerization is a straightforward way to measure one of the final steps of MLKL activation before execution of cell death. After MLKL is trimerized, it moves to the cell surface creating pores which facilitate rapid cell death. This method takes advantage of MLKL trimers being resistant to denaturization by SDS and boiling while fully denaturing with DTT. For time points, see Note 5.

1. Prepare 1 × 10^6 cells by infecting or treating with chemical reagents suspected of inducing necroptosis (see Note 6).

2. At various time points scrape cells into media using the blunt end of a p1000 pipette tip.

3. Centrifuge @ 1000 × g for 10′ and gently remove media from pellet (see Note 6).

4. Resuspend pellet thoroughly in 100 µL of 1× MLKL loading buffer without DTT. Separate half of sample and add DTT (see Note 11).

5. Add all of the sample to the Qiashredder and spin at maximum speed for 3′.

6. Heat all samples for at least 10′ at 95 °C.

7. Load onto a 7.5% polyacrylamide gel (see Note 9).

8. Run slowly (70 V) until the 50 kDa marker is 2/3 of the way down the gel.

9. Transfer to nitrocellulose membrane for 18 h at 15 V in 4 °C in CAPS transfer buffer with magnetic spinner turned to slow.

10. Block for 1 h with MBB.

11. Add primary antibody (MLKL see Note 3) overnight at 4 °C (rinse with TBST).

12. Wash with TBST 3× at RT for 5 min.

[9.] If you are pouring the gel, the interface between the stacking and separating gels must be perfect. Isopropanol can be substituted for saturated isobutanol for a cleaner transition.

13. Add secondary antibody and incubate for 2 h at RT in ADB.

14. Wash with TBST 3× at RT for 15 min.

15. Expose and develop blot.

16.

Co-Immunoprecipitation

We have validated this co-immunoprecipitation protocol to identify interactions between DAI and RIPK3 and to detect MLKL tyrosine phosphorylation (see Figure5-3). We can also find interactions between RIP3 and DAI by co-immunoprecipitation (Co-IP) (see Figure 4-4). Each of these pull-downs will require a different timeline (see Note 5).

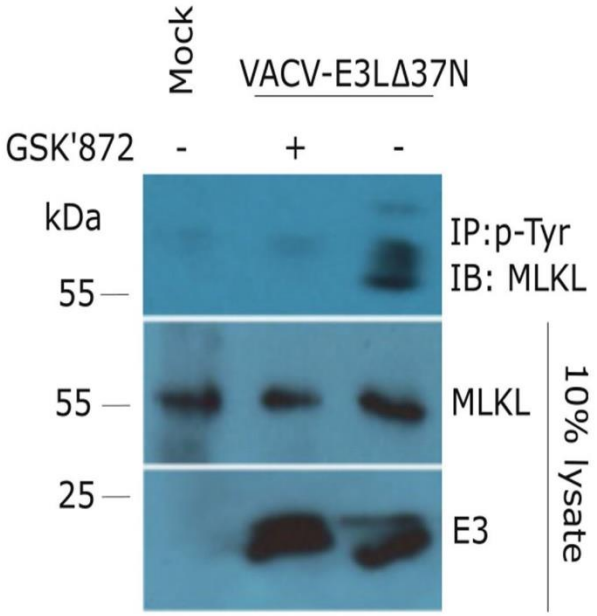

Figure 5-3 CoIP to Measure MLL Phosphor Tyrosine

L929 cells pretreated with type 1 interferon (IFN) were infected with VACV-E3LΔ37N and harvested at 4 h postinfection. Lysates then were immunoprecipitated as described in Subheading 3.3 using phosphotyrosine-specific antibody. Immunoprecipitated proteins and input lysate were run on a Western blot and probed for MLKL.

[10.] Add 0.1% β-mercaptoethanol to stripping buffer immediately before use.

[11.] Very fresh β-mercaptoethanol can be used in place of DTT. However, we have seen that this application is highly sensitive to oxidation and recommend using DTT for more consistent results.

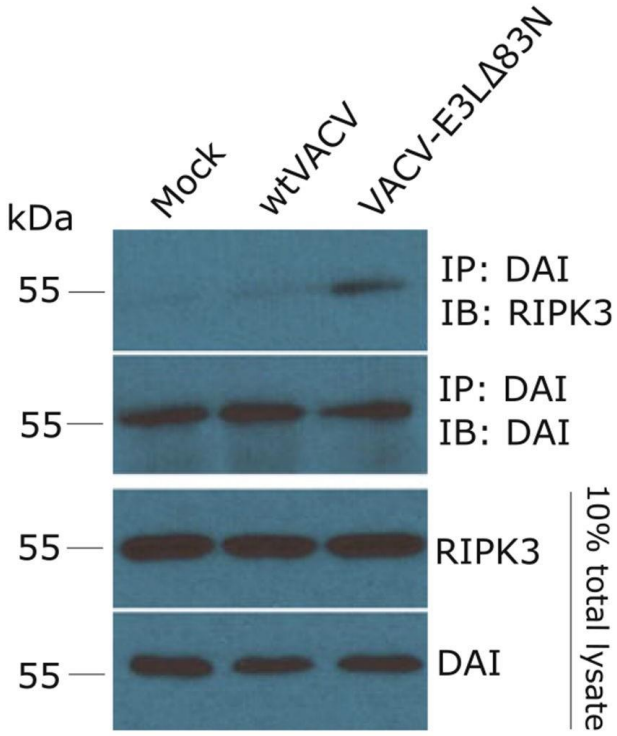

Figure 5-4 CoIP to determine activator of necroptosis

L929 cells pretreated with type 1 IFN were infected with VACV-E3LΔ83N. At 2 h postinfection, lysates were harvested and subjected to immunoprecipitation by antibodies specific for DAI as described in Subheading 3.3. Immunoprecipitated protein and input lysate were run on Western blots and probed with antibody for RIPK3.

1. Prepare 2 × 10^6 cells by infecting or treating with chemical reagents suspected of inducing necroptosis (see Note 6).
2. At 2 h posttreatment or postinfection, aspirate the media and wash cells with 1 mL cold PBS.
3. Scrape cells into cold PBS using the blunt end of a p1000 and transfer the suspension to a microcentrifuge tube.
4. Centrifuge at 1000 × g for 10 min at 4 °C.
5. Remove PBS (supernatant) carefully, not disturbing the pellet (see Note 6).
6. Lyse cells by resuspending the pellet in 100 µL ice-cold NDB and incubating on ice for 5 min.
7. Add 120 µL ice-cold Buffer I (see Note 12).
8. Measure 80 µL of 25% (v/v) raw bead slurry per sample (protein A/G agarose) and spin the slurry at 500 × g for 5 min (see Note 13).

9. Wash the pellet of beads with 1 mL Buffer I and spin again.

10. Perform a total of three washes (see Note 12).

11. Pre-clear samples, by adding 20 µL of washed 50% protein A/G PLUS-Agarose slurry to the collected cell lysates.

12. Incubate with rotation at 4 °C for 30–60 min.

13. Pellet beads (500 × g for 5 min) (see Note 14).

14. Transfer 200 µL of the supernatant into a fresh tube for immunoprecipitation (discard beads used for pre-clearing; the other 40 µL of the lysate will be the total lysate control) (see Note 14).

15. Add the bait antibody (see Note 3) to the 200 µL of cell lysate.

16. Incubate with rotation overnight at 4 °C.

17. Add 20 µL of the previously prepared 50% protein A/G PLUS-Agarose slurry to each sample.

18. Incubate with rotation for 60–90 min at 4 °C.

19. Pellet the bead-antibody-protein complexes by centrifugation at 500 × g for 5 min and set aside the supernatant to be kept as a control (see Note 14).

20. Wash the beads to remove proteins with nonspecific binding by adding 1 mL of Buffer I.

[12.] If necessary, lysates can be stored at −80 °C until a more suitable time for processing.

[13.] The commercial beads we use come as 25% (v/v) slurry. They need to be resuspended to a 50% (v/v) final concentration of beads. For this experiment, each sample requires 20 µL of the 50% slurry for both pre-clearing and immunoprecipitation. For ten samples, that will be 20 µL × 2 × 10 = 400 µL of 50% final slurry concentration. Therefore, you will need 400 µL x 2 = 800 µL of the 25% slurry. After washing the 800 µL of 25% slurry, you have roughly 200 µL of solid beads and add 200 µL buffer I to dilute to the final concentration of 400 µL 50% slurry.

[14.] These can be kept at −80 °C as a control.

21. Centrifuge at 500 × g for 5 min. Preserve a fraction of the supernatant as a control (see Note 14).

22. Repeat the wash for a total of three times.

23. When removing supernatant after last wash, leave about 15 µL of Buffer I on top of the bead slurry in the tube. Add at least 15 µL of 2× denaturing loading buffer containing 20–50 µM DTT.

24. To release the antibody-protein complexes from the beads, heat the samples at 95 °C for 10–15 min.

25. Pellet the beads by centrifugation at 500 × g for 10 min. Transfer the supernatant to a fresh tube. The pellet can be kept as a control for successful release of antibody-protein complexes (see Note 14).

26. Run two 10% PAGE-SDS gels at 100 V. One gel should be run for the immunoprecipitated fraction, and another one for the total lysate control from **step 14**.

27. Transfer to nitrocellulose membrane in 1× CAPS transfer buffer with added methanol for 1 h at 100 V.

28. Block for 1 h with membrane blocking buffer (MBB). Rinse with TBST until no longer cloudy.

29. Add primary antibody overnight at 4 °C in antibody dilution buffer (ADB) (see Notes 3 and 2) (rinse with TBST).

30. Rinse 3× with TBST at RT for 5 min.

31. Add secondary antibody. Incubate for 2 hr at RT in ADB.

32. Wash with TBST 3× at RT for 5 min.

33. Expose and image blot.

34. Strip the blot by incubating in stripping buffer (see Note 9) for 15 min at 56 °C.

35. Block for 1 h at RT. Rinse with TBST until no longer cloudy.

36. Add primary antibody overnight at 4 °C (rinse with TBST) (see Notes 3 and 15).

37. Rinse 3× with TBST at RT for 5 min.

38. Add secondary antibody. Incubate for 2 h at RT in ADB.

39. Wash with TBST 3× at RT for 5 min.

40. Expose and image blot.

Necrosome Cross-Linking

Necrosome cross-linking uses an amine-reactive crosslinker, DSP, to covalently cross-link all proteins in the necrosome shifting their weight on a PAGE gel to >250 kDa (see Figure5-5). It is helpful for looking at interactions between proteins that cannot easily be detected by Co-IP (see Subheading 3.4) and can readily be used to analyze animal and human tissue samples frozen in liquid nitrogen. It is not as specific as Co-IP but can be used with other methods to demonstrate protein inclusion in the necrosome. For timelines, see Note 5.

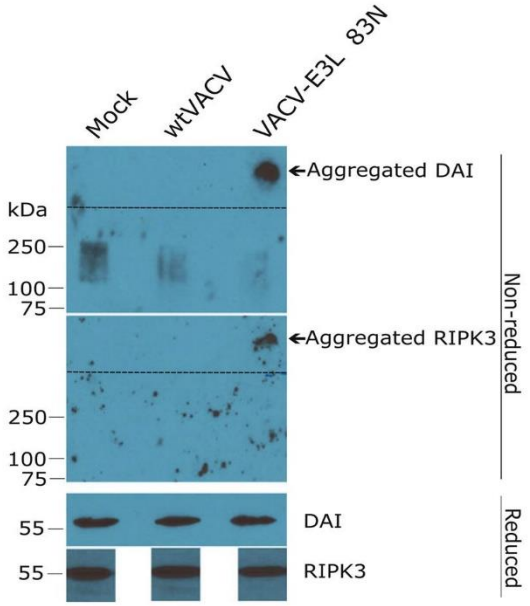

Figure 5-5 Cross-linking to Determine the Activator of Necroptosis

L929 cells pretreated with type 1 IFN were infected with VACV-E3LΔ83N. At 2 h post infection, cells were harvested and cross-linked according to the protocol described in Subheading 3.4. Lysates were then run on Western blots and probed with antibodies against DAI and RIPK3.

---

[15] When probing the co-immunoprecipitation blots, you will look for both the protein targeted by the bait antibody in the IP and associated proteins. The first primary antibody probe should be against associated proteins. Stripping and re-probing for other associated proteins can be done up to two more times. The final probe should be against the protein pulled down during the IP.

1. For tissue culture experiments prepare 2 × 10^6 cells by infecting or treating with chemical reagents suspected of inducing necroptosis (see Note 6).
2. At 2 h posttreatment or postinfection, aspirate the media and wash cells with 1 mL room-temperature reaction buffer (1× PBS) (see Note 16).
3. Scrape cells into the PBS using the blunt end of a p1000 and transfer the suspension to a microcentrifuge tube.
4. Centrifuge at 1000 × g for 10 min.
5. Remove PBS (supernatant) carefully, not disturbing the pellet (see Note 7).
6. For treatments done in vivo (mice) or tissues collected from a diseased individual (human), homogenize about 5 mg tissue per sample by grinding in liquid nitrogen. The protocol can be scaled up for 25 mg (see Note 17).
7. Resuspend pelleted cells in 100 µL or ground tissue in PBS at a concentration of 5 mg/100 µL.
8. Add 1 µL Halt™ Protease and Phosphatase Inhibitor Cocktail (in case some cells disrupt).
9. Add 8 µL of freshly prepared (see Note 4) 25 mM DSP crosslinker for a final concentration of 2 mM (see Note 18).
10. Incubate at room temperature for 30 min or on ice for 2 h with rotation (see Note 17).
11. Add 2 µL of stop solution: 1 M Tris pH 7.5 (for a final concentration of 20 mM).
12. Incubate for 15 min at room temperature with rotation (see Note 17).
13. Centrifuge at 1000 × g for 10 min at 4 °C.

[16.] Alternatively, 10–25 mM HEPES, bicarbonate/carbonate, and borate buffers pH 7–9 can be used as the reaction buffer.

[17.] For 25 mg of tissue several of the times need to be extended. Step 10: Cross-link by rotating for 1 h at RT or 4 h at 4 °C. Step 12: Incubate with the stop solution for 30 min at RT with rotation. Step 15: Lyse with RIPA for 30 min at 4 °C (with rotation).

14. Remove the supernatant carefully (see Note 7).

15. Add 120 µL of ice-cold RIPA lysis buffer (see Note 1) and incubate on ice for 10 min (see Note 17).

16. Add 60 µL of 4× SDS sample buffer without DTT (see Note 14).

17. Load onto a 10% polyacrylamide gel (see Note 9).

18. Run at 80 V until the sample is past the stacking gel and then at 130 V through the separating gel.

19. Transfer to nitrocellulose membrane for 18 h at 20 V at 4 °C in CAPS transfer buffer with a low-speed magnetic stirrer (see Note 19).

20. Block for 1 h at RT.

21. Add primary antibody overnight at 4 °C (rinse with TBST) (see Note 3).

22. Rinse 3× with TBST at RT for 5 min.

23. Add secondary antibody. Incubate for 2 h at RT in ADB.

24. Wash with TBST 3× at RT for 5 min.

25. Expose and develop blot (see Note 20).

26. For total lysate controls, reduce 50 µL of the cross-linked samples by adding DTT to a final concentration of 50 µM (5.5 µL for 50 µL samples) and incubating the sample first at 37 °C for 1 h and then at 95 °C for 5–10 min.

27. Load on a 10% polyacrylamide gel.

28. Run at 80 V until the sample is past the stacking gel and then at 130 V through the separating gel.

[18.] A final concentration of 1–2 µM is recommended. 2 µM works for L929 cells and brain tissue samples, but the concentration may need adjusting for other tissues and cell types.

[19.] Do not discard the stacking gel; many macromolecular complexes will be present in this part of gel. The entire gel (stacking + separating) should be transferred.

29. Transfer to nitrocellulose membrane in 1× CAPS transfer buffer with added methanol for 1 h at 100 V.

30. Block for 1 h with MBB. Rinse with TBST until no longer cloudy.

31. Add primary antibody overnight at 4 °C (rinse with TBST); see Note 3.

32. Rinse 3× with TBST at RT for 5 min.

33. Add secondary antibody. Incubate for 2 h at RT in ADB.

34. Wash with TBST 3× at RT for 5 min.

35. Expose and image blot (see Note 20).

[20.] Blots can be stripped and probed up to three times. The cross-linked and total lysate control blots should be probed with the same antibodies.

Acknowledgments

We would like to thank Nobuko Fukushima and James Bonner for technical assistance and Dr. Heather Koehler and Dr. Edward Mocarski for sharing expertise in necroptosis through consultation and protocol optimization.

References

1. Holler N, Zaru R, Micheau O et al. (2000) Fas triggers an alternative, caspase-8–independent cell death pathway using the kinase RIP as effector molecule. Nat Immunol 1:489–495. 10.1038/82732 [PubMed: 11101870]
2. Vercammen D, Beyaert R, Denecker G et al. (1998) Inhibition of caspases increases the sensitivity of L929 cells to necrosis mediated by tumor necrosis factor. J Exp Med 187:1477–1485. 10.1084/ jem.187.9.1477 [PubMed: 9565639]
3. Huang Z, Wu S-Q, Liang Yet al. (2015) RIP1/RIP3 binding to HSV-1 ICP6 initiates necroptosis to restrict virus propagation in mice. Cell Host Microbe 17:229–242. 10.1016/j.chom.2015.01.002 [PubMed: 25674982]
4. Petrie EJ, Sandow JJ, Lehmann WIL et al. (2019) Viral MLKL homologs subvert Necroptotic cell death by sequestering cellular RIPK3. Cell Rep 28:3309–3319.e5. 10.1016/j.celrep.2019.08.055 [PubMed: 31553902]
5. Zhang S, Tang M, Luo H et al. (2017) Necroptosis in neurodegenerative diseases: a potential therapeutic target. Cell Death Dis 8: e2905–e2905. 10.1038/cddis.2017.286 [PubMed: 28661482]
6. Hanus J, Anderson C, Wang S (2015) RPE necroptosis in response to oxidative stress and in AMD. Ageing Res Rev 24:286–298. 10.1016/j.arr.2015.09.002 [PubMed: 26369358]
7. Bonnet MC, Preukschat D, Welz P-S et al. (2011) The adaptor protein FADD protects epidermal keratinocytes from necroptosis in vivo and prevents skin inflammation. Immunity 35:572–582. 10.1016/j.immuni.2011.08.014 [PubMed: 22000287]
8. Moriwaki K, Bertin J, Gough PJ et al. (2015) Differential roles of RIPK1 and RIPK3 in TNFinduced necroptosis and chemotherapeutic agent-induced cell death. Cell Death Dis 6: e1636– e1636. 10.1038/cddis.2015.16 [PubMed: 25675296]
9. Bozec D, Iuga AC, Roda G et al. (2016) Critical function of the necroptosis adaptor RIPK3 in protecting from intestinal tumorigenesis. Oncotarget 7:46384–46400. 10.18632/oncotarget.10135 [PubMed: 27344176]

10. Oberst A, Dillon CP, Weinlich R et al. (2011) Catalytic activity of the caspase-8-FLIPL complex inhibits RIPK3-dependent necrosis. Nature 471:363–367. 10.1038/nature09852 [PubMed: 21368763]

11. Wang H, Sun L, Su L et al. (2014) Mixed lineage kinase domain-like protein MLKL causes necrotic membrane disruption upon phosphorylation by RIP3. Mol Cell 54:133–146. 10.1016/ j.molcel.2014.03.003 [PubMed: 24703947]

12. Tanzer MC, Tripaydonis A, Webb AI et al. (2015) Necroptosis signalling is tuned by phosphorylation of MLKL residues outside the pseudokinase domain activation loop. Biochem J 471:255–265. 10.1042/BJ20150678 [PubMed: 26283547]

13. Rodriguez DA, Weinlich R, Brown S et al. (2016) Characterization of RIPK3-mediated phosphorylation of the activation loop of MLKL during necroptosis. Cell Death & Differ 23:76-88. 10.1038/cdd.2015.70

14. Najafov A, Mookhtiar AK, Luu HS et al. (2019) TAM kinases promote necroptosis by regulating oligomerization of MLKL. Mol Cell 75:457–468.e4. 10.1016/j.molcel.2019.05.022 [PubMed: 31230815]

15. Dondelinger Y, Declercq W, Montessuit S et al. (2014) MLKL compromises plasma membrane integrity by binding to phosphatidylinositol phosphates. Cell Rep 7:971–981. 10.1016/ j.celrep.2014.04.026 [PubMed: 24813885]

16. Dovey CM, Diep J, Clarke BP et al. (2018) MLKL requires the inositol phosphate code to execute necroptosis. Mol Cell 70:936–948.e7. 10.1016/j.molcel.2018.05.010 [PubMed: 29883610]

17. de Almagro MC, Goncharov T, Izrael-Tomasevic A et al. (2017) Coordinated ubiquitination and phosphorylation of RIP1 regulates necroptotic cell death. Cell Death Different 24:26–37. 10.1038/ cdd.2016.78

18. Kaiser WJ, Sridharan H, Huang C et al. (2013) Toll-like receptor 3-mediated necrosis via TRIF, RIP3, and MLKL. J Biol Chem 288:31268–31279. 10.1074/jbc.M113.462341 [PubMed: 24019532]

19. Upton JW, Kaiser WJ, Mocarski ES (2012) DAI/ZBP1/DLM-1 complexes with RIP3 to mediate virus-induced programmed necrosis that is targeted by murine cytomegalovirus vIRA. Cell Host Microbe 11:290–297. 10.1016/jxhom.2012.01.016 [PubMed: 22423968]

20. Baker MODG, Shanmugam N, Pham CLL et al. (2020) RHIM-based protein:protein interactions in microbial defence against programmed cell death by necroptosis. Semin Cell Dev Biol 99:86–95. 10.1016/j.semcdb.2018.05.004 [PubMed: 29738881]

21. Jang T, Zheng C, Li J et al. (2014) Structural study of the RIPoptosome core reveals a helical assembly for kinase recruitment. Biochemistry 53:5424–5431. 10.1021/bi500585u [PubMed: 25119434]

CHAPTER 6

CONCLUSIONS AND FUTURE OUTLOOK

Recognition of Canonical dsRNA

Both the dsRNA binding domain and the Z-NA binding domain of VACV E3 protein critically inhibit the innate immune system to allow pathogenesis in mice (160). While the C-terminal dsRNA binding domain's target and function was easily identified, the role of the N-terminus has been less clearly defined. Early studies demonstrated that PKR recognized dsRNA at late times after infection with VACV E3 N-terminal deletion proteins (159, 178). PKR recognition of dsRNA was supported by data from MEF cells harvested from the commonly used mouse strain,129/Sv, with either WT or PKR-/- genotypes (76, 185). These data demonstrated that PKR was solely responsible for inhibiting VACV E3 N-terminal deletion mutants in this cell line. The data from Chapter 2 of this thesis supports these findings as we demonstrate that reducing total dsRNA in VACV E3Δ37N restores viral growth in IFN treated MEF 129 WT cells. Furthermore, MPXV subverts the PKR response by making less total and free dsRNA than VACV. Viral mutants and their phenotypes used in this study are described in Table 1, and cells and their phenotypes are described in Table 2.

After initially characterizing these MEF 129 cells with and without PKR in the previous studies in our lab, 8 week old PKR-/- mice were infected intranasally (IN) with VACV WT and VACV E3Δ37N. The study showed that knocking out PKR in the animal did not restore weight loss of VACV E3Δ37N to what was seen in VACV WT (76). Logistic complications obtaining the mice led to an experimental design that is difficult to compare to the rest of the literature for VACV E3Δ37N IN infections. For intranasal pathogenesis studies, mice are typically infected with VACV at 4-5 weeks old. Because this study did not include an age-matched PKR +/+ infection, it is difficult to draw conclusions relative to previously published studies. Additionally, most studies with VACV E3Δ37N have been done in C57BL/6J mice rather than 129/Sv mice. The PKR -/- mice were generated by knocking PKR out of 129/Sv embryos, implanting them into mice, and then back-crossing the PKR-/- progeny with wild-type C57BL/6J to F2 progeny (197). Papers

using these PKR -/- mice by different authors have referred to these mice and their MEFs as having either 129 or BL6 backgrounds despite tracing back to the same original publication (71, 198–204). It is not clear if any of the labs referring to the PKR-/- mice as C57BL/6 mice have performed additional back-crosses. It is important to have information about the lineage to better understand the differences between the MEF and mouse data, but unfortunately the literature is unclear. This is further obfuscated by data demonstrating that the effects of PKR-/- on two different transgenic mouse models yield different results (205, 206).

In order to look at spread throughout the different organs of the mouse following intranasal infection, we infected mice using 5(10^5) PFU which was previously determined to be the LD_{50} of VACV E3Δ37N in 4.5 week old mice (207). Clinical scores are demonstrated in Figure 4-9 and spread to outer organs in Figure 4-10. The experimental design is different than the design of the PKR -/- mouse study where the goal was to look for restoration of pathogenesis through weight loss (76). For example, in that study, the group with the highest dose was 1(10^6) PFU/mouse which was substantially less than the VACV E3Δ83N of 4(10^7) PFU (207). Additionally, the mice in that study were twice as old leading to VACV WT appearing attenuated by not killing any of the mice. Furthermore, this study did not measure viral spread PKR -/- mice restored spread to any organs. The spread data from Figure 4-10 in this dissertation can be more accurately compared to a previously published intranasal spread experiment in IFN-α/βR -/- mice (76). In that assay, 4 week old mice were infected with 10 times the LD_{50} of VACV E3Δ83N and euthanized at 6 days post infection to measure spread throughout the mouse. They determined that knocking out the IFN α/β receptor restored VACV E3Δ83N spread to brain, lungs, and spleen similarly to our results that of VACV E3Δ37N low dsRNA mutants restored spread to the spleen. Unfortunately, the control virus with a WT E3 locus and low dsRNA (VACV mutA24) did not spread to the brain or lungs preventing us from gathering meaningful data about spread of VACV E3Δ37N IBTR mutants to those organs. The mouse phenotype of VACV mutA24 has never been described, so we were not expecting it to be attenuated.

The results from the in vitro cell experiments from Chapter 2 and the in vivo mouse experiments described in Chapter 4 inform future research and directions that should be taken in several key areas. First, it is critical to understand why VACV E3 N-terminal deletion mutants are not rescued by PKR -/- in mice. Future experiments should include determination of the LD_{50} of VACV E3 N-terminal deletion mutants in PKR -/- mice and detailed analysis of what tissues the virus spreads to in these mice. Furthermore, because VACV mutA24 showed attenuation in the mice, the low dsRNA producing VACV E3Δ37N viruses should be reverted to WT E3 as the positive control for tissue spread instead of relying on VACV WT. It would also be helpful to determine the LD_{50} of the VACV E3Δ37N IBTR viruses and the WT E3 revertant viruses. Additionally, the role of dsRNA in viral pathogenesis has not been fully described. Screening known VACV IBTR mutants for attenuation in mice could be used to better understand the role those proteins play during infection. Additionally, if most IBTR mutants are attenuated in mice, dsRNA may positively contribute to pathogenesis in VACV infections.

Other future experiments could include determining how MPXV makes less dsRNA than VACV. Analysis from previous studies demonstrates that the genes most often responsible for IBT resistance (A18R, A24R, G2R, H5R, J3R, and J6R) are highly conserved between MPXV and VACV (173). Additionally, previous studies have demonstrated that IBT resistance could not be rescued by swapping out A18R, A24R, G2R, H5R, J3R, and J6R in VACV with their MPXV homologues (unpublished). It is likely that MPXV lost dsRNA production before losing VACV E3 N-terminus expression which means there was selective pressure against dsRNA.

Finally, while we have established the importance of the N-terminus for dsRNA sequestration, we have not shown how it sequesters dsRNA. Research from others demonstrated that there is no reduction in binding affinity to dsRNA in VACV E3Δ37N compared to E3 WT *in vitro* (164). However ,other research revealed a nuclear location signal in the N-terminus of E3 (208). Now that imaging technologies have improved, future studies could use pre-established virus expressing GFP tagged E3 to determine where E3 localizes during infection. Furthermore, point mutants in the N-terminus of E3 have been identified that disturb nuclear localization (208).

Previous studies were only able to determine whether or not these mutations altered nuclear localization. Now, we have identified that MEF 129 cells rely solely on dsRNA recognition by PKR for VACV E3Δ37N IFN sensitivity and can screen the non-nuclear localizing E3 mutants for reduced growth in IFN treated cells.

Recognition of Z-form Nucleic Acid

While the Z form of nucleic acid has been hypothesized to have a functional role in cells since its discovery, the tools have only recently been developed to explore what that role might be. To study this, we will use L929 cells which were established from CH3/An subcutaneous fibroblasts and spontaneously immortalized by repeated splitting leaving the necroptosis pathway intact. Previous research demonstrated that VACV E3 N-terminal deletion mutants were interferon sensitive through the DAI and necroptosis pathway (130). Chapter 3 demonstrates that the pathogen associated molecular pattern recognized by DAI is an RNA molecule recognizable by antibodies to the Z-form conformation. Furthermore, it depends on VACV early mRNA expression, and reduction of dsRNA in VACV E3Δ37N infections does not restore the wild-type phenotype.

Future experiments will need to determine what RNA is being converted into Z-form and how it transitions. While early VACV mRNA expression is necessary for necroptosis, it does not necessarily mean that those are the Z-RNAs. One publication has reported early dsRNA capable of activating PKR formed only in VACV ΔK1 virus (209). However, strand-specific sequencing analysis of poxvirus mRNA only yielded two potential sites for early dsRNA to form. One is the junction between K7R and F1L, the other is the junction between A46R and A47L (30). It is possible that the transcripts are from mRNA or mitochondrial RNA and not from poxvirus though. Transcription patterns of VACV are different in HeLa and L929s cells. HeLa cells produce more late RNA whereas in L929, more early transcripts are produced (52). Additionally, late RNA is less stable than early RNA in HeLa cells, but in L929 cells both early and late RNA have an equal intermediate phenotype for stability (52). One hypothesis is that early transcription induces a

change in the cells that allows RNA to convert to the Z-form. It has been proposed that stress granules induced by infection are creating a favorable microenvironment for conversion (210, 211). Furthermore, oxidative stress can lead to necroptosis via mitochondrial dysfunction (212, 213). Recent cryo-EM of dsRNA being processed by the mitochondrial protein MDA5 also suggest that ZRNA might be formed there (145, 214). Future studies will need to confirm the sequences of the Z-RNA, look for detailed cellular localization, and determine what other proteins are necessary for their conversion to the Z form.

In the animal models, clinical symptoms of VACV E3Δ83N can increase in DAI -/-, RIP3 -/-, and MLKL -/- (three critical necroptosis proteins) mice (130). DAI -/- mice were made with modified 129 embryos, injected into C57BL/6 mice, and backcrossed to the F2 generation (215). RIP3 -/- mice were generated in 129 R1 ES cells and injected in C57BL/6N mice before 4 generations of back crosses (216). MLKL -/- were generated in C57BL/6 mice (123). Further studies demonstrated that in these knockout mice, the LD_{50} of VACV E3Δ83N increased but was not fully restored in intranasal and intracranial infections (157). However, pathogenesis of VACV E3Δ37N was fully restored in DAI -/- and MLKL -/- mice after intranasal infections. This indicates that the primary pathway restricting E3 N-terminal deletion mutants in mice is DAI and necroptosis. Previous pathogenesis studies of VACV E3 N-terminal deletion mutant intranasal infections of these knockout mice only looked at spread to the lungs and brain (130, 157). Future pathogenesis studies should quantify virus in the other organs. Similar to our findings in Figure 4-8, previous studies also determined intracranial infections of MLKL -/- mice took longer to develop symptoms than WT mice for all VACV mutants (157).

Inhibition in JC Cells

We used JC cells to study VACV E3Δ37N replication because of the high correlation between growth in multi-step growth curves in JC cells and intracranial LD_{50s} in WT mice (Figure 1) (172). The JC cell line was established from a spontaneous primary mammary adenocarcinoma in a BALB/ cROS mouse. Previous research demonstrated that VACV E3Δ37N

was being inhibited before it could begin DNA replication or make intermediate and late transcripts (167). In chapter 4 of this thesis, I demonstrated that inhibition of DAI and a dsRNA sensor are both necessary to restore growth in JC cells. These results have been confirmed by other lab members who have determined that either knocking out DAI or PKR can restore both cell viability and viral replication (unpublished). Furthermore, unlike the L929 cells, in JC cells reduction of dsRNA in VACV E3Δ37N mutants partially restores cell death. It does not however restore growth in untreated JCs. Inhibition of RIP3 kinase activity and reduction of dsRNA are both required to fully restore the JC phenotype.

While we have determined that inhibition of both PKR and DAI are needed to allow viral replication, we still do not understand how these pathways interact. Future studies include cross-linking JC cells to determine if PKR and DAI are both interacting with RIP3. It is also unexpected that unlike L929 cells, loss of dsRNA can partially inhibit necroptosis. Preliminary data demonstrates that inhibitors of dsRNA replication inhibit MLKL phosphorylation unlike what happens in L929 cells where only inhibition of early transcription can block necroptosis indicating that either there are multiple pathways that lead to ZRNA formation or that DAI activation in JC cells also requires PKR activation. ZRNA staining has not been done in JC cells and will be necessary to confirm what PAMP is being recognized to inhibit virus growth

Inhibition of RIP3 kinase activity fully restores cell viability in VACV E3Δ37N infections, but cannot alone restore viral replication suggesting that necroptosis is not the sole pathway of viral inhibition. MLKL knock out JC cells do not permit VACV E3Δ37N replication confirming that necroptosis is not the sole pathway of inhibition (unpublished). RIP3 has other roles in the cell that might be being used to inhibit virus (115). A RIP3 knockout cell line might help determine if replication is restored will be critical to determining how the cells are inhibiting the virus.

Because of the correlation between JC growth and intracranial pathogenesis, we decided to test the VACV E3Δ37 IBTR mutants during intracranial infections. The intracranial (IC) experiment from this study shown in Figure 4-8 was initially designed to look for P-MLKL staining in brains, but the staining did not happen. In order to draw conclusions about intracranial

infections, a future experiment must measure IC LD_{50s} in WT and MLKL -/- mice of VACV E3Δ37N, the VACV E3Δ37N IBTR mutants, and VACV E3Δ37N IBTR to WT E3 revertants. If the JC cells are truly indicative of intracranial pathogenesis, the VACV E3Δ37N IC LD_{50} will be slightly increased in the MLKL-/- mice, and the VACV E3Δ37N IBTR IC LD50 will be fully restored in the MLKL -/- mice. For this experiment, VACV E3Δ37N IBTR7 would need to be used as VACV E3Δ37N IBTR3 was partially attenuated in intranasal infections through its low dsRNA mutation. Determining what matters in an infected host *in vivo* will be critical to determining what cell lines best represent the actual function of E3.

Overall, this study determined that two of our cell lines work as model systems to study canonical dsRNA (MEF 129) or ZRNA (L929). It also determined that a third cell line chosen due to its similarity with intracranial pathogenesis in mice (JC) has a more complex system of identifying a VACV E3Δ37N infection. Further studies will be needed to determine what this cell line's mechanism of action is. Finally, the role of each of these pathways in mice is still nebulous and will require additional experiments to clarify the extent of how these pathways interact.

Figure 6-1 Overview of Findings in this Dissertation. The MEF 129 cells are totally dependent on PKR and eIF2α phosphorylation while the L929 cells restrict viral growth solely through DAI and necroptosis. In JC cells, both are somehow working together to inhibit viral replication. In animal models, removal of the DAI/necroptosis genes rescues pathogenesis in high doses. LD50s are not fully restored to VACV WT though indicating there may be more going on.

Figure 6-1 Overview of findings in this dissertation.

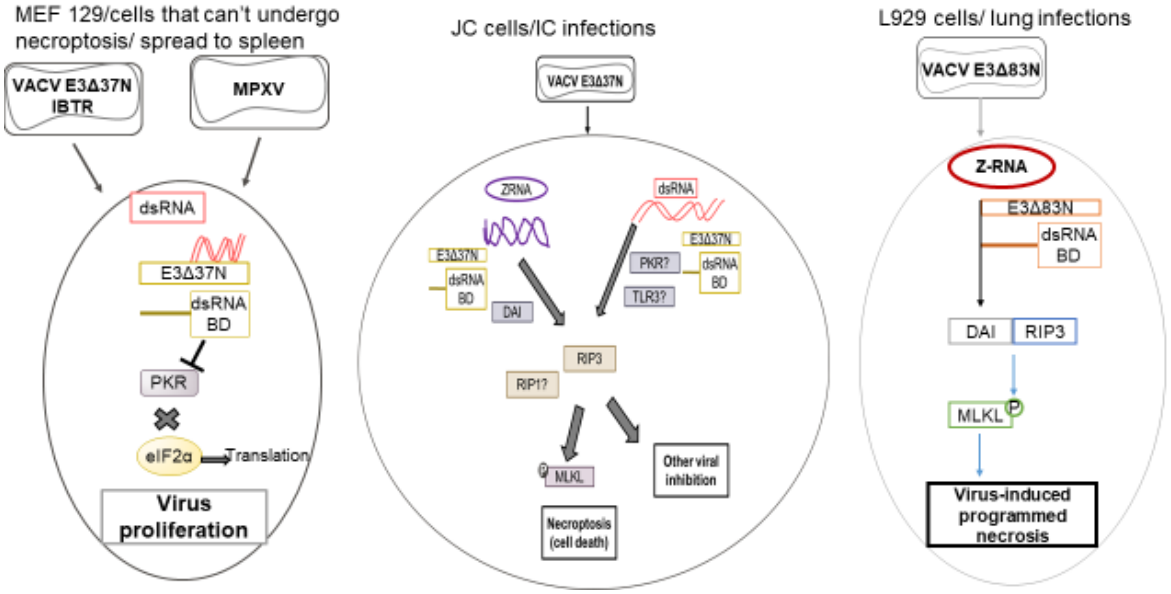

Table 6-1 Viruses Used in This Study

Table 6-1: Viruses and their phenotypes									
System	**Phenotype**	**VACV WT**	**VACV mutA24**	**VACV E3Δ83N**	**VACV E3Δ37N**	**VACV E3Δ37N IBTR3**	**VACV E3Δ37N IBTR7**	**MPXV**	**VACV ΔE3::F3**
	E3 locus	WT	WT	N-deleted	N-deleted	N-deleted	N-deleted	N-deleted	N-deleted
HeLa	dsRNA	+++	-	+++	+++	-	+	+	+++
	free dsRNA	-	-	+++	+++	-	-	-	+++
	PKR activation	-	-	Late	Late	-	-	-	Late
MEF 129	PKR activation	-	-	Late	Late	-	-	-	nd
	IFN sensitivity	-	-	+++	+++	-	-	-	nd
L929	IFN sensitivity	-	-	+++	+++	+++	+++	++	+++
	IFN sensitivity with RIP3 kinase inhibitor	-	-	-	-	-	-	-	nd
	Cell death	-	-	+++	+++	+++	+++	+	nd
	Cell death with RIP3 kinase inhibitor	-	-	-	-	-	-	-	-
JC	Replication	+++	+++	-	-	-	-	++	-
	Replication with RIP3 kinase inhibitor	+++	+++	nd	+	+++	+++	+++	nd
	Cell death	-	-	++	++	+	+	+	nd
	Cell death with RIP3 kinase inhibitor	-	-	-	-	-	-	-	nd
Mice	IN pathogenesis at VACV E3Δ37N LD50	+++	-	nd	+++	-	+++	nd	nd
	Spread to spleen	+++	++	nd	-	++	++	nd	nd

Table 6-2 Cell Phenotypes Used in This Study

Table 6-2: Cell lines and their phenotypes				
		MEF 129	**L929**	**JC**
Background	Mouse strain	129/Sv	CH3	Balb/cROS
	Cell type	embryonic fibroblast	subcutaneous fibroblast	breast adenocarcinoma
	Immortalization	SV40	repeated splitting	cancer
	DAI expression	IFN stimulated	IFN stimulated	constitutive
	PKR expression	IFN stimulated	IFN stimulated	consitutive
	Necroptosis capable	-	+	+
Virus growth	VACV WT	+++	+++	+++
	MPXV	+++	IFN sensitive	+++
	VACV E3Δ37N	IFN sensitive	IFN sensitive	-
	VACV E3Δ37N IBTR	IFN sensitive	IFN sensitive	-
Restricting PAMP sensor	VACV E3Δ37N	PKR	DAI	PKR + DAI
	VACV E3Δ37N IBTR	-	DAI	DAI or RIP3 kinase
Death	VACV E3Δ37N	-	+++	++
	VACV E3Δ37N IBTR	-	+++	+

REFERENCES

1. Chowdhury EK, Khan II, Dhar BK. Catastrophic impact of Covid-19 on the global stock markets and economic activities. Business and Society Review n/a.

2. Almeida V, Barrios S, Christl M, De Poli S, Tumino A, van der Wielen W. 2021. The impact of COVID-19 on households´ income in the EU. J Econ Inequal https://doi.org/10.1007/s10888-021-09485-8.

3. 2021. CDC Newsroom. CDC.

4. Yinka-Ogunleye A, Aruna O, Ogoina D, Aworabhi N, Eteng W, Badaru S, Mohammed A, Agenyi J, Etebu EN, Numbere T-W, Ndoreraho A, Nkunzimana E, Disu Y, Dalhat M, Nguku P, Mohammed A, Saleh M, McCollum A, Wilkins K, Faye O, Sall A, Happi C, Mba N, Ojo O, Ihekweazu C. 2018. Reemergence of Human Monkeypox in Nigeria, 2017. Emerg Infect Dis 24:1149–1151.

5. Yinka-Ogunleye A, Aruna O, Dalhat M, Ogoina D, McCollum A, Disu Y, Mamadu I, Akinpelu A, Ahmad A, Burga J, Ndoreraho A, Nkunzimana E, Manneh L, Mohammed A, Adeoye O, Tom-Aba D, Silenou B, Ipadeola O, Saleh M, Adeyemo A, Nwadiutor I, Aworabhi N, Uke P, John D, Wakama P, Reynolds M, Mauldin MR, Doty J, Wilkins K, Musa J, Khalakdina A, Adedeji A, Mba N, Ojo O, Krause G, Ihekweazu C, Mandra A, Davidson W, Olson V, Li Y, Radford K, Zhao H, Townsend M, Burgado J, Satheshkumar PS. 2019. Outbreak of human monkeypox in Nigeria in 2017–18: a clinical and epidemiological report. The Lancet Infectious Diseases 19:872–879.

6. Mauldin MR, McCollum AM, Nakazawa YJ, Mandra A, Whitehouse ER, Davidson W, Zhao H, Gao J, Li Y, Doty J, Yinka-Ogunleye A, Akinpelu A, Aruna O, Naidoo D, Lewandowski K, Afrough B, Graham V, Aarons E, Hewson R, Vipond R, Dunning J, Chand M, Brown C, Cohen-Gihon I, Erez N, Shifman O, Israeli O, Sharon M, Schwartz E, Beth-Din A, Zvi A, Mak TM, Ng YK, Cui L, Lin RTP, Olson VA, Brooks T, Paran N, Ihekweazu C, Reynolds MG. 2020. Exportation of Monkeypox virus from the African continent. J Infect Dis jiaa559.

7. Reed KD, Melski JW, Graham MB, Regnery RL, Sotir MJ, Wegner MV, Kazmierczak JJ, Stratman EJ, Li Y, Fairley JA, Swain GR, Olson VA, Sargent EK, Kehl SC, Frace MA, Kline R, Foldy SL, Davis JP, Damon IK. 2004. The Detection of Monkeypox in Humans in the Western Hemisphere. New England Journal of Medicine 350:342–350.

8. Hutson C, Lee K, Abel J, Carroll D, Montgomery J, Olson V, Li Y, Davidson W, Hughes C, Dillon M, Spurlock P, Kazmierczak J, Austin C, Miser L, Sorhage F, Howell J, Davis J, Reynolds M, Braden Z, Regnery R. 2007. Monkeypox zoonotic associations: Insights from laboratory evaluation of animals associated with the multi-state US outbreak. The American journal of tropical medicine and hygiene 76:757–68.

9. Likos AM, Sammons SA, Olson VA, Frace AM, Li Y, Olsen-Rasmussen M, Davidson W, Galloway R, Khristova ML, Reynolds MG, Zhao H, Carroll DS, Curns A, Formenty P, Esposito JJ, Regnery RL, Damon IKY 2005. A tale of two clades: monkeypox viruses. Journal of General Virology 86:2661–2672.

10. Rezza G. 2019. Emergence of human monkeypox in west Africa. The Lancet Infectious Diseases 19:797–799.

11. Magnus P von, Andersen EK, Petersen KB, Birch-Andersen A. 1959. A Pox-Like Disease in Cynomolgus Monkeys. Acta Pathologica Microbiologica Scandinavica 46:156–176.

12. Marennikova SS, Šeluhina EM, Mal'ceva NN, Čimiškjan KL, Macevič GR. 1972. Isolation and properties of the causal agent of a new variola-like disease (monkeypox) in man. Bull World Health Organ 46:599–611.

13. Reynolds MG, Carroll DS, Olson VA, Hughes C, Galley J, Likos A, Montgomery JM, Suu-Ire R, Kwasi MO, Root JJ, Braden Z, Abel J, Clemmons C, Regnery R, Karem K, Damon IK. 2010. A Silent Enzootic of an Orthopoxvirus in Ghana, West Africa: Evidence for Multi-Species Involvement in the Absence of Widespread Human Disease. The American Journal of Tropical Medicine and Hygiene 82:746–754.

14. Simpson K, Heymann D, Brown CS, Edmunds WJ, Elsgaard J, Fine P, Hochrein H, Hoff NA, Green A, Ihekweazu C, Jones TC, Lule S, Maclennan J, McCollum A, Mühlemann B, Nightingale E, Ogoina D, Ogunleye A, Petersen B, Powell J, Quantick O, Rimoin AW, Ulaeato D, Wapling A. 2020. Human monkeypox – After 40 years, an unintended consequence of smallpox eradication. Vaccine 38:5077–5081.

15. McFadden G. 2005. Poxvirus tropism. Nat Rev Microbiol 3:201–213.

16. Buller RM, Palumbo GJ. 1991. Poxvirus pathogenesis. Microbiol Rev 55:80–122.

17. Chung CS, Hsiao JC, Chang YS, Chang W. 1998. A27L protein mediates vaccinia virus interaction with cell surface heparan sulfate. J Virol 72:1577–1585.

18. Hsiao JC, Chung CS, Chang W. 1999. Vaccinia virus envelope D8L protein binds to cell surface chondroitin sulfate and mediates the adsorption of intracellular mature virions to cells. J Virol 73:8750–8761.

19. Lin CL, Chung CS, Heine HG, Chang W. 2000. Vaccinia virus envelope H3L protein binds to cell surface heparan sulfate and is important for intracellular mature virion morphogenesis and virus infection in vitro and in vivo. J Virol 74:3353–3365.

20. Chiu W-L, Lin C-L, Yang M-H, Tzou D-LM, Chang W. 2007. Vaccinia virus 4c (A26L) protein on intracellular mature virus binds to the extracellular cellular matrix laminin. J Virol 81:2149–2157.

21. Whitbeck JC, Foo C-H, Ponce de Leon M, Eisenberg RJ, Cohen GH. 2009. Vaccinia virus exhibits cell-type-dependent entry characteristics. Virology 385:383–391.

22. Perino J, Foo CH, Spehner D, Cohen GH, Eisenberg RJ, Crance J-M, Favier A-L. 2011. Role of sulfatide in vaccinia virus infection. Biol Cell 103:319–331.

23. Izmailyan R, Hsao J-C, Chung C-S, Chen C-H, Hsu PW-C, Liao C-L, Chang W. 2012. Integrin β1 Mediates Vaccinia Virus Entry through Activation of PI3K/Akt Signaling. J Virol 86:6677–6687.

24. Senkevich TG, Ojeda S, Townsley A, Nelson GE, Moss B. 2005. Poxvirus multiprotein entry-fusion complex. Proceedings of the National Academy of Sciences 102:18572–18577.

25. Schmidt FI, Bleck CKE, Mercer J. 2012. Poxvirus host cell entry. Current Opinion in Virology 2:20–27.

26. Joklik WK. 1964. The intracellular uncoating of poxvirus DNA: I. The fate of radioactively-labeled rabbitpox virus. Journal of Molecular Biology 8:263–276.

27. Joklik WK. 1964. The intracellular uncoating of poxvirus DNA: II. The molecular basis of the uncoating process. Journal of Molecular Biology 8:277–288.

28. Kates JR, McAuslan BR. 1967. MESSENGER RNA SYNTHESIS BY A “COATED” VIRAL GENOME*. Proc Natl Acad Sci U S A 57:314–320.

29. Kilcher S, Schmidt FI, Schneider C, Kopf M, Helenius A, Mercer J. 2014. siRNA Screen of Early Poxvirus Genes Identifies the AAA+ ATPase D5 as the Virus Genome-Uncoating Factor. Cell Host & Microbe 15:103–112.

30. Yang Z, Reynolds SE, Martens CA, Bruno DP, Porcella SF, Moss B. 2011. Expression Profiling of the Intermediate and Late Stages of Poxvirus Replication ▿. J Virol 85:9899–9908.

31. Da Fonseca F, Moss B. 2003. Poxvirus DNA topoisomerase knockout mutant exhibits decreased infectivity associated with reduced early transcription. Proceedings of the National Academy of Sciences 100:11291–11296.

32. Broyles SS. 2003. Vaccinia virus transcription. Journal of General Virology 84:2293–2303.

33. Broyles SS, Moss B. 1986. Homology between RNA polymerases of poxviruses, prokaryotes, and eukaryotes: nucleotide sequence and transcriptional analysis of vaccinia virus genes encoding 147-kDa and 22-kDa subunits. Proc Natl Acad Sci U S A 83:3141–3145.

34. Magee WE, Miller OV. 1968. Initiation of Vaccinia Virus Infection in Actinomycin D-pretreated Cells. J Virol 2:678–685.

35. Martin S, Moss B. 1975. Modification of RNA by mRNA guanylyltransferase and mRNA (guanine-7-)methyltransferase from vaccinia virions. Journal of Biological Chemistry 250:9330–9335.

36. Cong P, Shuman S. 1992. Methyltransferase and subunit association domains of vaccinia virus mRNA capping enzyme. Journal of Biological Chemistry 267:16424–16429.

37. Higman MA, Bourgeois N, Niles EG. 1992. The vaccinia virus mRNA (guanine-N7-)-methyltransferase requires both subunits of the mRNA capping enzyme for activity. Journal of Biological Chemistry 267:16430–16437.

38. Mao X, Shuman S. 1994. Intrinsic RNA (guanine-7) methyltransferase activity of the vaccinia virus capping enzyme D1 subunit is stimulated by the D12 subunit. Identification of amino acid residues in the D1 protein required for subunit association and methyl group transfer. Journal of Biological Chemistry 269:24472–24479.

39. Hillen HS, Bartuli J, Grimm C, Dienemann C, Bedenk K, Szalay AA, Fischer U, Cramer P. 2019. Structural Basis of Poxvirus Transcription: Transcribing and Capping Vaccinia Complexes. Cell 179:1525-1536.e12.

40. Yuen L, Moss B. 1987. Oligonucleotide sequence signaling transcriptional termination of vaccinia virus early genes. Proceedings of the National Academy of Sciences 84:6417–6421.

41. Tate J, Gollnick P. 2015. The role of vaccinia termination factor and cis-acting elements in vaccinia virus early gene transcription termination. Virology 485:179–188.

42. Gershon PD, Ahn B-Y, Garfield M, Moss B. 1991. Poly(A) polymerase and a dissociable polyadenylation stimulatory factor encoded by vaccinia virus. Cell 66:1269–1278.

43. DeLange AM, McFadden G. 1986. Sequence-nonspecific replication of transfected plasmid DNA in poxvirus-infected cells. Proceedings of the National Academy of Sciences 83:614–618.

44. Merchlinsky M, Moss B. 1986. Resolution of linear minichromosomes with hairpin ends from circular plasmids containing vaccinia virus concatemer junctions. Cell 45:879–884.

45. De Silva FS, Lewis W, Berglund P, Koonin EV, Moss B. 2007. Poxvirus DNA primase. Proceedings of the National Academy of Sciences 104:18724–18729.

46. Wang TS-E, Wong SW, Korn D. 1989. Human DNA polymerase α: predicted functional domains and relationships with viral DNA polymerases. The FASEB Journal 3:14–21.

47. Willer DO, Mann MJ, Zhang W, Evans DH. 1999. Vaccinia Virus DNA Polymerase Promotes DNA Pairing and Strand-Transfer Reactions. Virology 257:511–523.

48. Willer DO, Yao X-D, Mann MJ, Evans DH. 2000. In Vitro Concatemer Formation Catalyzed by Vaccinia Virus DNA Polymerase. Virology 278:562–569.

49. Duesberg PH, Colby C. 1969. On the Biosynthesis and Structure of Double-Stranded RNA in Vaccinia Virus-Infected Cells. Proceedings of the National Academy of Sciences of the United States of America 64:396–403.

50. Colby C, Duesberg PH. 1969. Double-stranded RNA in Vaccinia Virus Infected Cells. 5197. Nature 222:940–944.

51. Boone RF, Parr RP, Moss B. 1979. Intermolecular duplexes formed from polyadenylylated vaccinia virus RNA. J Virol 30:365–374.

52. Oda K-I, Joklik WK. 1967. Hybridization and sedimentation studies on “early” and “late” vaccinia messenger RNA. Journal of Molecular Biology 27:395–419.

53. Sebring ED, Salzman NP. 1967. Metabolic Properties of Early and Late Vaccinia Virus Messenger Ribonucleic Acid. J Virol 1:550–558.

54. Liu R, Moss B. 2016. Opposing Roles of Double-Stranded RNA Effector Pathways and Viral Defense Proteins Revealed with CRISPR-Cas9 Knockout Cell Lines and Vaccinia Virus Mutants. J Virol 90:7864–7879.

55. Liu S-W, Katsafanas GC, Liu R, Wyatt LS, Moss B. 2015. Poxvirus Decapping Enzymes Enhance Virulence by Preventing the Accumulation of dsRNA and the Induction of Innate Antiviral Responses. Cell Host & Microbe 17:320–331.

56. Burgess HM, Mohr I. 2015. Cellular 5′-3′ mRNA Exonuclease Xrn1 Controls Double-Stranded RNA Accumulation and Anti-Viral Responses. Cell Host & Microbe 17:332–344.

57. Cantu F, Cao S, Hernandez C, Dhungel P, Spradlin J, Yang Z. 2020. Poxvirus-encoded decapping enzymes promote selective translation of viral mRNAs. PLOS Pathogens 16:e1008926.

58. Morgan C. 1976. The insertion of DNA into vaccinia virus. Science 193:591–592.

59. Griffiths G, Roos N, Schleich S, Locker JK. 2001. Structure and Assembly of Intracellular Mature Vaccinia Virus: Thin-Section Analyses. J Virol 75:11056–11070.

60. Smith GL, Law M. 2004. The exit of Vaccinia virus from infected cells. Virus Research 106:189–197.

61. Schmelz M, Sodeik B, Ericsson M, Wolffe EJ, Shida H, Hiller G, Griffiths G. 1994. Assembly of vaccinia virus: the second wrapping cisterna is derived from the trans Golgi network. J Virol 68:130–147.

62. Sivan G, Weisberg AS, Americo JL, Moss B. 2016. Retrograde Transport from Early Endosomes to the trans-Golgi Network Enables Membrane Wrapping and Egress of Vaccinia Virus Virions. J Virol 90:8891–8905.

63. Dey M, Cao C, Dar AC, Tamura T, Ozato K, Sicheri F, Dever TE. 2005. Mechanistic link between PKR dimerization, autophosphorylation, and eIF2alpha substrate recognition. Cell 122:901–913.

64. Cole JL. 2007. Activation of PKR: an open and shut case? Trends Biochem Sci 32:57–62.

65. Kuhen KL, Samuel CE. 1999. Mechanism of interferon action: functional characterization of positive and negative regulatory domains that modulate transcriptional activation of the human RNA-dependent protein kinase Pkr promoter. Virology 254:182–195.

66. Pathak VK, Schindler D, Hershey JW. 1988. Generation of a mutant form of protein synthesis initiation factor eIF-2 lacking the site of phosphorylation by eIF-2 kinases. Mol Cell Biol 8:993–995.

67. Dar AC, Dever TE, Sicheri F. 2005. Higher-Order Substrate Recognition of eIF2α by the RNA-Dependent Protein Kinase PKR. Cell 122:887–900.

68. Der SD, Yang Y-L, Weissmann C, Williams BRG. 1997. A double-stranded RNA-activated protein kinase-dependent pathway mediating stress-induced apoptosis. Proc Natl Acad Sci U S A 94:3279–3283.

69. Gil J, Esteban M. 2000. The interferon-induced protein kinase (PKR), triggers apoptosis through FADD-mediated activation of caspase 8 in a manner independent of Fas and TNF-α receptors. Oncogene 19:3665–3674.

70. Kibler KV, Shors T, Perkins KB, Zeman CC, Banaszak MP, Biesterfeldt J, Langland JO, Jacobs BL. 1997. Double-stranded RNA is a trigger for apoptosis in vaccinia virus-infected cells. Journal of Virology 71:1992–2003.

71. Kumar A, Yang YL, Flati V, Der S, Kadereit S, Deb A, Haque J, Reis L, Weissmann C, Williams BR. 1997. Deficient cytokine signaling in mouse embryo fibroblasts with a targeted deletion in the PKR gene: role of IRF-1 and NF-kappaB. EMBO J 16:406–416.

72. Ishii T, Kwon H, Hiscott J, Mosialos G, Koromilas AE. 2001. Activation of the I kappa B alpha kinase (IKK) complex by double-stranded RNA-binding defective and catalytic inactive mutants of the interferon-inducible protein kinase PKR. Oncogene 20:1900–1912.

73. Gil J, Rullas J, García MA, Alcamí J, Esteban M. 2001. The catalytic activity of dsRNA-dependent protein kinase, PKR, is required for NF-kappaB activation. Oncogene 20:385–394.

74. Thapa RJ, Nogusa S, Chen P, Maki JL, Lerro A, Andrake M, Rall GF, Degterev A, Balachandran S. 2013. Interferon-induced RIP1/RIP3-mediated necrosis requires PKR and is licensed by FADD and caspases. PNAS 110:E3109–E3118.

75. Lee SB, Esteban M. 1993. The Interferon-Induced Double-Stranded RNA-Activated Human p68 Protein Kinase Inhibits the Replication of Vaccinia Virus. Virology 193:1037–1041.

76. White SD, Jacobs BL. 2012. The Amino Terminus of the Vaccinia Virus E3 Protein Is Necessary To Inhibit the Interferon Response. Journal of Virology 86:5895–5904.

77. Hartmann R, Justesen J, Sarkar SN, Sen GC, Yee VC. 2003. Crystal Structure of the 2′-Specific and Double-Stranded RNA-Activated Interferon-Induced Antiviral Protein 2′-5′-Oligoadenylate Synthetase. Molecular Cell 12:1173–1185.

78. Kodym R, Kodym E, Story MD. 2009. 2'-5'-Oligoadenylate synthetase is activated by a specific RNA sequence motif. Biochem Biophys Res Commun 388:317–322.

79. Silverman RH, Weiss SR. 2014. Viral phosphodiesterases that antagonize double-stranded RNA signaling to RNase L by degrading 2-5A. J Interferon Cytokine Res 34:455–463.

80. Zeng M, Qi M, Wang Y, Xu R, Wu Y, Li M, Zheng X, Feng W. 2020. 5-O-methyldihydroquercetin and cilicicone B isolated from Spina Gleditsiae ameliorate lipopolysaccharide-induced acute kidney injury in mice by inhibiting inflammation and oxidative stress via the TLR4/MyD88/TRIF/NLRP3 signaling pathway. International Immunopharmacology 80:106194.

81. Han J-Q, Barton DJ. 2002. Activation and evasion of the antiviral 2'-5' oligoadenylate synthetase/ribonuclease L pathway by hepatitis C virus mRNA. RNA 8:512–525.

82. Liang S-L, Quirk D, Zhou A. 2006. RNase L: Its biological roles and regulation. IUBMB Life 58:508–514.

83. Bisbal C, Silverman RH. 2007. Diverse functions of RNase L and implications in pathology. Biochimie 89:789–798.

84. Samuel CE. 2012. ADARs, Viruses and Innate Immunity. Curr Top Microbiol Immunol 353:10.1007/82_2011_148.

85. George CX, Gan Z, Liu Y, Samuel CE. 2011. Adenosine Deaminases Acting on RNA, RNA Editing, and Interferon Action. J Interferon Cytokine Res 31:99–117.

86. Patterson JB, Samuel CE. 1995. Expression and regulation by interferon of a double-stranded-RNA-specific adenosine deaminase from human cells: evidence for two forms of the deaminase. Mol Cell Biol 15:5376–5388.

87. Athanasiadis A, Placido D, Maas S, Brown BA, Lowenhaupt K, Rich A. 2005. The crystal structure of the Zbeta domain of the RNA-editing enzyme ADAR1 reveals distinct conserved surfaces among Z-domains. J Mol Biol 351:496–507.

88. Liu Y, Lei M, Samuel CE. 2000. Chimeric double-stranded RNA-specific adenosine deaminase ADAR1 proteins reveal functional selectivity of double-stranded RNA-binding domains from ADAR1 and protein kinase PKR. Proc Natl Acad Sci U S A 97:12541–12546.

89. Huynh TP, Jacobs BL, Hogue B, Chang Y, Ugarova T, Arizona State University. 2013. Characterization of Host Responses to Vaccinia Virus InfectionASU Electronic Theses and Dissertations. Arizona State University.

90. Reikine S, Nguyen JB, Modis Y. 2014. Pattern Recognition and Signaling Mechanisms of RIG-I and MDA5. Frontiers in Immunology 5:342.

91. Feng M, Ding Z, Xu L, Kong L, Wang W, Jiao S, Shi Z, Greene MI, Cong Y, Zhou Z. 2013. Structural and biochemical studies of RIG-I antiviral signaling. Protein Cell 4:142–154.

92. Berke IC, Modis Y. 2012. MDA5 cooperatively forms dimers and ATP-sensitive filaments upon binding double-stranded RNA. The EMBO Journal 31:1714–1726.

93. Yoneyama M, Onomoto K, Jogi M, Akaboshi T, Fujita T. 2015. Viral RNA detection by RIG-I-like receptors. Current Opinion in Immunology 32:48–53.

94. Weber F. 2015. The catcher in the RIG-I. Cytokine 76:38–41.

95. Seth RB, Sun L, Ea C-K, Chen ZJ. 2005. Identification and Characterization of MAVS, a Mitochondrial Antiviral Signaling Protein that Activates NF-κB and IRF3. Cell 122:669–682.

96. Xu L-G, Wang Y-Y, Han K-J, Li L-Y, Zhai Z, Shu H-B. 2005. VISA Is an Adapter Protein Required for Virus-Triggered IFN-β Signaling. Molecular Cell 19:727–740.

97. Kawai T, Takahashi K, Sato S, Coban C, Kumar H, Kato H, Ishii KJ, Takeuchi O, Akira S. 2005. IPS-1, an adaptor triggering RIG-I- and Mda5-mediated type I interferon induction. Nat Immunol 6:981–988.

98. Paz S, Sun Q, Nakhaei P, Romieu-Mourez R, Goubau D, Julkunen I, Lin R, Hiscott J. 2006. Induction of IRF-3 and IRF-7 phosphorylation following activation of the RIG-I pathway. Cell Mol Biol (Noisy-le-grand) 52:17–28.

99. Sharma S. 2003. Triggering the Interferon Antiviral Response Through an IKK-Related Pathway. Science 300:1148–1151.

100. Fitzgerald KA, McWhirter SM, Faia KL, Rowe DC, Latz E, Golenbock DT, Coyle AJ, Liao S-M, Maniatis T. 2003. IKKε and TBK1 are essential components of the IRF3 signaling pathway. Nat Immunol 4:491–496.

101. Brisse M, Ly H. 2019. Comparative Structure and Function Analysis of the RIG-I-Like Receptors: RIG-I and MDA5. Frontiers in Immunology 10:1586.

102. Matsumoto M, Seya T. 2008. TLR3: Interferon induction by double-stranded RNA including poly(I:C). Advanced Drug Delivery Reviews 60:805–812.

103. Doyle SE, Vaidya SA, O'Connell R, Dadgostar H, Dempsey PW, Wu T-T, Rao G, Sun R, Haberland ME, Modlin RL, Cheng G. 2002. IRF3 Mediates a TLR3/TLR4-Specific Antiviral Gene Program. Immunity 17:251–263.

104. Takemura R, Takaki H, Okada S, Shime H, Akazawa T, Oshiumi H, Matsumoto M, Teshima T, Seya T. 2015. PolyI:C–Induced, TLR3/RIP3-Dependent Necroptosis Backs Up Immune Effector–Mediated Tumor Elimination *In Vivo*. Cancer Immunol Res 3:902–914.

105. Salaun B, Coste I, Rissoan M-C, Lebecque SJ, Renno T. 2006. TLR3 Can Directly Trigger Apoptosis in Human Cancer Cells. J Immunol 176:4894–4901.

106. Li M, Beg AA. 2000. Induction of Necrotic-Like Cell Death by Tumor Necrosis Factor Alpha and Caspase Inhibitors: Novel Mechanism for Killing Virus-Infected Cells. Journal of Virology 74:7470–7477.

107. Vandenabeele P, Galluzzi L, Vanden Berghe T, Kroemer G. 2010. Molecular mechanisms of necroptosis: an ordered cellular explosion. 10. Nature Reviews Molecular Cell Biology 11:700–714.

108. Feoktistova M, Geserick P, Kellert B, Dimitrova DP, Langlais C, Hupe M, Cain K, MacFarlane M, Häcker G, Leverkus M. 2011. cIAPs Block Ripoptosome Formation, a RIP1/Caspase-8 Containing Intracellular Cell Death Complex Differentially Regulated by cFLIP Isoforms. Molecular Cell 43:449–463.

109. Moriwaki K, Chan FK-M. 2016. Regulation of RIPK3- and RHIM-dependent Necroptosis by the Proteasome. J Biol Chem 291:5948–5959.

110. Holler N, Zaru R, Micheau O, Thome M, Attinger A, Valitutti S, Bodmer J-L, Schneider P, Seed B, Tschopp J. 2000. Fas triggers an alternative, caspase-8–independent cell death pathway using the kinase RIP as effector molecule. 6. Nature Immunology 1:489–495.

111. Vanlangenakker N, Bertrand MJM, Bogaert P, Vandenabeele P, Vanden Berghe T. 2011. TNF-induced necroptosis in L929 cells is tightly regulated by multiple TNFR1 complex I and II members. Cell Death Dis 2:e230–e230.

112. Jang T, Zheng C, Li J, Richards C, Hsiao Y-S, Walz T, Wu H, Park HH. 2014. Structural Study of the RIPoptosome Core Reveals a Helical Assembly for Kinase Recruitment. Biochemistry 53:5424–5431.

113. Tenev T, Bianchi K, Darding M, Broemer M, Langlais C, Wallberg F, Zachariou A, Lopez J, MacFarlane M, Cain K, Meier P. 2011. The Ripoptosome, a Signaling Platform that Assembles in Response to Genotoxic Stress and Loss of IAPs. Molecular Cell 43:432–448.

114. Moriwaki K, Bertin J, Gough PJ, Orlowski GM, Chan FK. 2015. Differential roles of RIPK1 and RIPK3 in TNF-induced necroptosis and chemotherapeutic agent-induced cell death. 2. Cell Death & Disease 6:e1636–e1636.

115. Nogusa S, Thapa RJ, Dillon CP, Liedmann S, Oguin TH, Ingram JP, Rodriguez DA, Kosoff R, Sharma S, Sturm O, Verbist K, Gough PJ, Bertin J, Hartmann BM, Sealfon SC, Kaiser WJ, Mocarski ES, López CB, Thomas PG, Oberst A, Green DR, Balachandran S. 2016. RIPK3 Activates Parallel Pathways of MLKL-Driven Necroptosis and FADD-Mediated Apoptosis to Protect against Influenza A Virus. Cell Host & Microbe 20:13–24.

116. Murphy JM, Vince JE. 2015. Post-translational control of RIPK3 and MLKL mediated necroptotic cell death. F1000Res 4.

117. Murphy JM, Czabotar PE, Hildebrand JM, Lucet IS, Zhang J-G, Alvarez-Diaz S, Lewis R, Lalaoui N, Metcalf D, Webb AI, Young SN, Varghese LN, Tannahill GM, Hatchell EC, Majewski IJ, Okamoto T, Dobson RCJ, Hilton DJ, Babon JJ, Nicola NA, Strasser A, Silke J, Alexander WS. 2013. The Pseudokinase MLKL Mediates Necroptosis via a Molecular Switch Mechanism. Immunity 39:443–453.

118. Rodriguez DA, Weinlich R, Brown S, Guy C, Fitzgerald P, Dillon CP, Oberst A, Quarato G, Low J, Cripps JG, Chen T, Green DR. 2016. Characterization of RIPK3-mediated phosphorylation of the activation loop of MLKL during necroptosis. 1. Cell Death & Differentiation 23:76–88.

119. Cai Z, Jitkaew S, Zhao J, Chiang H-C, Choksi S, Liu J, Ward Y, Wu L, Liu Z-G. 2014. Plasma membrane translocation of trimerized MLKL protein is required for TNF-induced necroptosis. 1. Nature Cell Biology 16:55–65.

120. Gong Y-N, Guy C, Olauson H, Becker JU, Yang M, Fitzgerald P, Linkermann A, Green DR. 2017. ESCRT-III Acts Downstream of MLKL to Regulate Necroptotic Cell Death and Its Consequences. Cell 169:286-300.e16.

121. Najafov A, Mookhtiar AK, Luu HS, Ordureau A, Pan H, Amin PP, Li Y, Lu Q, Yuan J. 2019. TAM Kinases Promote Necroptosis by Regulating Oligomerization of MLKL. Molecular Cell 75:457-468.e4.

122. Weber K, Roelandt R, Bruggeman I, Estornes Y, Vandenabeele P. 2018. Nuclear RIPK3 and MLKL contribute to cytosolic necrosome formation and necroptosis. Commun Biol 1:1–13.

123. Wu J, Huang Z, Ren J, Zhang Z, He P, Li Y, Ma J, Chen W, Zhang Y, Zhou X, Yang Z, Wu S-Q, Chen L, Han J. 2013. Mlkl knockout mice demonstrate the indispensable role of Mlkl in necroptosis. Cell Res 23:994–1006.

124. Dondelinger Y, Declercq W, Montessuit S, Roelandt R, Goncalves A, Bruggeman I, Hulpiau P, Weber K, Sehon CA, Marquis RW, Bertin J, Gough PJ, Savvides S, Martinou J-C, Bertrand MJM, Vandenabeele P. 2014. MLKL Compromises Plasma Membrane Integrity by Binding to Phosphatidylinositol Phosphates. Cell Reports 7:971–981.

125. Dovey CM, Diep J, Clarke BP, Hale AT, McNamara DE, Guo H, Brown NW, Cao JY, Grace CR, Gough PJ, Bertin J, Dixon SJ, Fiedler D, Mocarski ES, Kaiser WJ, Moldoveanu T, York JD, Carette JE. 2018. MLKL Requires the Inositol Phosphate Code to Execute Necroptosis. Molecular Cell 70:936-948.e7.

126. Wang H, Sun L, Su L, Rizo J, Liu L, Wang L-F, Wang F-S, Wang X. 2014. Mixed Lineage Kinase Domain-like Protein MLKL Causes Necrotic Membrane Disruption upon Phosphorylation by RIP3. Molecular Cell 54:133–146.

127. Kaiser WJ, Sridharan H, Huang C, Mandal P, Upton JW, Gough PJ, Sehon CA, Marquis RW, Bertin J, Mocarski ES. 2013. Toll-like Receptor 3-mediated Necrosis via TRIF, RIP3, and MLKL. J Biol Chem 288:31268–31279.

128. Rebsamen M, Heinz LX, Meylan E, Michallet M-C, Schroder K, Hofmann K, Vazquez J, Benedict CA, Tschopp J. 2009. DAI/ZBP1 recruits RIP1 and RIP3 through RIP homotypic interaction motifs to activate NF-κB. EMBO reports 10:916–922.

129. Upton JW, Kaiser WJ, Mocarski ES. 2012. DAI/ZBP1/DLM-1 Complexes with RIP3 to Mediate Virus-Induced Programmed Necrosis that Is Targeted by Murine Cytomegalovirus vIRA. Cell Host & Microbe 11:290–297.

130. Koehler H, Cotsmire S, Langland J, Kibler KV, Kalman D, Upton JW, Mocarski ES, Jacobs BL. 2017. Inhibition of DAI-dependent necroptosis by the Z-DNA binding domain of the vaccinia virus innate immune evasion protein, E3. Proceedings of the National Academy of Sciences 114:11506–11511.

131. Koehler HS, Cotsmire S, Zhang T, Balachandran S, Upton JW, Langland J, Kalman D, Jacobs BL, Mocarski ES. 2020. Competition between E3 and ZBP1 for Z-RNA Dictates Susceptibility to Vaccinia Virus-Induced Necroptosis. ID 3717768. SSRN Scholarly Paper, Social Science Research Network, Rochester, NY.

132. Shubina M, Tummers B, Boyd DF, Zhang T, Yin C, Gautam A, Guo XJ, Rodriguez DA, Kaiser WJ, Vogel P, Green DR, Thomas PG, Balachandran S. 2020. Necroptosis restricts influenza A virus as a stand-alone cell death mechanism. Journal of Experimental Medicine 217.

133. Zhang T, Yin C, Boyd DF, Quarato G, Ingram JP, Shubina M, Ragan KB, Ishizuka T, Crawford JC, Tummers B, Rodriguez DA, Xue J, Peri S, Kaiser WJ, López CB, Xu Y,

Upton JW, Thomas PG, Green DR, Balachandran S. 2020. Influenza Virus Z-RNAs Induce ZBP1-Mediated Necroptosis. Cell 180:1115-1129.e13.

134. Dickerson RE, Drew HR, Conner BN, Wing RM, Fratini AV, Kopka ML. 1982. The anatomy of A-, B-, and Z-DNA. Science 216:475–485.

135. Hall K, Cruz P, Tinoco I, Jovin TM, van de Sande JH. 1984. 'Z-RNA'—a left-handed RNA double helix. Nature 311:584–586.

136. Azorin F, Nordheim A, Rich A. 1983. Formation of Z-DNA in negatively supercoiled plasmids is sensitive to small changes in salt concentration within the physiological range. The EMBO Journal 2:649–655.

137. Ellison MJ, Feigon J, Kelleher RJ, Wang AHJ, Habener JF, Rich A. 1986. An assessment of the Z-DNA forming potential of alternating dA-dT stretches in supercoiled plasmids. Biochemistry 25:3648–3655.

138. Nordheim A, Lafer EM, Peck LJ, Wang JC, David Stollar B, Rich A. 1982. Negatively supercoiled plasmids contain left-handed Z-DNA segments as detected by specific antibody binding. Cell 31:309–318.

139. Wittig B, Dorbic T, Rich A. 1991. Transcription is associated with Z-DNA formation in metabolically active permeabilized mammalian cell nuclei. PNAS 88:2259–2263.

140. Davis PW, Adamiak RW, Tinoco I. 1990. Z-RNA: The solution NMR structure of r(CGCGCG). Biopolymers 29:109–122.

141. de Reuver R, Dierick E, Wiernicki B, Staes K, Seys L, De Meester E, Muyldermans T, Botzki A, Lambrecht BN, Van Nieuwerburgh F, Vandenabeele P, Maelfait J. 2021. ADAR1 interaction with Z-RNA promotes editing of endogenous double-stranded RNA and prevents MDA5-dependent immune activation. Cell Reports 36:109500.

142. Placido D, Brown BA, Lowenhaupt K, Rich A, Athanasiadis A. 2007. A Left-Handed RNA Double Helix Bound by the Zα Domain of the RNA-Editing Enzyme ADAR1. Structure 15:395–404.

143. Brown BA, Lowenhaupt K, Wilbert CM, Hanlon EB, Rich A. 2000. The zalpha domain of the editing enzyme dsRNA adenosine deaminase binds left-handed Z-RNA as well as Z-DNA. Proc Natl Acad Sci U S A 97:13532–13536.

144. Liddicoat BJ, Piskol R, Chalk AM, Ramaswami G, Higuchi M, Hartner JC, Li JB, Seeburg PH, Walkley CR. 2015. RNA editing by ADAR1 prevents MDA5 sensing of endogenous dsRNA as nonself. Science 349:1115–1120.

145. Herbert A. 2021. To "Z" or not to "Z": Z-RNA, self-recognition, and the MDA5 helicase. PLOS Genetics 17:e1009513.

146. Schwartz T, Behlke J, Lowenhaupt K, Heinemann U, Rich A. 2001. Structure of the DLM-1?Z-DNA complex reveals a conserved family of Z-DNA-binding proteins. Nature Structural Biology 8:761.

147. Cotsmire SM, Szczerba M, Jacobs BL. 2021. Detecting Necroptosis in Virus-Infected Cells, p. 199–216. *In* Lucas, AR (ed.), Viruses as Therapeutics: Methods and Protocols. Springer US, New York, NY.

148. Thapa RJ, Ingram JP, Ragan KB, Nogusa S, Boyd DF, Benitez AA, Sridharan H, Kosoff R, Shubina M, Landsteiner VJ, Andrake M, Vogel P, Sigal LJ, tenOever BR, Thomas PG, Upton JW, Balachandran S. 2016. DAI Senses Influenza A Virus Genomic RNA and Activates RIPK3-Dependent Cell Death. Cell Host Microbe 20:674–681.

149. Zheng M, Kanneganti T-D. 2020. The regulation of the ZBP1-NLRP3 inflammasome and its implications in pyroptosis, apoptosis, and necroptosis (PANoptosis). Immunological Reviews 297:26–38.

150. Kuriakose T, Man SM, Malireddi RKS, Karki R, Kesavardhana S, Place DE, Neale G, Vogel P, Kanneganti T-D. 2016. ZBP1/DAI is an innate sensor of influenza virus triggering the NLRP3 inflammasome and programmed cell death pathways. Sci Immunol 1:aag2045.

151. Kesavardhana S, Kuriakose T, Guy CS, Samir P, Malireddi RKS, Mishra A, Kanneganti T-D. 2017. ZBP1/DAI ubiquitination and sensing of influenza vRNPs activate programmed cell death. Journal of Experimental Medicine 214:2217–2229.

152. Jiao H, Wachsmuth L, Kumari S, Schwarzer R, Lin J, Eren RO, Fisher A, Lane R, Young GR, Kassiotis G, Kaiser WJ, Pasparakis M. 2020. Z-nucleic-acid sensing triggers ZBP1-dependent necroptosis and inflammation. Nature 580:391–395.

153. Sridharan H, Ragan KB, Guo H, Gilley RP, Landsteiner VJ, Kaiser WJ, Upton JW. 2017. Murine cytomegalovirus IE3-dependent transcription is required for DAI/ZBP1-mediated necroptosis. EMBO reports 18:1429–1441.

154. Guo H, Gilley RP, Fisher A, Lane R, Landsteiner VJ, Ragan KB, Dovey CM, Carette JE, Upton JW, Mocarski ES, Kaiser WJ. 2018. Species-independent contribution of ZBP1/DAI/DLM-1-triggered necroptosis in host defense against HSV1. Cell Death Dis 9:1–11.

155. Maelfait J, Liverpool L, Bridgeman A, Ragan KB, Upton JW, Rehwinkel J. 2017. Sensing of viral and endogenous RNA by ZBP1/DAI induces necroptosis. The EMBO Journal 36:2529–2543.

156. Yang D, Liang Y, Zhao S, Ding Y, Zhuang Q, Shi Q, Ai T, Wu S-Q, Han J. 2020. ZBP1 mediates interferon-induced necroptosis. Cell Mol Immunol 17:356–368.

157. Subramanian S. 2020. Necroptosis: Role in Poxvirus Pathogenesis and Oncolytic Virotherapy. Doctoral Dissertation, Arizona State University.

158. Chang H-W, Jacobs BL. 1993. Identification of a Conserved Motif That Is Necessary for Binding of the Vaccinia Virus E3L Gene Products to Double-Stranded RNA. Virology 194:537–547.

159. Langland JO, Jacobs BL. 2004. Inhibition of PKR by vaccinia virus: role of the N- and C-terminal domains of E3L. Virology 324:419–429.

160. Brandt TA, Jacobs BL. 2001. Both Carboxy- and Amino-Terminal Domains of the Vaccinia Virus Interferon Resistance Gene, E3L, Are Required for Pathogenesis in a Mouse Model. Journal of Virology 75:850–856.

161. Brandt T, Heck MC, Vijaysri S, Jentarra GM, Cameron JM, Jacobs BL. 2005. The N-terminal domain of the vaccinia virus E3L-protein is required for neurovirulence, but not induction of a protective immune response. Virology 333:263–270.

162. Shors T, Kibler KV, Perkins KB, Seidler-Wulff R, Banaszak MP, Jacobs BL. 1997. Complementation of Vaccinia Virus Deleted of the E3L Gene by Mutants of E3L. Virology 239:269–276.

163. Thakur M, Seo EJ, Dever TE. 2014. Variola virus E3L Z domain, but not its Z-DNA binding activity, is required for PKR inhibition. RNA 20:214–227.

164. Pearcy M. Identification and characterization of the multiple domains of the vaccinia virus E3L protein. Ph.D., Arizona State University, United States -- Arizona.

165. Zhang P, Jacobs BL, Samuel CE. 2008. Loss of Protein Kinase PKR Expression in Human HeLa Cells Complements the Vaccinia Virus E3L Deletion Mutant Phenotype by Restoration of Viral Protein Synthesis. J Virol 82:840–848.

166. Sharp TV, Moonan F, Romashko A, Joshi B, Barber GN, Jagus R. 1998. The Vaccinia Virus E3L Gene Product Interacts with both the Regulatory and the Substrate Binding Regions of PKR: Implications for PKR Autoregulation. Virology 250:302–315.

167. Arndt WD, Cotsmire S, Trainor K, Harrington H, Hauns K, Kibler KV, Huynh TP, Jacobs BL. 2015. Evasion of the Innate Immune Type I Interferon System by Monkeypox Virus. J Virol 89:10489–10499.

168. Kim Y-G, Muralinath M, Brandt T, Pearcy M, Hauns K, Lowenhaupt K, Jacobs BL, Rich A. 2003. A role for Z-DNA binding in vaccinia virus pathogenesis. Proceedings of the National Academy of Sciences 100:6974–6979.

169. Bera BCh, Shanmugasundaram K, Barua S, Anand T, Riyesh T, Vaid RK, Virmani N, Bansal M, Shukla BN, Malik P, Singh RK. 2012. Sequence and phylogenetic analysis of host-range (E3L, K3L, and C7L) and structural protein (B5R) genes of buffalopox virus isolates from buffalo, cattle, and human in India. Virus Genes 45:488–498.

170. Kim Y-G, Muralinath M, Brandt T, Pearcy M, Hauns K, Lowenhaupt K, Jacobs BL, Rich A. 2003. A role for Z-DNA binding in vaccinia virus pathogenesis. PNAS 100:6974–6979.

171. Muralinath M. The role of the amino terminus of E3L in vaccinia virus pathogenesis. Ph.D., Arizona State University, United States -- Arizona.

172. Hauns KD. Expression of cellular anti-viral antagonists from vaccinia virus to study the innate immune response and Z -DNA. Ph.D., Arizona State University, United States -- Arizona.

173. Arndt WD, White SD, Johnson BP, Huynh T, Liao J, Harrington H, Cotsmire S, Kibler KV, Langland J, Jacobs BL. 2016. Monkeypox virus induces the synthesis of less dsRNA than

vaccinia virus, and is more resistant to the anti-poxvirus drug, IBT, than vaccinia virus. Virology 497:125–135.

174. Chen N, Li G, Liszewski MK, Atkinson JP, Jahrling PB, Feng Z, Schriewer J, Buck C, Wang C, Lefkowitz EJ, Esposito JJ, Harms T, Damon IK, Roper RL, Upton C, Buller RML. 2005. Virulence differences between monkeypox virus isolates from West Africa and the Congo basin. Virology 340:46–63.

175. Fine PEM, Jezek Z, Grab B, Dixon H. 1988. The Transmission Potential of Monkeypox Virus in Human Populations. Int J Epidemiol 17:643–650.

176. Reynolds MG, Wauquier N, Li Y, Satheshkumar PS, Kanneh LD, Monroe B, Maikere J, Saffa G, Gonzalez J-P, Fair J, Carroll DS, Jambai A, Dafae F, Khan SH, Moses LM. 2019. Human Monkeypox in Sierra Leone after 44-Year Absence of Reported Cases. Emerg Infect Dis 25:1023–1025.

177. Fenner F, Henderson DA, Arita I, Jezek Z, Ladnyi ID, Organization WH. 1988. Smallpox and its eradication. World Health Organization.

178. Langland JO, Jacobs BL. 2002. The Role of the PKR-Inhibitory Genes, E3L and K3L, in Determining Vaccinia Virus Host Range. Virology 299:133–141.

179. Bratke KA, McLysaght A, Rothenburg S. 2013. A survey of host range genes in poxvirus genomes. Infection, Genetics and Evolution 14:406–425.

180. Clemens MJ. 1997. PKR--a protein kinase regulated by double-stranded RNA. Int J Biochem Cell Biol 29:945–949.

181. de Veer MJ, Holko M, Frevel M, Walker E, Der S, Paranjape JM, Silverman RH, Williams BR. 2001. Functional classification of interferon-stimulated genes identified using microarrays. J Leukoc Biol 69:912–920.

182. Dey M, Mann BR, Anshu A, Mannan MA. 2014. Activation of Protein Kinase PKR Requires Dimerization-induced cis-Phosphorylation within the Activation Loop*. Journal of Biological Chemistry 289:5747–5757.

183. Farrell PJ, Balkow K, Hunt T, Jackson RJ, Trachsel H. 1977. Phosphorylation of initiation factor eIF-2 and the control of reticulocyte protein synthesis. Cell 11:187–200.

184. Levin D, London IM. 1978. Regulation of protein synthesis: Activation by double-stranded RNA of a protein kinase that phosphorylates eukaryotic initiation factor 2. Proceedings of the National Academy of Sciences 75:1121–1125.

185. Duerst RJ, Morrison LA. 2004. Herpes simplex virus 2 virion host shutoff protein interferes with type I interferon production and responsiveness. Virology 322:158–167.

186. Cresawn SG, Prins C, Latner DR, Condit RC. 2007. Mapping and phenotypic analysis of spontaneous isatin-β-thiosemicarbazone resistant mutants of vaccinia virus. Virology 363:319–332.

187. Cresawn SG, Condit RC. 2007. A targeted approach to identification of vaccinia virus postreplicative transcription elongation factors: Genetic evidence for a role of the H5R gene in vaccinia transcription. Virology 363:333–341.

188. Prins C, Cresawn SG, Condit RC. 2004. An Isatin-β-thiosemicarbazone-resistant Vaccinia Virus Containing a Mutation in the Second Largest Subunit of the Viral RNA Polymerase Is Defective in Transcription Elongation. J Biol Chem 279:44858–44871.

189. Langland JO, Jacobs BL. 2004. Inhibition of PKR by vaccinia virus: role of the N- and C-terminal domains of E3L. Virology 324:419–429.

190. Huhn GD, Bauer AM, Yorita K, Graham MB, Sejvar J, Likos A, Damon IK, Reynolds MG, Kuehnert MJ. 2005. Clinical Characteristics of Human Monkeypox, and Risk Factors for Severe Disease. Clin Infect Dis 41:1742–1751.

191. Brandt T, Heck MC, Vijaysri S, Jentarra GM, Cameron JM, Jacobs BL. 2005. The N-terminal domain of the vaccinia virus E3L-protein is required for neurovirulence, but not induction of a protective immune response. Virology 333:263–270.

192. Sun L, Wang H, Wang Z, He S, Chen S, Liao D, Wang L, Yan J, Liu W, Lei X, Wang X. 2012. Mixed Lineage Kinase Domain-like Protein Mediates Necrosis Signaling Downstream of RIP3 Kinase. Cell 148:213–227.

193. Cho Y, Challa S, Moquin D, Genga R, Ray TD, Guildford M, Chan FK-M. 2009. Phosphorylation-Driven Assembly of the RIP1-RIP3 Complex Regulates Programmed Necrosis and Virus-Induced Inflammation. Cell 137:1112–1123.

194. Yang C, Li J, Yu L, Zhang Z, Xu F, Jiang L, Zhou X, He S. 2017. Regulation of RIP3 by the transcription factor Sp1 and the epigenetic regulator UHRF1 modulates cancer cell necroptosis. Cell Death Dis 8:e3084–e3084.

195. Koo G-B, Morgan MJ, Lee D-G, Kim W-J, Yoon J-H, Koo JS, Kim SI, Kim SJ, Son MK, Hong SS, Levy JMM, Pollyea DA, Jordan CT, Yan P, Frankhouser D, Nicolet D, Maharry K, Marcucci G, Choi KS, Cho H, Thorburn A, Kim Y-S. 2015. Methylation-dependent loss of RIP3 expression in cancer represses programmed necrosis in response to chemotherapeutics. Cell Res 25:707–725.

196. Koehler H, Cotsmire S, Zhang T, Balachandran S, Upton JW, Langland J, Kalman D, Jacobs BL, Mocarski ES. 2021. Vaccinia virus E3 prevents sensing of Z-RNA to block ZBP1-dependent necroptosis. Cell Host & Microbe 29:1266-1276.e5.

197. Yang Y-L, F.L.Reis L, Pavlovic J, Aguzzi A, Schafer R, Kumar A, R.G.Williams B, Aguet M, Weissmann C. 1995. Deficient signaling in mice devoid of double-stranded RNA-dependent protein kinase. The EMBO Journal 14:6095–6106.

198. Rice AD, Turner PC, Embury JE, Moldawer LL, Baker HV, Moyer RW. 2011. Roles of Vaccinia Virus Genes E3L and K3L and Host Genes PKR and RNase L during Intratracheal Infection of C57BL/6 Mice. J Virol 85:550–567.

199. Bergmann M, Garcia-Sastre A, Carnero E, Pehamberger H, Wolff K, Palese P, Muster T. 2000. Influenza Virus NS1 Protein Counteracts PKR-Mediated Inhibition of Replication. J Virol 74:6203–6206.

200. Schulz O, Pichlmair A, Rehwinkel J, Rogers NC, Scheuner D, Kato H, Takeuchi O, Akira S, Kaufman RJ, Sousa CR e. 2010. Protein Kinase R Contributes to Immunity against Specific Viruses by Regulating Interferon mRNA Integrity. Cell Host & Microbe 7:354–361.

201. Schierhorn KL, Jolmes F, Bespalowa J, Saenger S, Peteranderl C, Dzieciolowski J, Mielke M, Budt M, Pleschka S, Herrmann A, Herold S, Wolff T. 2017. Influenza A Virus Virulence Depends on Two Amino Acids in the N-Terminal Domain of Its NS1 Protein To Facilitate Inhibition of the RNA-Dependent Protein Kinase PKR. J Virol 91:e00198-17.

202. Khabar KSA, Dhalla M, Siddiqui Y, Zhou A, Al-Ahdal MN, Der SD, Silverman RH, Williams BRG. 2000. Effect of Deficiency of the Double-Stranded RNA-Dependent Protein Kinase, PKR, on Antiviral Resistance in the Presence or Absence of Ribonuclease L: HSV-1 Replication Is Particularly Sensitive to Deficiency of the Major IFN-Mediated Enzymes. Journal of Interferon & Cytokine Research 20:653–659.

203. Sawicki DL, Silverman RH, Williams BR, Sawicki SG. 2003. Alphavirus Minus-Strand Synthesis and Persistence in Mouse Embryo Fibroblasts Derived from Mice Lacking RNase L and Protein Kinase R. J Virol 77:1801–1811.

204. Goodman DE, Pretto CD, Krepostman TA, Carnahan KE, Spindler KR. 2019. Enhanced Replication of Mouse Adenovirus Type 1 following Virus-Induced Degradation of Protein Kinase R (PKR). mBio 10:e00668-19.

205. Abraham N, Stojdl DF, Duncan PI, Méthot N, Ishii T, Dubé M, Vanderhyden BC, Atkins HL, Gray DA, McBurney MW, Koromilas AE, Brown EG, Sonenberg N, Bell JC. 1999. Characterization of Transgenic Mice with Targeted Disruption of the Catalytic Domain of the Double-stranded RNA-dependent Protein Kinase, PKR *. Journal of Biological Chemistry 274:5953–5962.

206. Baltzis D, Li S, Koromilas AE. 2002. Functional Characterization of pkr Gene Products Expressed in Cells from Mice with a Targeted Deletion of the N terminus or C terminus Domain of PKR *. Journal of Biological Chemistry 277:38364–38372.

207. Brandt TA. The dual domains of the vaccinia virus E3L gene: In vivo and in vitro studies. Ph.D., Arizona State University, United States -- Arizona.

208. Perkins KB. The role of the amino terminus of E3L in vaccinia virus replication. Ph.D., Arizona State University, United States -- Arizona.

209. Willis KL, Langland JO, Shisler JL. 2011. Viral Double-stranded RNAs from Vaccinia Virus Early or Intermediate Gene Transcripts Possess PKR Activating Function, Resulting in NF-κB Activation, When the K1 Protein Is Absent or Mutated *. Journal of Biological Chemistry 286:7765–7778.

210. Chiang DC, Li Y, Ng SK. 2021. The Role of the Z-DNA Binding Domain in Innate Immunity and Stress Granules. Frontiers in Immunology 11:3779.

211. Szczerba MB. 2021. Stress Granule-Mediated Mechanism of the Cellular Death Pathway Necroptosis Induced Through Oxidative Stress and Viral Infection. Ph.D., Arizona State University, United States -- Arizona.

212. Hanus J, Anderson C, Wang S. 2015. RPE necroptosis in response to oxidative stress and in AMD. Ageing Research Reviews 24:286–298.

213. Han Q, Zhang J, Sun Q, Xu Y, Teng X. 2020. Oxidative stress and mitochondrial dysfunction involved in ammonia-induced nephrocyte necroptosis in chickens. Ecotoxicology and Environmental Safety 203:110974.

214. Yu Q, Qu K, Modis Y. 2018. Cryo-EM Structures of MDA5-dsRNA Filaments at Different Stages of ATP Hydrolysis. Mol Cell 72:999-1012.e6.

215. Ishii KJ, Kawagoe T, Koyama S, Matsui K, Kumar H, Kawai T, Uematsu S, Takeuchi O, Takeshita F, Coban C, Akira S. 2008. TANK-binding kinase-1 delineates innate and adaptive immune responses to DNA vaccines. Nature 451:725–729.

216. Newton K, Sun X, Dixit VM. 2004. Kinase RIP3 Is Dispensable for Normal NF-κBs, Signaling by the B-Cell and T-Cell Receptors, Tumor Necrosis Factor Receptor 1, and Toll-Like Receptors 2 and 4. Mol Cell Biol 24:1464–1469.

APPENDIX A

CHAPTER 2 SUPPLIMENTARY INFORMATION

Figure 2-S1: Detailed screen of plaques

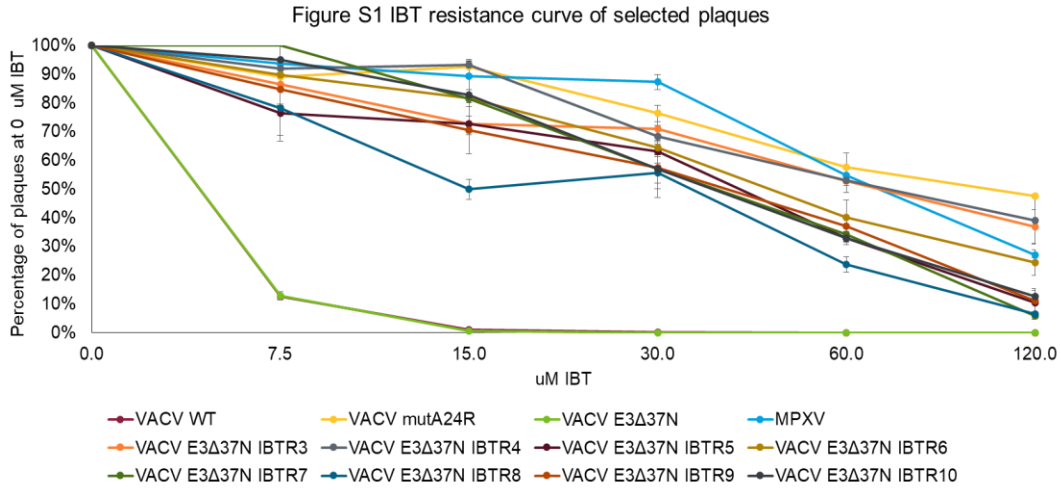

Figure 2-S1 Generating IBTR mutants

After picking plaques from IBT treated infections, the plaques underwent a preliminary screen. Two IBT dependent plaques were picked (data not shown) and eight IBT resistant plaques were picked. These plaques underwent one round of expansion before undergoing more detailed study. We measured the IBT sensitivity curve of each plaque compared to VACV WT, VACV E3Δ37N, VACV mutA24R, and MPXV. We selected plaque 3 (VACV E3Δ37N IBTR3) due to its similarity with VACV mutA24R. We selected plaque 7 (VACV E3Δ37N IBTR7) because it had an intermediate phenotype. Error bars represent standard error after three biological replicates.

Figure 2-S2 Free dsRNA flow cytometry validation

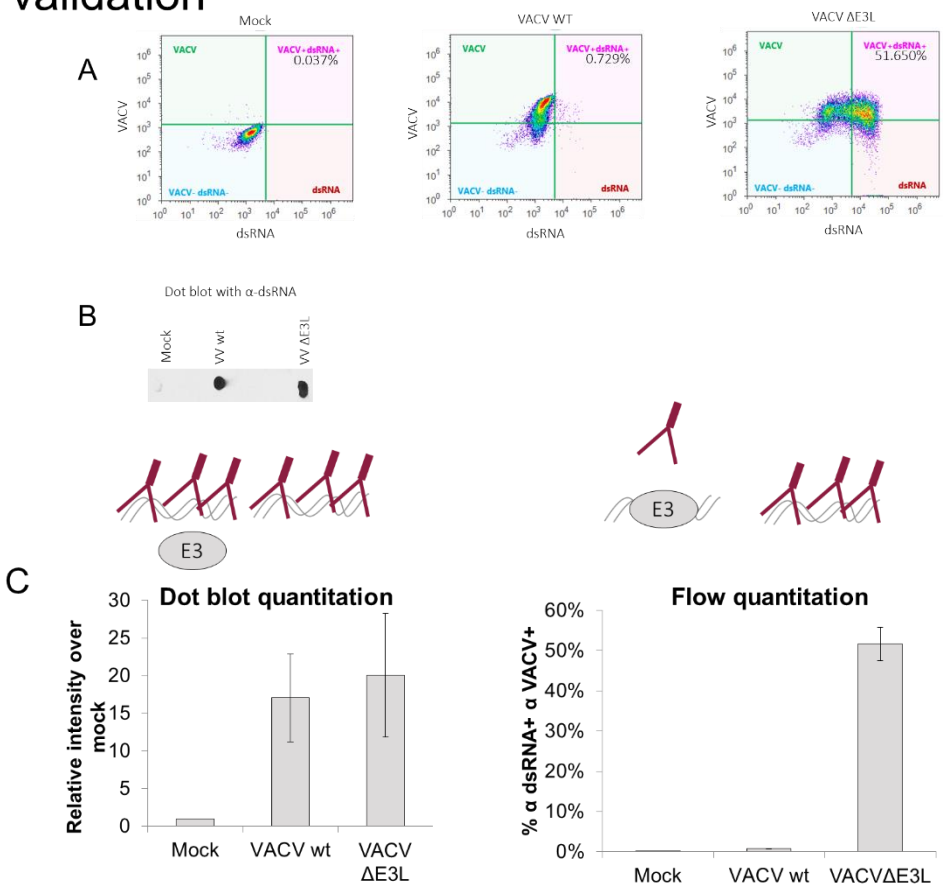

Figure 2-S2 Free dsRNA flow cytometry validation

HeLa cells were infected with mock, VACV WT, or VACV ΔE3 at an MOI of 5 for 6 hours. They were then either fixed with formaldehyde and stained for flow cytometry (A), or RNA lysates were harvested and purified (B). Cells were stained for flow with polyclonal anti-VACV antibody and monoclonal anti-dsRNA antibody, J2. Results were quantified and plotted with error bars representing standard error (C).

APPENDIX B

CHAPTER 3 SUPPLIMENTARY INFORMATION

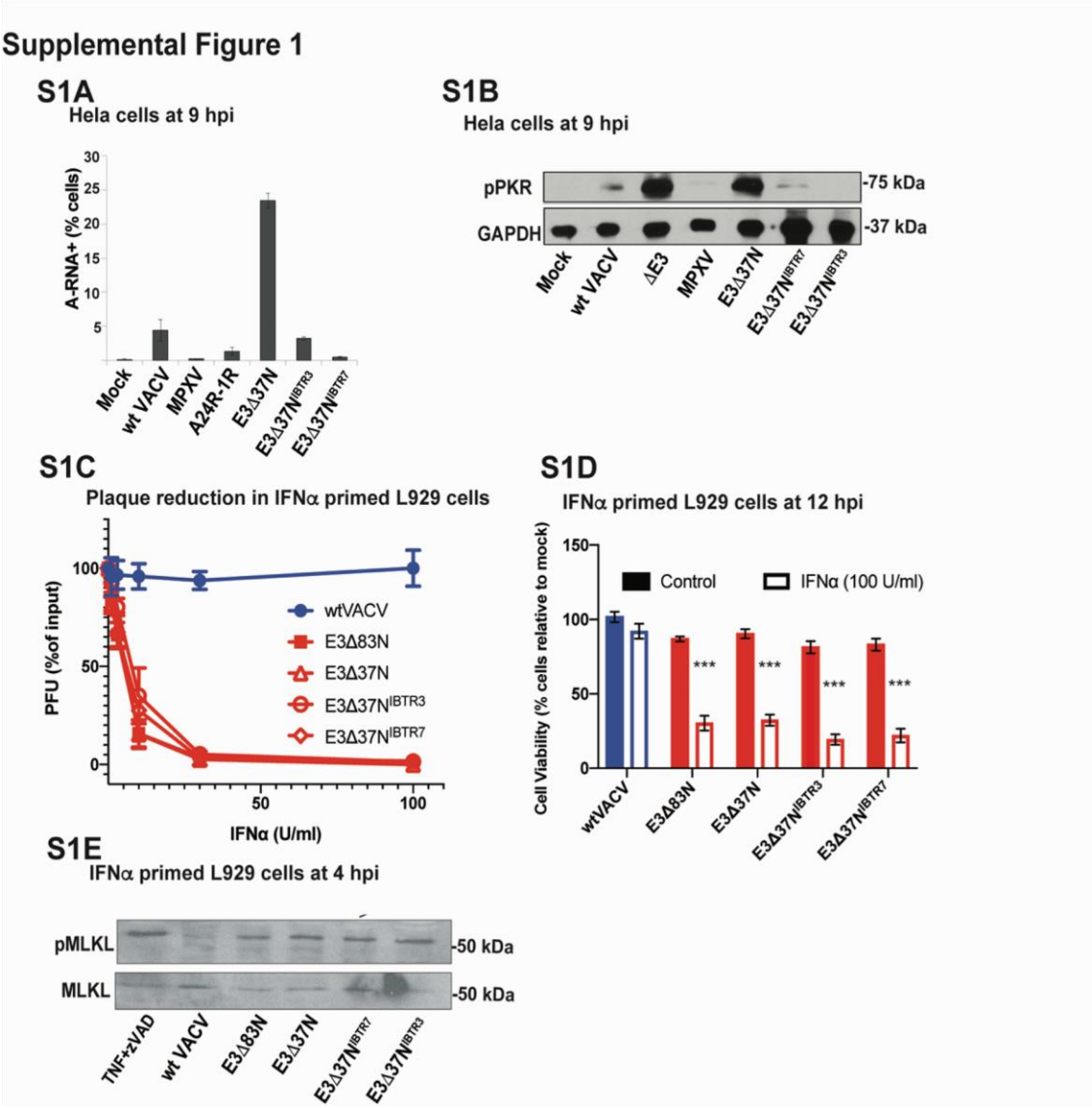

Supplemental Figure 3-1.

(S1A) Flow cytometric evaluation of free A-RNA in Hela cells. Cells were either left uninfected (Mock) or infected with wt VACV, MPXV, A24R-R1, E3Δ37N, E3Δ37N^{IBTR3} or E3Δ37N^{IBTR7} (MOI of 5). Following fixation and permeabilization at 9 hpi, the frequency of A-RNA^{+} cells was determined by flow cytometry with the J2 antibody. Single cell suspensions were generated and gated to exclude doublets.

(S1B) IB of Hela cells for activated PKR that were either left uninfected (Mock) or infected with wt VACV, MPXV, E3Δ37N, E3Δ37N^{IBTR3} or E3Δ37N^{IBTR7} (MOI of 5). Lysates were harvested at 9

hpi, denatured and separated by SDS-PAGE prior to transfer and detection of phospho-PKR (pPKR).

(S1C) Plaque reduction assays were carried out on L929 cells as described in Figure 1.

(S1D) L929 cells either left untreated or IFNa-pretreated as described in Figure 1 and infected (MOI of 5) with the indicated viruses. Cell viability was determined by Sytox dye exclusion as described in Figure 1.

(S1E) IB of L929 cell lysates as described in Figure 1. Error bars represent the SD. Statistical significance was determined as described in Figure 1. Each set of data is representative of three replicates except for panel A, C and D which compiles the results of the replicates. Statistical significance was determined as described in Figure 1.

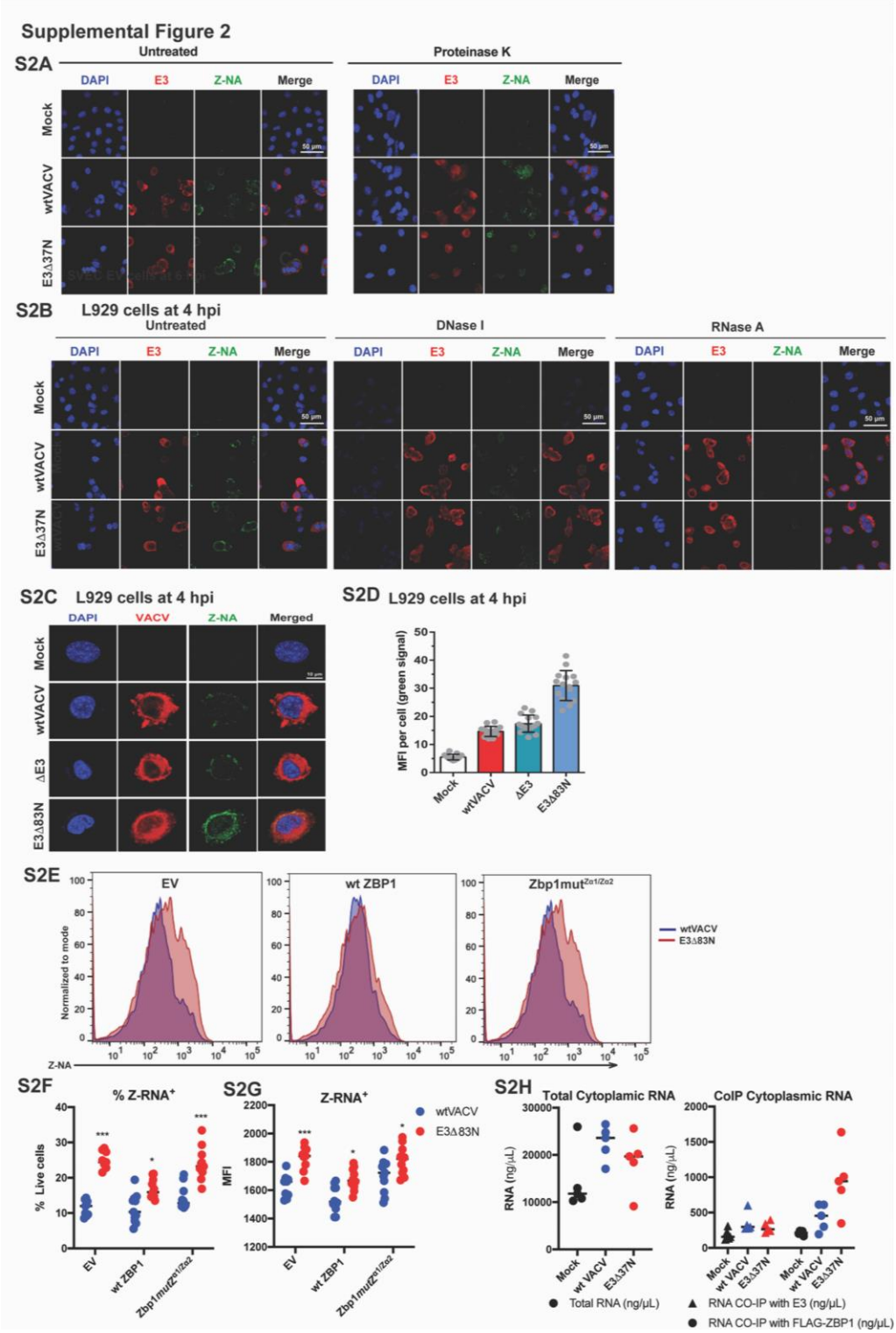

Supplemental Figure 3-2.

(S2A) Confocal immunofluorescent micrographs showing a field of L929 cells evaluated as single cells in Figure 5A.

(S2B) Confocal immunofluorescent micrographs showing a field of L929 cells evaluated as single cells in Figure 5C. **(S2C)** Confocal immunofluorescent micrographs evaluating single L929 cells infected with additional VACV mutants, E3Δ83N and ΔE3.

(S2D) Quantification of the median fluorescence intensity of Z-NA signal intensity of 20 individual cells from S2C analyzed as described in Figure 5B.

(S2E) Flow cytometric evaluation of Z-NA, showing representative flow cytometric histograms employed for evaluation shown in S2F and S2G. SVEC-derived EV, wt ZBP1 and Zbp1*mut*$^{Za1/Za2}$ cells were infected with wt VACV or E3Δ83N (MOI of 5), UV-crosslinked at 6 hpi, fixed and permeabilized, DNase I treated and evaluated for the presence of Z-NA by flow cytometry with anti-Z-NA antibody. Single cell suspensions were evaluated by employing gating to exclude doublets and dead cells.

(S2F) Proportion of Z-NA positive cells from 10 to 12 replicate flow cytometric histograms infected and treated as described in S2E.

(S2G) MFI of Z-NA+ SVEC-derived EV, wt ZBP1 and ZBP1*mut*$^{Za1/Za2}$ cells following infection at a MOI of 5 with wt VACV or E3Δ83N. Cells were infected, treated and harvested as described in Panel S2E.

(S2H) Quantification of total RNA (left panel) or co-IP (right panel) of either ZBP1- or E3-associated RNA extracted from Mock or infected SVEC-derived wt ZBP1 cells and used to calculate proportions depicted in Figure 5D.

Error bars represent the SD. Each set of data is representative of three replicates which compiles the results of the replicates. Statistical significance was determined as described in Figure 1.